Chem Soc Rev

REVIEW ARTICLE

View Article Online
View Journal | View Issue

Cite this: *Chem. Soc. Rev.*, 2018, **47**, 3152

Wearable energy sources based on 2D materials

Fang Yi,†[a] Huaying Ren,†[ab] Jingyuan Shan,†[ab] Xiao Sun,[ab] Di Wei *[c] and Zhongfan Liu*[ac]

Received 11th December 2017

DOI: 10.1039/c7cs00849j

rsc.li/chem-soc-rev

Wearable energy sources are in urgent demand due to the rapid development of wearable electronics. Besides flexibility and ultrathin thickness, emerging 2D materials present certain extraordinary properties that surpass the properties of conventional materials, which make them advantageous for high-performance wearable energy sources. Here, we provide a comprehensive review of recent advances in 2D material based wearable energy sources including wearable batteries, supercapacitors, and different types of energy harvesters. The crucial roles of 2D materials in the wearable energy sources are highlighted. Based on the current progress, the existing challenges and future prospects are outlined and discussed.

1. Introduction

Since the smart watch IBM WatchPad 1.0 running Linux was released in 2000, a rapid succession of various wearable smart gizmos have come to the fore.[1,2] The smart devices today can not only run algorithms alone, but can also be connected together into groups to form the internet of things.[3] People can get personalized information and communicate with the world by carrying devices such as mobile phones, in-ear monitors or earphones, smart watches or bands, glasses, rings, and even smart tattoos (Fig. 1).[4–8] These wearable smart devices offer plenty of applications while obeying stringent size constrains, which poses a great challenge to their power supply components. Besides reducing the power consumption,[9,10] increasing the energy density of the power supply component and developing a sustainable power system that provides power by harvesting energy from the ambient environment are two solutions to address this challenge. Furthermore, wearable electronics are now undergoing fast development following the trend of lighter weight, thinner thickness, more conformable to the curved contours of the human body and more adaptable to the

[a] Center for Nanochemistry, Beijing Science and Engineering Center for Nanocarbons, Beijing National Laboratory for Molecular Sciences, College of Chemistry and Molecular Engineering, Peking University, Beijing 100871, P. R. China. E-mail: zfliu@pku.edu.cn
[b] Academy for Advanced Interdisciplinary Studies, Peking University, Beijing 100871, P. R. China
[c] Beijing Graphene Institute, Beijing 100094, P. R. China. E-mail: weidi-cnc@pku.edu.cn
† These authors contributed equally to the work.

Fang Yi

Fang Yi received her BS degree from Central South University, and PhD degree from the University of Science and Technology Beijing, in Prof. Yue Zhang's group. She was a visiting PhD student at Georgia Institute of Technology, in Prof. Zhong Lin Wang's group, from 08/2013 to 08/2015. She is now a postdoc at Peking University, in Prof. Zhongfan Liu's group. Her research interest focuses on energy conversion and storage, self-powered power systems, and self-powered sensors.

Huaying Ren

Huaying Ren received her BS degree from the School of Chemistry and Chemical Engineering at Shandong University in 2013. She is currently a graduate student in Center for Nanochemistry, College of Chemistry and Molecular Engineering at Peking University, in Prof. Zhongfan Liu's group. Her research is focused on controlled synthesis of high-quality graphene and its applications in photothermal and wearable sensing devices.

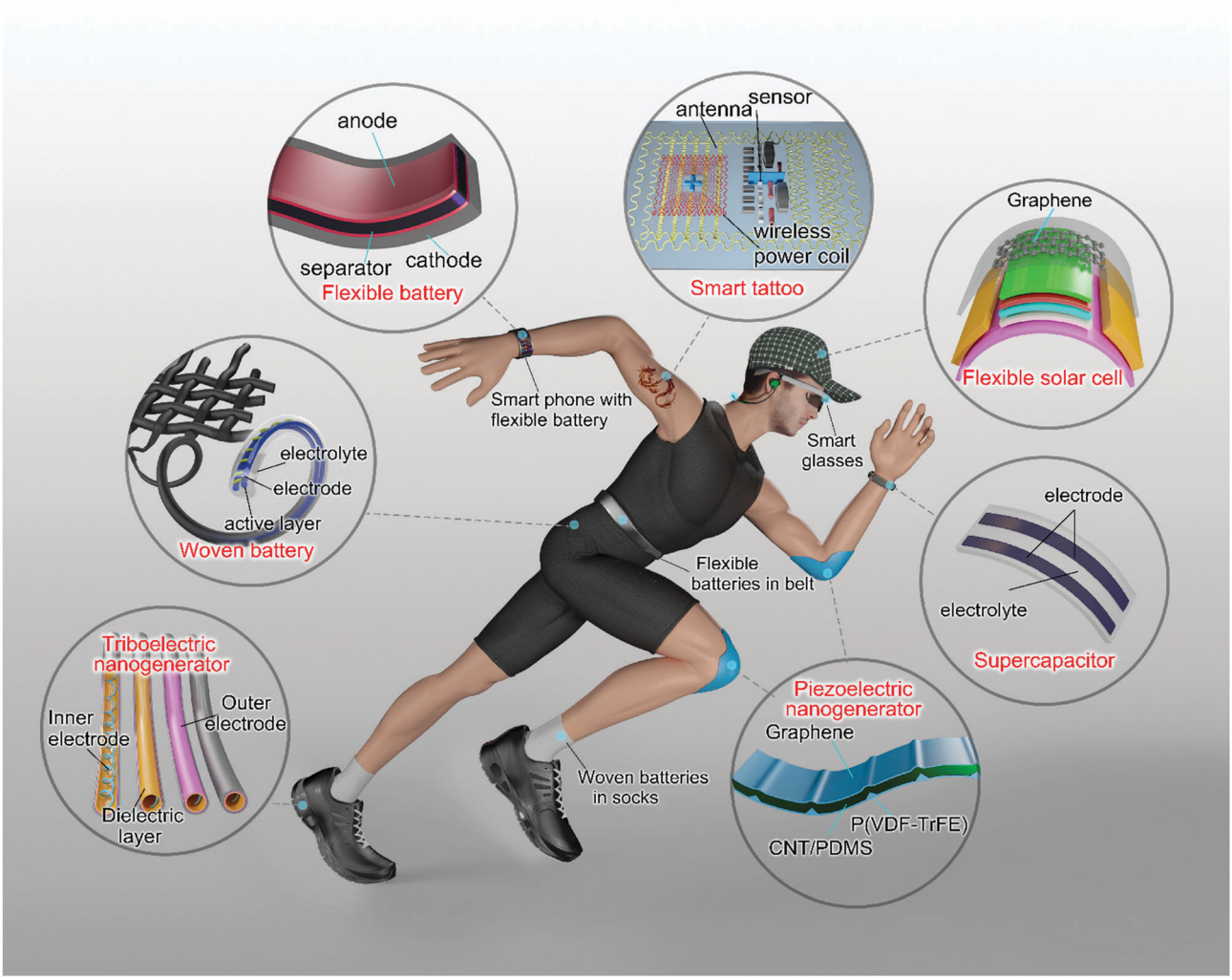

Fig. 1 Schematic illustration of wearable energy sources and devices in near future.

body movements,[11–15] which requires the power supply components to meet these standards. Although integrating the conventional rigid energy supply component with the other electronic components onto a flexible substrate is a stopgap to tackle this issue, this approach introduces additional weight to the device and compromises customer experience. Therefore, wearable energy sources with light weight, thin thickness, flexibility, in addition to high energy density and power density, operational safety, long-term stability, and low cost are urgently needed.

Jingyuan Shan

Jingyuan Shan received her BS degree from the School of Material Science and Engineering at Shandong University in 2016. She is currently a PhD candidate in Center for Nanochemistry, College of Chemistry and Molecular Engineering at Peking University, in Prof. Zhongfan Liu's group. Her research mainly focuses on controlled synthesis of graphene and its applications in wearable energy devices.

Xiao Sun

Xiao Sun received her BS degree from the College of Chemistry and Chemical Engineering at Lanzhou University in 2014. She is currently pursuing a PhD in Center for Nanochemistry, College of Chemistry and Molecular Engineering at Peking University, in Prof. Zhongfan Liu's group. Her research is focused on graphene based radio frequency, especially its applications in wearable devices.

Batteries and supercapacitors are two common energy storage devices that are used as power supplies for electronics. Compared with supercapacitors, batteries have a higher energy density and are the most widely used power supply components for electronics in the present day.[16–20] Specifically, rechargeable batteries have been given more attention due to their long-term cycle life and less environmental impact. Rechargeable lithium ion batteries (LIBs) have been the subject of intense research interest for decades due to their high energy density and long service life.[21,22] Other rechargeable batteries based on abundant elements such as sodium (Na) and aluminum (Al) have also been intensively studied owing to their low cost; furthermore, Al-ion batteries show superiority in terms of high safety and good cyclic stability.[23,24] Supercapacitors, on the other hand, possess a higher power density and longer cycle lifetime,[25–28] and have been widely applied to deliver power for portable consumer electronics, computer memory back-up systems, stop-start systems of automobiles, *etc.* The excellent cycle lifetime of supercapacitors also makes them more suitable to act as the energy storage component of sustainable power systems that power electronics by harvesting energy. Thus, developing wearable high-performance batteries and supercapacitors is a promising route to meet the demand for wearable energy sources.

An alternative type of energy source to energy storage devices is the energy harvesters. There are various forms of renewable energy in the ambient environment that can be scavenged, such as solar radiation, body motion, and body heat. Correspondingly, solar cells can scavenge energy from sunlight;[29,30] piezoelectric and triboelectric nanogenerators are desirable to harvest biomechanical energy due to their light weight, low cost and high energy conversion efficiency;[31–35] and thermoelectric nanogenerators can scavenge energy from body heat.[36,37] It should be kept in mind, though, that energy harvesters often need to combine with energy storage devices to form a sustainable power system so as to provide a stable direct current (DC) power supply because some energy harvesters work intermittently (*e.g.*, solar cells) or generate electrical pulses with irregular magnitudes (*e.g.*, piezoelectric and triboelectric nanogenerators).[38–40] With wearable energy harvesters, the wearable devices can be powered by the energy harvested from the ambient environment, or even achieve a sustainable operation when the amount of energy scavenged by the energy harvesters is higher than that consumed by the electronics. Hence, developing wearable energy harvesters is also a promising approach to satisfy the demand for wearable energy sources.

In recent years, plenty of two-dimensional (2D) materials have sprung up, such as graphene and graphene oxide (GO),[41–47] graphyne,[48,49] graphdiyne,[50,51] transition metal dichalcogenides (TMDs),[52–54] transition metal oxides (TMOs),[55] transition metal carbides/carbonitrides (MXenes),[56,57] black phosphorus (BP),[58,59] *etc.* These novel 2D materials usually feature in-plane covalent bonds and inter-layer van der Waals interactions. It is believed that the atomic-scale thickness of 2D materials makes them flexible, which is a decisive strength for use in wearable energy devices, advantageously satisfying the requirements of thin thickness and good flexibility.[60] What's more, since a wealth of unusual physical phenomena occur when charge and heat transport is confined to a plane, 2D materials present certain extraordinary properties that are different from the properties of their bulky counterparts.[61] These unique properties of 2D materials and their diverse incorporations make them promising for wearable energy storage devices and energy harvesters. For example, for batteries, the 2D crystalline structure can facilitate the intercalation/deintercalation of ions, buffer the volume expansion of electrode materials and enhance the surface/interface Li storage properties; for supercapacitors, the unique structure of MXenes can enable fast electron supply, offer a redox-active layer surface and allow high proton accessibility; for solar cells, 2D TMDs have tunable band gaps and are predicted to absorb more incident sunlight than conventional Si or GaAs with the same thickness; for piezoelectric nanogenerators, some 2D TMDs such as MoS_2 show layer-dependent

Di Wei

Di Wei received his PhD from Åbo Akademi University in Finland. After a postdoctoral fellowship at Cambridge University in the UK, he became a senior research scientist at Nokia Technologies Cambridge. He was one of the initiators of the research in the field of nanocarbon and graphene technologies in Nokia. He became the executive director of Beijing Graphene Institute in 2017 and holds the fellowship at Wolfson College Cambridge University and adjunct professorship at Åbo Akademi University. His research interests cover applications of nanotechnology in sensors and energy devices.

Zhongfan Liu

Zhongfan Liu received his PhD from the University of Tokyo in 1990. After a postdoctoral fellowship at the Institute for Molecular Science, Japan, he became an associate professor (1993), full professor (1993), and Cheung Kong Chair professor (1999) of Peking University. He was elected as the member of Chinese Academy of Science (CAS) in 2011. His research interests focus on low-dimensional carbon materials and novel 2D atomic crystals, targeting nanoelectronic and energy conversion devices together with the exploration of fundamental phenomena in nanoscale systems.

higher piezoelectricity than their bulky counterparts; for triboelectric nanogenerators, reduced graphene oxide (rGO) or MoS_2 introduced into the triboelectric layer can help trap electrons and increase the triboelectric charge density; for thermoelectric nanogenerators, some 2D IV–VI metal chalcogenides such as SnS_2 have higher electrical conductivity and lower thermal conductivity than their bulky counterparts that can lead to higher thermoelectricity.

In this review, we will summarize recent advances in the field of 2D materials for wearable energy sources, with an emphasis on the crucial roles that emerging 2D materials play in various types of wearable energy sources. Firstly, an overview of wearable batteries categorized according to battery types will be given. We will present the functions 2D materials serve, outline the performance improvements 2D materials bring about, and discuss the prospects and challenges. Secondly, an overview of wearable supercapacitors will be given. We will review wearable supercapacitors based on graphene and its derivatives categorized according to supercapacitor types, and discuss how they enhance the performance and what challenges they face. Other 2D materials such as MXenes, TMDs and TMOs for supercapacitors will also be mentioned, and the reasons for the high performance brought about by their unique structures will be analyzed. Thirdly, an exhaustive overview of wearable energy harvesters based on 2D materials will be presented, and the main focus will be on how 2D materials' unique properties help to improve the electrical outputs of various energy harvesters. Finally, we will outline each category of 2D materials, and highlight the advantages, prospects, and challenges of using them for wearable energy sources.

2. Wearable batteries

Among various energy storage systems, batteries have become one of the most promising power sources to meet the ever-increasing demand for high-performance electric devices, owing to their high energy density, long operating life, and good stability.[62,63] However, they are far from enough for the more power-hungry electronic devices. New batteries need to be urgently developed to meet the performance requirements of different devices.

As mentioned earlier, the remarkable progress in wearable electronic devices entails the development of wearable batteries. However, most current batteries are rigid and heavy due to the conventional manufacture method and the use of metallic current collectors. The key challenge for wearable batteries is to design and fabricate reliable materials for electrodes with high capacity, high rate capability, cycling stability, good conductivity and robust flexibility.[64] To achieve better battery performance and satisfy the wearable requirement, various 2D materials have been applied in batteries, along with the designs of material structure and battery configuration.[65–67]

2D materials, exhibiting much more exposed surface area than bulk materials, can provide abundant ion-insertion channels and shorter paths for fast ion diffusion, making them ideal candidates for high capacity batteries. The trend that 2D materials routinely outperform their bulk counterparts in terms of capacity and cycle life has been demonstrated in many emerging electrode materials.[68] The 2D crystalline structure holds a number of advantages over bulk materials, such as facilitating the intercalation/deintercalation of ions, buffering the volume expansion of electrode materials due to the elasticity of the 2D nanosheets, and enhancing surface/interface Li storage properties.[60]

Generally speaking, in traditional batteries based on the conventional coating method and metallic current collectors, the electrode materials may detach from the current collector by repeated deformation.[63] In comparison, the atomic-scale thickness of the layers of 2D materials offers good mechanical flexibility, and the nanoarchitecture design ensures good contact with other electrode materials, making them suitable for future wearable batteries.[69] With the numerous synthetic strategies and electrode designs, batteries based on 2D materials show enhanced performance under repeated deformation.

A large number of batteries based on 2D materials that are flexible, bendable, and even foldable have been reported, mainly by exploiting the various electrode configurations or material nanostructures to achieve excellent electrochemical and mechanical performances. In this section, we will highlight the recent progress in wearable batteries including Li-, Na- and Al-ion batteries as well as other types of batteries such as lithium–sulfur (Li–S) batteries, *etc.*

2.1 Wearable Li-ion batteries based on 2D materials

LIBs are among the best candidates for flexible energy-storage systems of wearable devices, bendable displays, implanted medical devices and so on. Since their first commercialization by Sony in 1991, LIBs have attracted growing attention and have been extensively applied as the power source for portable electronic devices, electric vehicles as well as large-scale energy-storage systems, owing to their high energy density, long-term cycle life, good stability, and comparatively low cost.[62]

2D materials with an expanded interlayer distance have open structures that not only facilitate the storage and efficient transport of ions, electrons, and mass, but also provide better tolerance to the volume change of electrode materials compared with their bulk counterparts.[70] Various 2D materials have been applied in LIBs to play diverse roles, which will be discussed below.

2.1.1 Graphene. Graphene, a two-dimensional material with a honeycomb structure, has attracted tremendous research interest in recent years, owing to its high carrier mobility, large surface area, chemical stability, flexibility, and desirable mechanical properties.

Graphene shows many superior properties such as high theoretical specific surface area (*ca.* 2630 $m^2 g^{-1}$),[71] high carrier mobility at room temperature ($\sim$10 000 $cm^2 V^{-1} s^{-1}$)[46] and high Young's modulus ($\sim$1 TPa),[72] making it a multifunctional material for wearable batteries. In the reported wearable LIBs, graphene presents superior performance in different roles, which can be classified into three models (Fig. 2): as an active

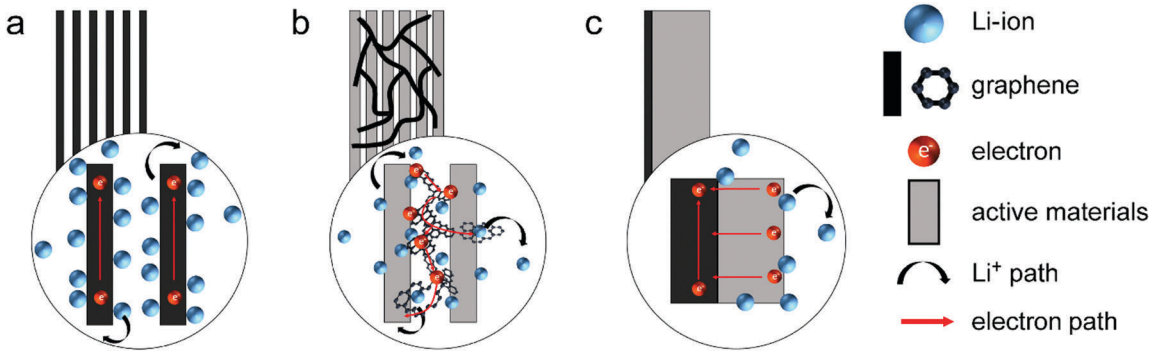

Fig. 2 Schematic illustration of the three roles of graphene in LIBs. All models have omitted other possible conducting additives and binders. (a) Graphene composites as active materials. (b) Graphene as a conducting additive. (c) Graphene as a current collector.

material to store Li ions, as a conducting additive and as a current collector. However, the easy reassembling and restacking structure results in negative effects such as poor reversibility and limited number of cycles, leading to the loss of all the predicted advantages of graphene.[17,73] Additionally, it is suggested that when the graphene sheet is mixed in a manner similar to conventional carbon additives during electrode preparation, it could negatively affect the Li^+ mobility because the perfect graphene monolayer is impermeable to all atoms under ambient conditions, thus worsening the electrochemical performance of the electrode.[74–76] Therefore, it is indispensable to have proper nanostructure design when graphene is applied in electrodes.

To further exploit these properties in various kinds of applications, versatile and reliable synthetic routes have been developed to prepare graphene and its composites, ranging from the bottom-up epitaxial growth to the top-down exfoliation of graphite by means of oxidation, intercalation, and/or sonication.[77] Different preparation methods lead to different structures and distinguished properties. Graphene prepared by chemical vapor deposition (CVD) methods possesses high carrier mobility which could promote the conductivity of the electrode but the yield is limited, while the low cost rGO with functional groups could achieve better binding with active materials but could result in reduced electron conductivity and the defects in rGO would cause irreversible capacity loss during cycling.

Graphene/graphene composites as active materials. Graphene has a relatively low potential of charge and discharge, and thus it usually acts as an anode in LIBs. Generally, the ideal active material for LIB anodes should have high reversible capacity, low insertion/deinsertion potentials, chemical stability during cycling, and high electrical and ionic conductivity for good rate performance.[78] Graphite is the most commonly used material in commercially available rechargeable LIBs as it meets most of these requirements; however, it presents some relevant limitations. Graphite has a limited theoretical capacity of 372 mA h g^{-1}, and its specific capacity also rapidly decays when high current loads are applied.

Different from graphite, in which Li-ions are intercalated between the stacked layers, monolayer graphene can theoretically store Li ions through an adsorption mechanism, both on its internal surfaces and in the empty nanopores that exist between the randomly arranged layers. This working mechanism results in a theoretical specific capacity of 744 mA h g^{-1} which is twice that of graphite,[79,80] and this may be even higher when defects and additional groups exist. Nevertheless, it is verified that the theoretical specific capacity of 744 mA h g^{-1} could not be fulfilled since the strong Coulombic repulsion of Li atoms facing opposite sides of the same graphene sheet results in lower binding energies[17,81,82] and there is a huge irreversible capacity loss after the first cycle. Therefore, although graphene can be used both as the anode for storing Li^+ and as a supporting skeleton in combination with other Li storage materials, we should have a critical insight into the graphene anodes.

Here, we review three representative structures: graphene paper, graphene aerogel and graphene ink.

Graphene paper. Graphene paper is one of the most reported materials for wearable batteries. Clearly, the graphene paper derives some unique properties from the nature of graphene and can serve as the functional anode of flexible LIBs. The fabrication of graphene papers has been reported previously.[83–86] It is well known that GO can be synthesized from commercially available, inexpensive graphite powder by oxidation using a typical Hummers method.[86] Then, graphene paper, or rGO paper, is usually fabricated by filtration of dispersions of the rGO solution.

Based on the general synthetic method, Wallace and coworkers demonstrated the flexible and robust graphene papers.[83] The process of vacuum filtration of the as-prepared dispersion results in the formation of ultrastrong paper-like materials exhibiting a relatively smooth surface with a shiny metallic luster on both sides. These graphene papers are mechanically strong and electrically conductive. Koratkar *et al.* introduced the photoflash and laser-reduction of GO to obtain similar freestanding graphene paper anodes.[87] Photothermal reduction of GO yields an expanded structure with micrometer-scale pores, cracks, and intersheet voids, enabling accessibility of Li ions to the underlying sheets of graphene and facilitating efficient intercalation kinetics at ultrafast charge/discharge rates of >100 °C. At charge/discharge rates of ~ 40 °C, the anodes delivered a steady capacity of ~ 156 mA h g_{anode}^{-1}

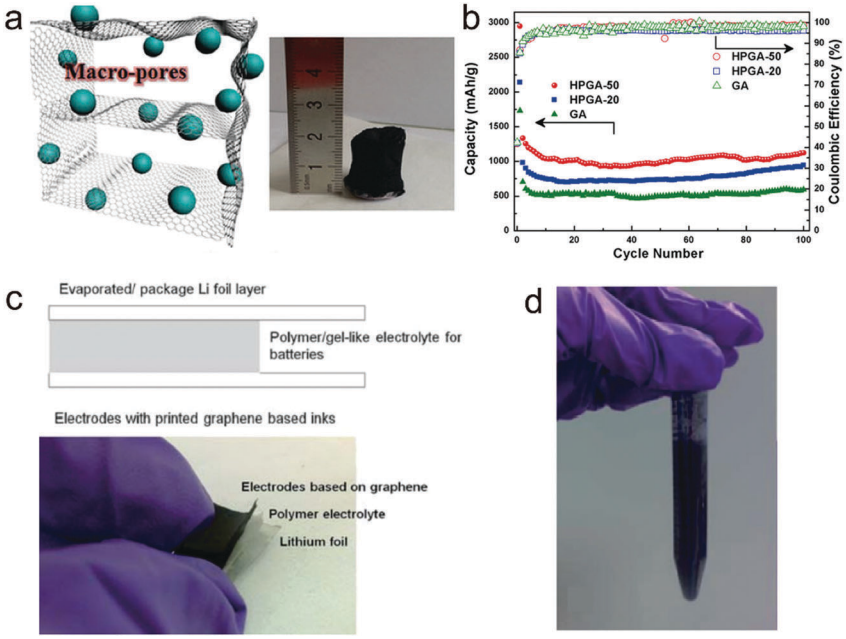

Fig. 3 Graphene based wearable LIBs, as active materials. (a) Schematic illustration of the morphological formation of the hierarchical porous graphene aerogel (HPGA). (b) Cycling performance and Coulombic efficiencies of HPGA-50 and HPGA-20 anodes compared with GA at 0.1 A g^{-1} with a voltage window of 0.1–3.0 V. Reproduced with permission from ref. 88. Copyright 2015, Nature Publishing Group. (c) Structure and image of the rechargeable lithium battery based on the graphene-ink cathode and polymer electrolyte. (d) Poly(sodium 4-styrenesulfonate)-modified graphene ink containing 0.2 M TiO_2 nanoparticles and 1 M $LiClO_4$. Reproduced with permission from ref. 18. Copyright 2011, the Royal Society of Chemistry.

continuously over 1000 charge/discharge cycles, providing a stable power density of $\sim$10 kW kg_{anode}^{-1}. The batteries also displayed outstanding stability and cycling ability.

Since the freestanding graphene paper is highly bendable, it is clearly a good candidate for flexible batteries. Indeed, these flexible graphene paper electrodes showed excellent cycling stability and high rate capability.[87] However, due to the fact that the layered structure of graphene tends to reassemble and restack, there will be unfavorable capacity decay during cycling. Hence, hierarchical structures of graphene have been proposed to prevent the restacking.

Graphene aerogel. The issue of reassembling and restacking of layered graphene could be addressed by the recently developed 3D graphene aerogels (GAs), which are assembled by cross-linking individual graphene sheets into a continuously interconnected macroporous network with large surface area, low mass density, and high electrical conductivity.[69] Compared with graphene sheets, the graphene aerogel demonstrated superior electrochemical and mechanical properties due to the cross-linked skeleton.

Ren *et al.* reported a novel 3D hierarchical porous graphene aerogel (HPGA) with uniform and tunable mesopores (*e.g.*, 21 and 53 nm) on graphene nanosheets.[88] The HPGA was prepared by a hydrothermal self-assembly process and an *in situ* carbothermal reaction. The size and distribution of the mesopores on the individual graphene nanosheet were uniform and could be tuned by controlling the sizes of the Co_3O_4 nanoparticles used in the hydrothermal reaction. This unique architecture of HPGA prevents the stacking of the graphene nanosheets and provides more electrochemically active sites that enhance the overall electrochemical storage significantly. As a battery anode in LIBs, HPGA exhibited superior electrochemical performance, including a high reversible specific capacity of 1100 mA h g^{-1} at a current density of 0.1 A g^{-1}, outstanding cycling stability and excellent rate performance (Fig. 3b). Even at a large current density of 20 A g^{-1}, the reversible capacity remained at 300 mA h g^{-1}, which is larger than those of the most reported porous carbon based anodes, suggesting that it is a promising candidate for LIBs. Unlike the graphene sheet, the cross-linked structure in the HPGA is not such fragile, but has superior mechanical properties.

Graphene ink. An important trend in wearable electronics is to deposit conductive ink on a flexible substrate such as polymer films, paper sheets or rubber slabs to form a flexible conductive electrode. A key issue in this approach is developing conductive ink with good dispersion. The dispersion of high concentrations of graphene in solution is still a great technical challenge due to the strong π–π stacking interactions between the planar graphene sheets.[89]

Graphene ink, prepared in the form of a colloidal suspension, containing polymeric binders and surfactant additives, has already been used as an electrode material for batteries and supercapacitors.[18] Wei and coworkers demonstrated an electrode fabricated from graphene ink, obtained from the chemical reduction of GO, deposited onto carbon fibers (Al foil as the current collector) and then constructed a full battery with a solid polymer electrolyte sandwiched between a Li foil anode and the cathode (Fig. 3c).[18] Unlike all other reported methods

that used conventional ways to fabricate electrodes by mixing the hybrid materials with poly(vinylidenefluoride) (PVDF) binders, in this case, the flexible and potentially printable electrodes are prepared by depositing suspensions of graphene nanoplatelets modified with large counter anions with TiO_2 nanoparticles and $LiClO_4$ (Fig. 3d). This battery delivered a specific capacity of 582 mA h g^{-1} in the initial discharging, which is approximately 78% of the theoretical capacity (744 mA h g^{-1}) of graphene sheets through the formation of Li_2C_6. This approach, being both versatile and scalable, can be adapted to a wide variety of applications. Despite the limited electrochemical performance of this work, it suggests a feasible route towards fully printable rechargeable Li batteries based on graphene inks and/or other 2D materials in solutions. Regarding the strong stacking interactions between layers of the 2D materials, it is important to obtain excellent dispersion to effectively overcome the interlayer stacking. Liu and coworkers developed a scalable and surface-oxygen assisted CVD route to produce a type of 3D biomorphic graphene powder materials, which preserves the 3D hierarchical structures of the original diatom frustules to effectively overcome the interlayer stacking and hence gives a high solution dispersion performance.[89] This suggests the potential of solution-processible electrodes for high electrochemical performance and good mechanical properties.

Graphene as a conducting additive. Due to their large surface area, good mechanical strength, and high mobility, graphene sheets can serve as a support in various flexible functional electrodes, endowing the electrodes with features of good flexibility, strong mechanical strength and efficient electrical conduction.[90]

During the composite preparation, graphene can act as a support for the growth of electroactive nanostructures that, in turn, hinder the restacking by lowering the van der Waals forces among the layers. As a result, graphene-based composites are less affected by agglomeration during electrode preparation, or by capacity fading during cycling.

Zhi and coworkers developed a kind of novel self-supporting binder-free silicon-based anodes *via* the encapsulation of silicon nanowires with dual adaptable apparels (overlapped graphene (G) sheaths and rGO overcoats), abbreviated as SiNW@G@rGO, as shown in Fig. 4.[91] The overlapped graphene sheets that were processed by a CVD method acted as adaptable but sealed sheaths, which encapsulated the silicon and prevented its direct exposure to the electrolyte. As a result, the structural and interfacial stabilization of silicon nanowires was achieved. Meanwhile, the flexible and conductive rGO overcoats accommodated the volume change of embedded SiNW@G nanocables and thus maintained the structural and electrical integrity of the architecture. As a result, the SiNW@G@rGO electrodes exhibited a high reversible specific capacity of 1600 mA h g^{-1} at 2.1 A g^{-1}, 80% capacity retention after 100 cycles, and superior rate capability (500 mA h g^{-1} at 8.4 A g^{-1}) on the basis of the total electrode weight.

Graphene layers provide a conducting matrix, as well as an elastic protective layer to buffer the volume change of silicon-based materials, thus realizing a stable silicon-based anode. However, when mixed improperly or in excessive amounts, the excellent impermeability of the 2D planar structure can impede the Li ion penetration. Hence, a rational design that allows graphene to serve as a conducting additive and also provides ample transport channels of Li ions is indispensable for new electrode structures.[92]

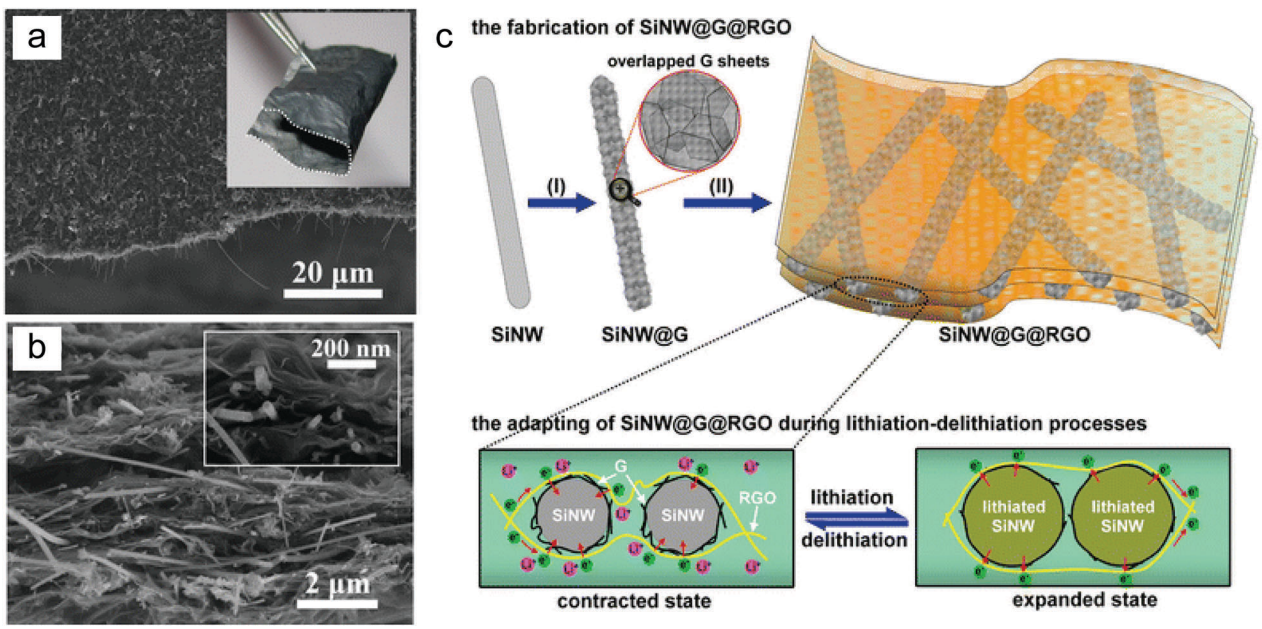

Fig. 4 Graphene based wearable LIBs, as conducting additives. (a and b) Characterization of the rGO-sandwiched SiNW@G nanocables (SiNW@G@RGO): (a) low magnification SEM image. The inset shows the optical image of a bent SiNW@G@rGO film with the dashed line highlighting its edges. (b) Cross-sectional SEM image. The inset shows an enlarged cross-sectional view. (c) Schematic illustration of the fabrication (upper panel) and adapting (lower panel) of SiNW@G@rGO. Reproduced with permission from ref. 91. Copyright 2013, American Chemical Society.

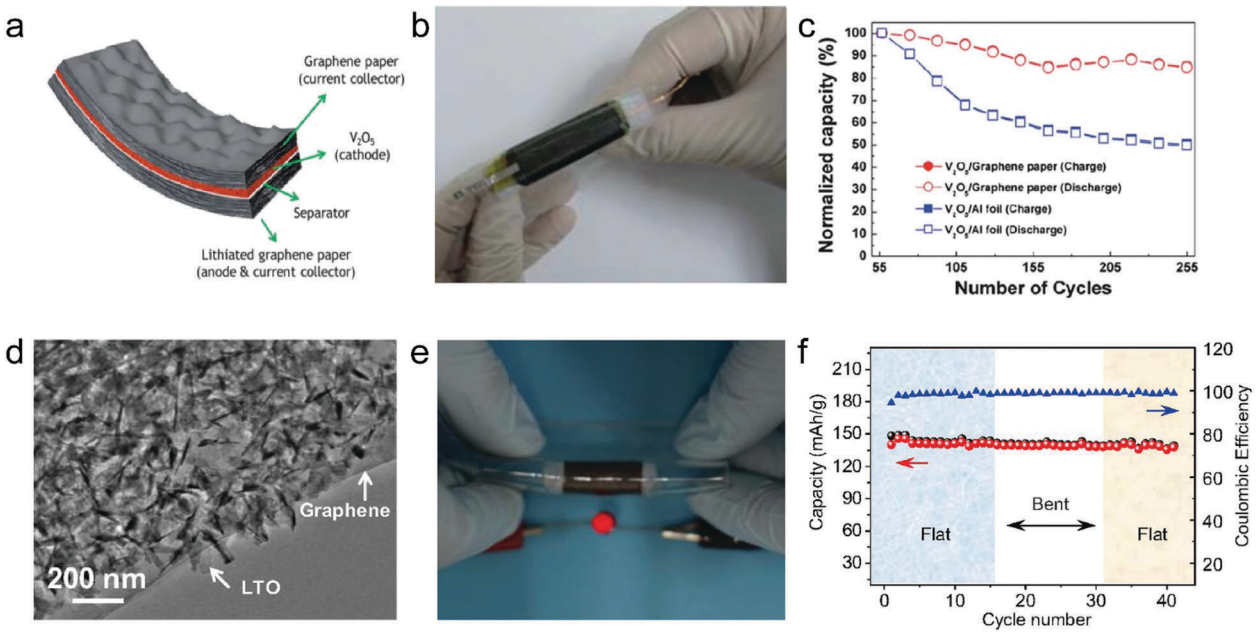

Fig. 5 Graphene based wearable LIBs, as current collectors. (a) Schematic drawing of the flexible LIB based on graphene paper. (b) The battery is thin, lightweight, and flexible enough to be rolled up or twisted. (c) Cycling performance of V_2O_5/graphene paper and V_2O_5/Al foil up to 200 cycles at a current density of 20 mA cm^{-2}. Reproduced with permission from ref. 93. Copyright 2011, the Royal Society of Chemistry. (d) TEM image of the LTO/GF. (e) Lighting a red LED device under bending. (f) Cyclic performance of the battery in the flat and bent states. Reproduced with permission from ref. 94. Copyright 2012, National Academy of Science.

Graphene as a current collector. As a multifunctional material, graphene can not only act as a conducting additive but could also be constructed as a current collector. The unique combination of graphene's outstanding properties such as high mechanical strength, large surface area, and superior electrical conductivity makes it a promising current collector material for wearable batteries.

Kang and coworkers demonstrated the freestanding graphene paper that can be used as a versatile multifunctional matrix for both cathode and anode in flexible LIBs (Fig. 5a–c).[93] Using flexible graphene paper and V_2O_5/graphene paper as anode and cathode materials, respectively, they fabricated a graphene-based flexible LIB. The graphene paper was made by a similar method as mentioned before, and the V_2O_5/graphene paper was fabricated by using a pulsed laser deposition technique. The graphene paper, with its good mechanical strength, large surface area and superior electrical conductivity, acts as both active material and current collector. The intrinsic wrinkles and ripples on the graphene surface ensure an intact contact with active materials. Thus, the V_2O_5/graphene paper exhibited a higher capacity and rate capability plus a better cycling life compared with a non-flexible conventional V_2O_5/Al foil electrode. The robust integration of graphene into the electrode ensures not only superior electrochemical performance over conventional electrode architecture, but also the capability of operation with full mechanical flexibility.

Recently, a highly conductive 3D graphene macrostructure, called the graphene foam (GF), was synthesized using a Ni foam template-directed CVD method. It consists of an interconnected graphene network to achieve high electrical conductivity and good mechanical strength. Based on this technique, Cheng and coworkers developed a flexible GF for LIBs for use as anode and cathode after loading the GF current collectors with $Li_4Ti_5O_{12}$ and $LiFePO_4$, respectively (Fig. 5d and e).[94] In this case, no metal current collectors, conducting additives, or binders were used. It is generally believed that the charge/discharge rate of a LIB depends critically on the migration rate of Li ions and electrons through the electrolyte and bulk electrodes into the active electrode materials. Obviously, the excellent electrical conductivity and pore structure of the hybrid electrodes enabled rapid electron and ion transport in this battery, leading to good high-rate performance and energy density, in addition to the capacity of being repeatedly bent to a radius of 5 mm without structural failure and performance loss. Combining the mechanical flexibility and high rate performance of these electrodes, a thin, lightweight and flexible LIB was demonstrated with an initial discharge capacity of 143 mA h g^{-1}, a Coulombic efficiency of 98% at 0.2 °C and an energy density of 110 W h kg^{-1} based on the total mass of the $Li_4Ti_5O_{12}$/GF anode and $LiFePO_4$/GF cathode. Furthermore, both the GF fabrication and the subsequent filling and loading of active materials can be easily scaled up, which opens up the possibility for large-scale fabrication of flexible batteries with high capacity to power flexible electronic devices that can be operated at a high power rate with short charging time.

2.1.2 Hydrogen substituted graphdiyne. Graphyne and graphdiyne, new molecular allotropes of carbon, are novel 2D carbon allotropes that feature assembled layers of sp and sp^2 hybridized carbon atoms and display chemical stability and good electrical conductivity.[95] With high charge mobility and

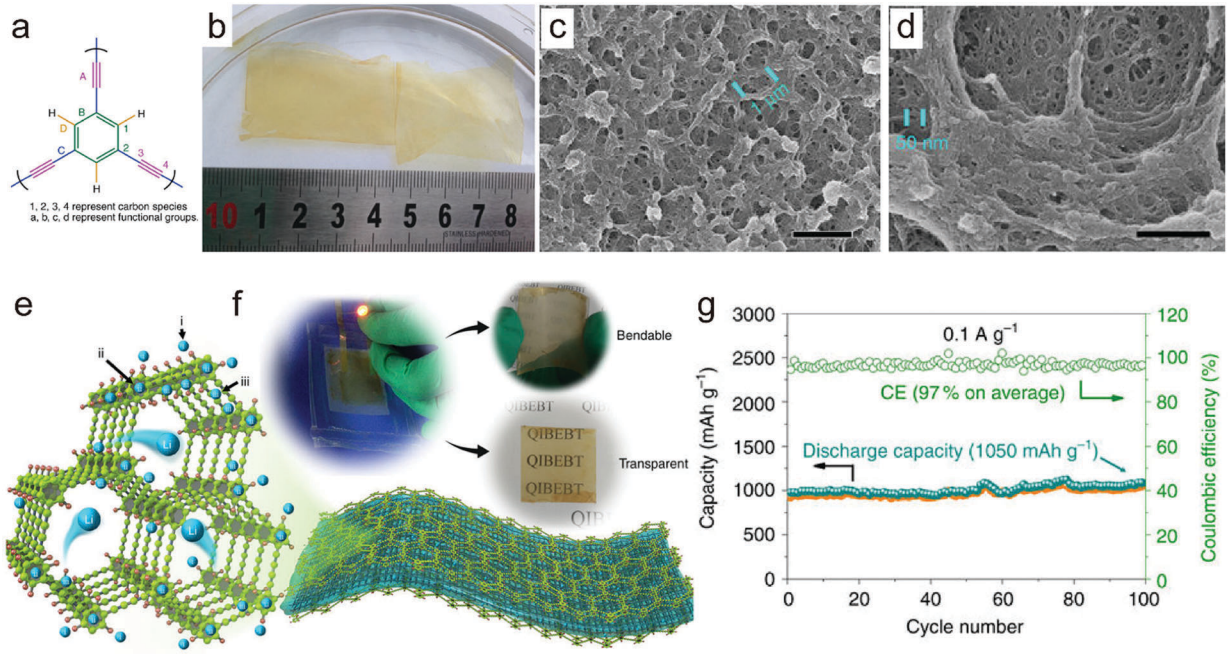

Fig. 6 Wearable LIBs based on hydrogen substituted graphdiyne (HsGDY). (a) Carbon species and functional groups in HsGDY. (b) The photograph of freestanding HsGDY films. (c and d) The SEM images of HsGDY. Scale bar: 2 μm (c); 500 nm (d). (e) The mechanism of Li storage. (f) A bendable transparent LIB made up of HsGDY. (g) The cycle performance of a flexible electrode at a current density of 0.1 A g^{-1}. Reproduced with permission from ref. 98. Copyright 2017, Nature Publishing Group.

high capacity for Li, graphyne and graphdiyne suggest potential applications in LIBs. In graphite, Li ion diffusion parallel to the plane of graphite (in-plane) is impeded by steric hindrance, while that perpendicular to the basal plane (out-of-plane) is hindered by the aromatic carbon rings. The unique atomic arrangement and electronic structures of graphyne and graphdiyne enable both in-plane and out-of-plane diffusion of Li ions with only moderate barriers of 0.52–0.57 eV.[96] The large number of triangular pores in the structure of graphdiyne endows it with more Li storage sites and facilitates Li ion adsorption, desorption and diffusion both in-plane and out-of-plane.[97]

Various studies have applied graphdiyne as the electrode for LIBs, in order to improve the capacity for Li storage. Some general conclusions can be drawn. For one thing, a larger pore size in the molecular structure favours ion diffusion. For another, the small ratio of H atoms increases the capacity, as it is reported that Li atoms can bind in the vicinity of H atoms in these hydrogen-containing carbons.[79] Li and coworkers fabricated a carbon-rich hydrogen-substituted graphdiyne (HsGDY) film through an *in situ* cross-coupling reaction of triethynylbenzene on copper foil, as shown in Fig. 6.[98] This novel material has the merits of good electronic conductivity like graphite with the pore structure (Fig. 6c and d) and convenient synthesis process of polymers. Furthermore, the hierarchical, porous 3D conductive structure provides a matrix for the hopping and transport of electrons to ensure high efficient charge collection and diffusion. As a result, this freestanding flexible electrode can achieve a highly improved reversible and stable capacity of 1050 mA h g^{-1} for LIBs, which is higher than those of intrinsic carbon allotropes and organic molecules. Moreover, the carbon-rich framework endows HsGDY with excellent mechanical properties, which can act as a bendable transparent electrode in LIBs (Fig. 6f). The organic film can act as a freestanding flexible electrode for not only LIBs but also sodium ion batteries (SIBs) with a reversible capability of 650 mA h g^{-1}.

Compared with other 2D materials such as graphene, the unique structure of graphdiyne, with its numerous large triangular pores, endows it with many Li ion storage sites and facilitates the rapid transport of electrons and ions. This new anode material provides a new concept for the design of high-performance flexible electrodes with high capacity and excellent cycling stability, thereby satisfying the requirements of next-generation wearable LIBs.[98]

2.1.3 Transition metal dichalcogenides (TMDs). As a typical TMD, MoS_2 has a layered structure with a high theoretical capacity (670 mA h g^{-1}), and therefore it has been intensively studied as the anode material for LIBs.[68] However, despite its high initial capacity, bulk MoS_2 normally shows quick capacity decay in the subsequent charge/discharge cycles or at increased charge/discharge rates. Besides, bulk MoS_2 in electrodes suffers from pulverization caused by the large volume expansion as well as the high energy barriers for intercalation of Li^+ ions into the interlayer space. In contrast, 2D MoS_2 nanosheets showed enhanced performance in LIBs, due to the shorter diffusion path length for Li^+ ions and enlarged surface active sites. The unique properties of TMDs engender their versatile uses in LIBs. In a recent report, 2D MoS_2 nanosheets prepared by exfoliation of bulk MoS_2 exhibited a reversible capacity of ~750 mA h g^{-1} after 50 charge/discharge cycles at a current density of 50 mA g^{-1},[99]

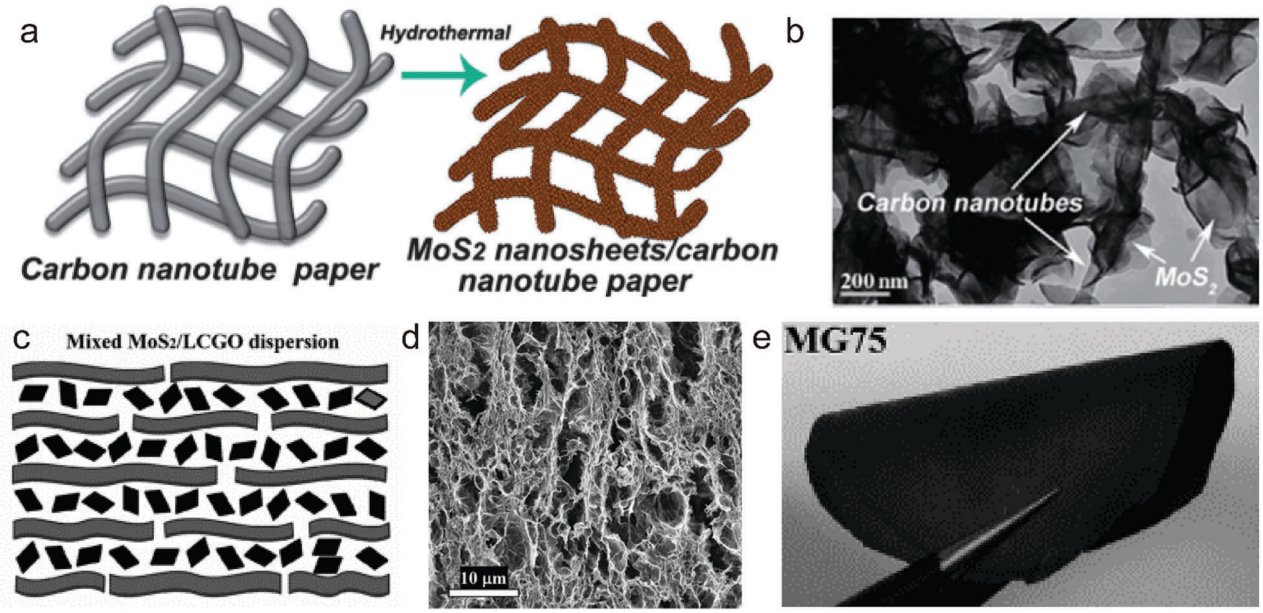

Fig. 7 Schematic illustration and the structure of the flexible electrode based on TMDs. (a) Schematic illustration of the synthesis of flexible 3D MoS_2 nanosheets/carbon nanotube paper. (b) TEM image of MoS_2 nanosheets/carbon nanotube paper. Reproduced with permission from ref. 101. Copyright 2011, John Wiley & Sons, Inc. (c) Schematic structure of MoS_2/liquid crystalline graphene oxide (LCGO) dispersions. (d) Cross-sectional SEM image of the MG film. (e) Flexibility demonstration of the MG film. Reproduced with permission from ref. 102. Copyright 2017, John Wiley & Sons, Inc.

and values of as high as 1290 mA h g^{-1} have been reported for nanostructured MoS_2/graphene composite electrodes. Similar results have also been found in other 2D nanomaterials, such as WS_2 and VS_2, clearly indicating the advantages and promising future of using 2D nanomaterials in batteries.

The large surface area and interlayer spaces of TMDs provide a convenient environment to accommodate Li^+ ions. Also, their relatively low operation voltage and high energy density render them potential candidates as anode materials in LIBs. Due to the relatively low conductivity and easy restacking character of the TMD sheets, hybridizing them with other materials (such as graphene, 3D graphene networks, carbon nanotubes, Fe_3O_4 nanoparticles, TiO_2 nanotubes, and carbon fibers) is one of the most attractive strategies to overcome the weakness of TMDs and further optimize their performance in LIBs.[100]

Zhang and coworkers reported a facile and scalable process to fabricate a flexible, 3D, and binder-free electrode architecture consisting of a highly conductive carbon nanotube paper (CNP) uniformly covered by MoS_2 nanosheets (Fig. 7a and b).[101] Its distinct advantages include a highly porous structure, a highly conductive pathway for electrons, fast transport channels for Li^+ ions and excellent mechanical strength. After 100 cycles, the MoS_2 nanosheets/CNP electrode maintained a discharge capacity of 1091 mA h g^{-1} with capacity retention of 90% for the initial discharge capacity of 1204 mA h g^{-1}, demonstrating its superior cycling stability. In comparison, although the discharge capacity of bulk MoS_2 in the first cycle was high (1209 mA h g^{-1}), its capacity retention was poor: the discharge capacity decreased to 264 mA h g^{-1} after 100 cycles, which was only approximately 22% of the initial value. By using the flexible MoS_2 nanosheets/CNP composite as a combined binder-free anode and a current collector, rechargeable batteries with excellent mechanical strength, high electrical conductivity, and superior electrochemical performance were obtained.

Wallace and coworkers combined the excellent electrochemical performance and inherent flexibility of atomically thin 2D MoS_2 along with the self-assembly properties of liquid crystalline graphene oxide (LCGO) dispersion to fabricate a porous anode for high-performance LIBs (Fig. 7c–e).[102] Flexible, freestanding MoS_2–rGO film with a 3D porous structure was fabricated *via* a facile spontaneous self-assembly process and subsequent freeze-drying. This is the first report of the one-pot self-assembly, gelation, and subsequent reduction of the MoS_2/LCGO composite to form a flexible, high-performance electrode for charge storage. The gelation process occurs directly in the mixed dispersion of MoS_2 and LCGO nanosheets at a low temperature (70 °C) and normal atmosphere (1 atm). The MG film with 75 wt% of MoS_2 exhibited a high reversible capacity of 800 mA h g^{-1} at a current density of 100 mA g^{-1}. It also demonstrated excellent rate capability and cycling stability, with no capacity drop over 500 charge/discharge cycles at a current density of 400 mA g^{-1}.

TMDs have a layered structure with higher theoretical capacity than graphite, making them more promising materials for LIBs. However, their low conductivity and easy restacking character require new structural design or hybridization with other materials. In addition, constructing porous 2D TMD nanosheets and mono- or few-layer TMDs and then assembling them into 3D macroscopic structures could increase the specific surface area and provide more ion channels compared with disordered TMD layers alone. Thus, higher capacitance and rate performance could be achieved for energy storage.[103]

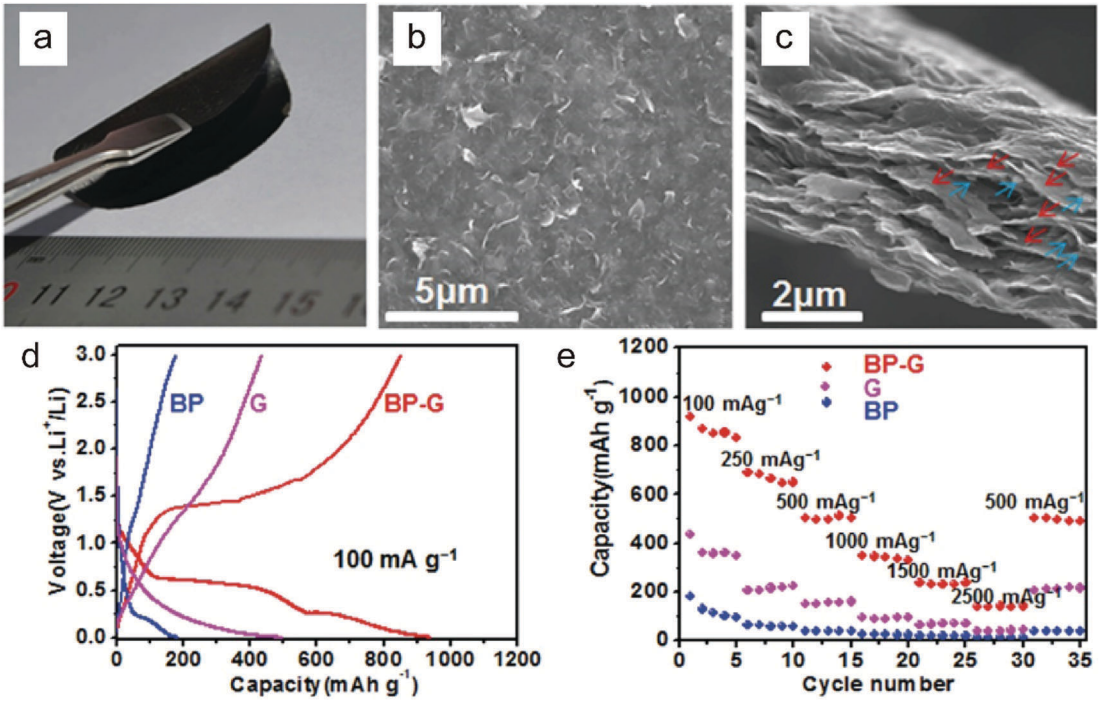

Fig. 8 Structure and electrochemical behaviors of the flexible BP–graphene (BP–G) hybrid paper. (a) Photograph of a BP–G hybrid paper, showing its good flexibility. (b) Top-view SEM and (c) cross-sectional SEM images of the BP–G hybrid paper, showing that the small BP nanosheets (indicated by blue arrows) are in close contact with the large graphene sheets (indicated by red arrows). (d) The second galvanostatic charge/discharge profiles of the BP nanosheet, graphene paper, and BP–G hybrid paper electrodes at a current density of 100 mA g^{-1}. (e) Rate performance of the BP nanosheet, graphene paper, and BP–G hybrid paper electrodes at different current densities. Reproduced with permission from ref. 105. Copyright 2016, John Wiley & Sons, Inc.

2.1.4 Black phosphorus (BP). In addition to the aforementioned 2D materials for flexible LIBs, atomically thin BP has also been considered recently as a reliable anode material in LIBs. BP, a rare allotrope of phosphorus, possesses a high theoretical specific capacity of 2596 mA h g^{-1}, which is approximately 7 times that of the widely used graphite (372 mA h g^{-1}), with a reasonable anode potential of discharge and charge, 0.9 and 0.45 V *versus* Li metal, respectively.[104]

Recently, Ren and coworkers reported a scalable and clean method to produce BP (Fig. 8).[105] Few-layer BP nanosheets were exfoliated in water by fully utilizing the hydrophilic nature of BP crystals. Then the obtained materials were combined with highly conductive graphene sheets *via* vacuum filtration. Owing to its great mechanical robustness, the BP/graphene hybrid paper exhibited superior flexibility as it can be bent to nearly 180° without breaking, which demonstrates its great potential for future flexible energy storage devices/systems. When the BP/graphene hybrid paper was employed as the anode in LIBs, it exhibited a high electrochemical Li storage capacity of 920 mA h g^{-1} at 100 mA g^{-1}, while the respective capacities for BP nanosheets and graphene paper electrodes were 180 mA h g^{-1} and 435 mA h g^{-1}, respectively (Fig. 8d). In addition, the hybrid paper also demonstrated a perfect synergistic effect and great improvement in rate capability and cycling performance. These results demonstrate the advantages of BP based 2D materials for flexible electrochemical energy storage applications.

Despite its high theoretical specific capacity of 2596 mA h g^{-1}, which surpasses those of most 2D materials, the synthesis of BP remains difficult. Currently, the mechanical exfoliation of bulk BP is still the main method of preparing atomically thin BP sheets, which obviously has a low yield and limits BP's utilization in energy storage applications.[105] In addition, the poor chemical stability of BP is still a serious impediment for further application.

2.1.5 Transition metal oxides (TMOs). Compared with 3D bulk crystals, ultrathin 2D TMOs normally show improved specific capacity and rate capacity, because their large surface area provides abundant active sites for Li ion storage and their shortened ion diffusion distance leads to fast ion transport. However, one of the disadvantages of ultrathin 2D nanomaterials is their tendency for aggregation during the electrode fabrication process, which significantly decreases their cycling stability. There are mainly two solutions to tackle this problem.

One effective way to solve this issue is to hybridize the ultrathin 2D nanomaterial with another type of nanomaterial to form hierarchical hybrid nanostructures. By doing so, the structural collapse and the aggregation of ultrathin 2D nanomaterials can be minimized and better cycling performance can be achieved for the electrode material.[60] Cheng and coworkers designed an anisotropic TiO_2/graphene sandwich paper (A-TO/GSP) electrode, in which Li^+ ion insertion and diffusion are anisotropic, by the controlled growth of TiO_2 nanosheets parallel to the surface of graphene paper (Fig. 9a–c).[106]

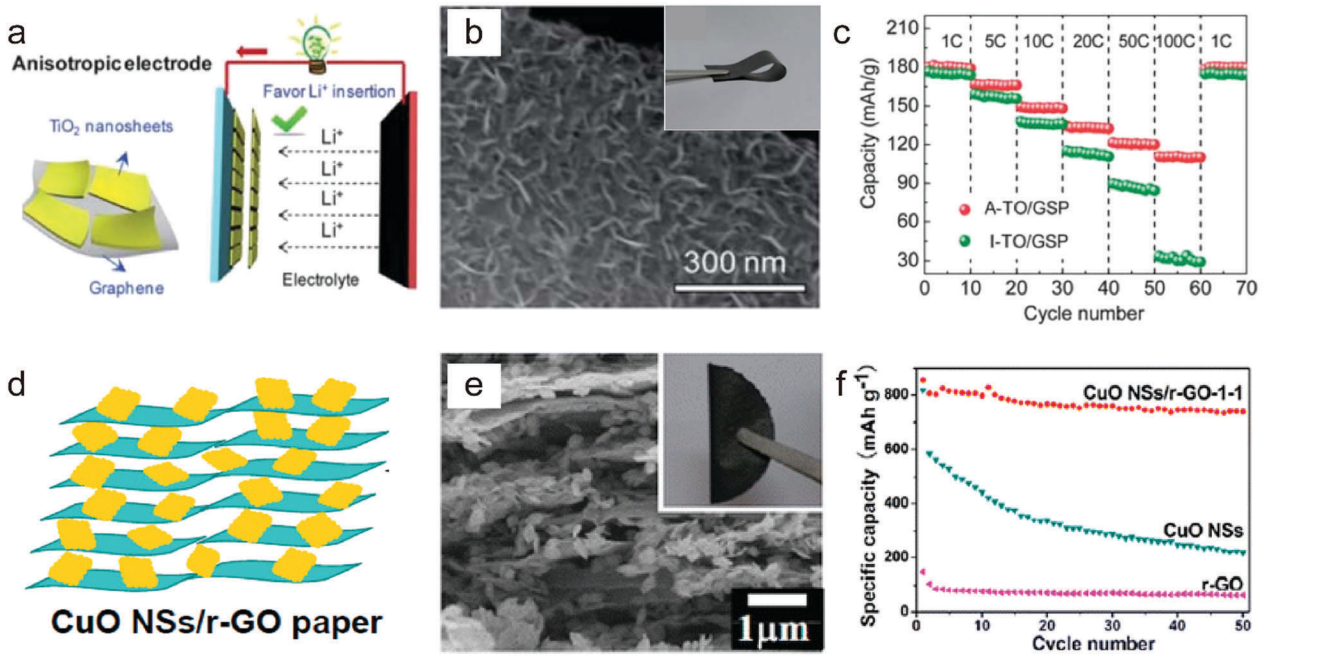

Fig. 9 Schematic illustration, structure and electrochemical behaviors of the flexible electrode based on TMOs. (a) Illustrations of A-TO/GSP for Li ion transport. (b) High magnification SEM image of LTO nanosheets in the anisotropic TiO_2/graphene sandwich paper (A-TO/GSP). The inset image shows a bent flexible A-TO/GSP. (c) Comparison of the specific capacity at different rates between the A-TO/GSP and I-TO/GSP electrodes. Reproduced with permission from ref. 106. Copyright 2013, the Royal Society of Chemistry. (d) Schematic representation of the synthesis procedure of CuO nanosheets/rGO paper. (e) Cross-sectional SEM image of the CuO nanosheets/rGO paper, which shows good flexibility (inset). (f) Cycling performance of rGO, CuO nanosheets, and CuO nanosheets/rGO-1-1, at a constant current density of 67 mA g^{-1}. Reproduced with permission from ref. 107. Copyright 2013, American Chemical Society.

The anisotropic electrode gives a gravimetric capacity of 112 mA h g^{-1} at an ultrahigh rate of 100 °C (corresponding to 36 s of charge/discharge), 3 times higher than that of a referenced isotropic electrode. The results indicate that such an anisotropic electrode can be useful in the search for high-power LIBs. This electrode is also flexible and can be bent into arbitrary shapes. Peng and coworkers reported a flexible freestanding CuO nanosheets/rGO hybrid lamellar paper (Fig. 9d–f).[107] It was fabricated through vacuum filtration and hydrothermal reduction processes. A unique 3D nanoporous network was achieved with the CuO nanosheets homogeneously embedded within the rGO layers. As a binder-free anode for LIBs, this hybrid lamellar composite paper demonstrated excellent cyclic retention with a specific capacity of 736.8 mA h g^{-1} after 50 cycles. This is much higher than those of the pristine CuO nanosheets and rGO film (219.1 mA h g^{-1} and 60.2 mA h g^{-1}, respectively) at the same current density of 67 mA g^{-1}. The high capacitance and excellent cycling performance were generated from the integrated nanoporous structure composed of CuO nanosheets spaced rGO layers. This structure offered electrically conducting channels with high efficiency, favoured electrolyte penetration, and buffered the volume variations during the lithiation and delithiation process. These outstanding electrochemical capabilities of CuO nanosheets/rGO paper hold great promise for flexible binder-free anodes for LIBs.

Besides hybridization with other nanomaterials, intrinsically engineering TMOs into porous or nanofluidic-type structures is also an effective way to tackle the aggregation problem.[108–111] For example, Yu and coworkers reported a two-step strategy for controlled synthesis of holey 2D TMO nanosheets with tunable pore sizes using GO as a sacrificial template.[108] The 2D holey $ZnMn_2O_4$ nanosheets inherit strong mechanical properties, maintaining the holey morphology and displaying minimal structural changes during the lithiation/delithiation processes. As a result, the 2D holey TMO nanosheets exhibit improved cycling stability. The nanofluidic structure by combining controlled interlayer spacing and surface functionalization can offer excellent electrochemical performance in LIBs.[111] In principle, a surface charged nanofluidic channel narrower than the Debye length of the electrolyte enables exclusive transport of oppositely charged ions, and ionic conductivity can be greatly enhanced in such unipolar ionic transport. Therefore, properly constructed 2D nanofluidic structures could achieve fast Li-ion transport. Moreover, the nanofluidic channels provide natural void space that can buffer volume changes during charge/discharge processes.

Wearable LIBs based on 2D materials show excellent specific capacity, rate capacity and electrochemical stability because of the large active surface area, shortened ion diffusion distance and superior structural stability of 2D materials. The performance of wearable LIBs with various 2D materials as electrode materials is summarized in Table 1.

2.2 Wearable non-Li-ion batteries based on 2D materials

2.2.1 Na-Ion batteries and Al-ion batteries. Currently, practical LIBs with very high energy density and long cycle life have

Table 1 Summary of performance of LIBs based on 2D materials[a]

2D material	Electrodes	Roles of 2D materials	Potential range applied (*vs.* Li^+/Li) (V)	Cycle number	Current density	Specific capacity	Wearablility	Ref.
Graphene	Photothermally reduced graphene	active materials	0.03–3	1000	40 °C	156 mA h g^{-1}	Flexible	87
Graphene	HPGA	Active materials	0.1–3.0	100	100 mA g^{-1}	1100 mA h g^{-1}	Flexible	88
Graphene	SiNW@G@rGO	Conducting additives	2–0.002	100	2100 mA g^{-1}	1600 mA h g^{-1}	Flexible	91
Graphene	V_2O_5/graphene paper	Current collector	3.8–1.7	200	20 μA cm^{-2}	19 μA h cm^{-2}	Flexible	93
Graphene	LTO/graphene foam	Current collector	0.8–2.5	130	200 °C	135 mA h g^{-1}	Flexible	94
HsGDY	HsGDY	Active materials	0.005–3	100	100 mA g^{-1}	1050 mA h g^{-1}	Flexible	98
Graphdiyne	Bulk graphdiyne powder	Active materials	0.005–4	200	50 mA g^{-1}	552 mA h g^{-1}	—	97
TMD	Li_2S@TiS_2	Active materials	1.8–2.6	400	0.2 °C (255 mA g^{-1})	1156 mA h g^{-1}	—	263
TMD	MG film	Active materials	0.01–3	500	100 mA g^{-1}	800 mA h g^{-1}	Flexible	102
TMD	MoS_2 NSs/CNP	Active materials	0.01–3.0	100	100 mA g^{-1}	1091 mA h g^{-1}	Flexible	101
BP	BP–G hybrid paper	Active materials	0.001–3	500	100 mA g^{-1}	920 mA h g^{-1}	Flexible	105
BP	BP–G	Active materials	0.01–2.0	100	0.2 °C	2786 mA h g^{-1}	—	104
MXene	Nb_2CT/CNT	Active materials	1.0–3.0	300	2.5 °C	430 mA h g^{-1}	Flexible	264
TMO	CuO NSs/r-GO	Active materials	0.01–3.0	50	0.1 °C (67 mA g^{-1})	736.8 mA h g^{-1}	Flexible	107
TMO	A-TO/GSP	Active materials	1.0–3.0	100	10 °C (1680 mA g^{-1})	147 mA h g^{-1}	Flexible	106

[a] Notes: SiNW@G@rGO: silicon nanowires (SiNWs) with dual adaptable apparels (overlapped graphene (G) sheaths and rGO overcoats); HPGA: hierarchical porous graphene aerogel; HsGDY: hydrogen substituted graphdiyne; MG film: MoS_2–reduced graphene oxide (MG) film; MoS_2 NSs/CNP: carbon nanotube paper (CNP) uniformly covered by MoS_2 nanosheets (NSs); BP–G: black phosphorus nanoparticle–graphite composite; CuO NSs/r-GO: CuO nanosheets (NSs)/rGO; A-TO/GSP: anisotropic TiO_2 (A-TO)/graphene sandwich papers (GSP).

been realized and have attracted extensive attention.[112] However, there are other potential issues for LIBs such as safety, cycle life, and poor low-temperature performance. What's more, as the use of large-format LIBs becomes widespread, the low abundance and uneven distribution of Li in the Earth's crust lead to increased price of the Li element, which in turn significantly affects the further extension of commercial LIBs.[113] Thus, there is an urgent need to explore rechargeable batteries based on abundant elements that also have low cost, high safety, and cycling stability. Up to now, a number of such batteries have been developed using cheap, earth-abundant elements, such as Na-ion,[113,114] Mg-ion,[115] and Al-ion batteries.[24]

Compared with Li^+, Na^+ has similar intercalation chemistry but much higher abundance and lower cost. These factors, as well as its low redox potential (slightly higher than that of Li), make SIBs a promising alternative to LIBs for state of the art batteries.[116,117] The large size of Na ions (0.102 nm in radius) requires a larger interlayer distance than LIBs. Thus, ultrathin 2D nanomaterials have also been explored as electrode materials for SIBs, such as graphene, TMDs, MXenes, and BP. Similar to wearable LIBs, SIBs can be designed to be wearable. But up to now, studies of wearable energy-storage devices have mainly focused on LIBs, while reports on SIBs have been very limited.

Yu and coworkers developed an Na-ion full battery using all stretchable components, based on graphene-modified poly(dimethylsiloxane) (PDMS) sponge electrodes and an elastic gel membrane (Fig. 10).[118] Fig. 10a shows the synthesis strategy for preparing the PDMS/rGO sponge from a sugar cube completely filled with PDMS precursors containing base/curing agents. In this work, they integrated 2D $VOPO_4$ nanosheets and commercial hard carbon as stretchable electrodes (based on the PDMS/rGO sponges), respectively. Clearly, the PDMS/rGO sponge/$VOPO_4$ electrodes displayed superior rate capability and good cycling stability. A stable capacity of ~126 mA h g^{-1} can be achieved at a current density of 50 mA g^{-1}. The electrode can deliver a capacity of up to ~83 mA h g^{-1} even at a high current density of 1.0 A g^{-1}. The high rate capability can be ascribed to the tailored properties of the PDMS/rGO sponge based electrodes, which include high electrochemical conductivity, stable porous architecture, as well as the robust mechanical deformability. Owing to the robust mechanical strength of PDMS/rGO, the battery exhibited high deformability: its electrochemical characteristics can be well-maintained under many different stretching conditions and after hundreds of stretch–release cycles. This novel design integrating all stretchable components provides a pathway toward the next generation of wearable energy devices in modern electronics.

Rechargeable Al-ion batteries have unique superiority in terms of battery safety, and they have gained increasing attention for wearable energy storage devices. Batteries based on Al also benefit from Al's three-electron redox properties (*i.e.* potential for high-capacity batteries), stability in the metallic state, and very high natural abundance.[119] Lu and coworkers reported plasma-etched graphene nanoribbons on highly porous 3D graphene (GNHPG) foam as the cathode material for rechargeable Al-ion batteries.[120] The freestanding and flexible pouch cell exhibited excellent performance: low charging voltage plateaus (cutoff voltage of 2.3 V, below which the battery has no side reactions), high discharge voltage plateaus near 2 V, a high capacity of about 123 mA h g^{-1} at a current density of 5000 mA g^{-1} with Coulombic efficiency higher than 98%, long cycle life (no capacity decay after more than 10 000 cycles), and high rate performance (148, 125, 123, 119, 116, and 111 mA h g^{-1} at current densities of 2000, 4000, 5000, 6000, 7000, and 8000 mA g^{-1}, respectively). In addition, the battery also showed fast charge and slow discharge (fully charged in 80 s and discharged over 3100 s). Although there was less information about the flexibility of the electrode and the

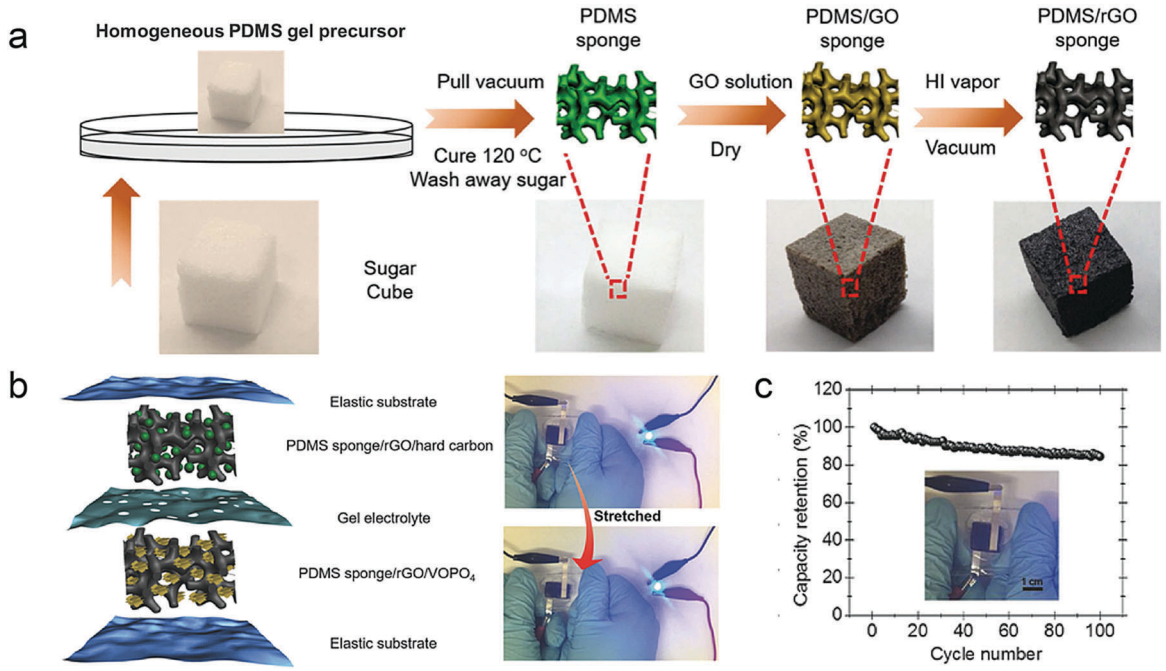

Fig. 10 Wearable SIBs based on graphene. (a) Schematic illustration of preparation steps of conductive PDMS/rGO sponge. While the PDMS/GO sponge (insulating) was brownish in color, once the material was reduced to rGO (conductive), the material appeared black. (b) Schematic illustration of the fabricated stretchable PDMS/rGO sponge/$VOPO_4$//PDMS/rGO sponge/hard carbon sodium-ion full battery and photographs of the stretchable sodium-ion full battery in the unstretched state (top) and stretched state with ~50% strain (bottom) to power a commercial LED light. (c) Cycling stability of the full battery at the rate of 1.0 °C. The inset image shows the full battery in the unstretched state. Reproduced with permission from ref. 118. Copyright 2017, John Wiley & Sons, Inc.

whole battery, these results are still promising for next-generation wearable batteries.

2.2.2 Li–S batteries. 2D materials can also be integrated into other kinds of batteries, such as Li–S batteries, Li–O_2 batteries, and some other novel batteries.

The theoretical specific capacity of Li–S batteries (1672 mA h g^{-1}) is much higher than those of traditional cathode materials. Therefore, the Li–S batteries are promising candidates for next-generation energy storage applications.[121–123] Nevertheless, it has been difficult to develop a practical Li–S battery partly due to the low electrical conductivity of sulfur, the dissolution of polysulfides in the electrolyte, and volume expansion of sulfur during discharge. Moreover, highly soluble polysulfides in the electrolyte, which can shuttle between the anode and cathode and form a deposit of solid Li_2S_2/Li_2S on the cathode and anode ("shuttle effect"), could cause an irreversible loss of S, which leads to low Coulombic efficiency, low cyclic capacity, and an increase in impedance.[124]

The adoption of hierarchically structured graphene and associated nanomaterials as a supporting matrix for Li–S batteries can partly overcome these obstacles, because of their good conductivity, fast e^-/Li^+ transport kinetics, large specific surface area, and high flexible characteristics.[69]

Cheng and coworkers developed a flexible Li–S battery electrode by using graphene foam (GF) as a current collector and host to achieve high sulfur loading through simple slurry infiltration (Fig. 11a–c).[123] The PDMS coating on the GF makes this interconnected network sufficiently robust, guaranteeing the flexibility of the cathode. The interconnected GF also provides efficient electron transport pathways, offers vast void space to accommodate a significant amount of sulfur and sufficient electrolyte, as well as provides a robust mechanical support. As shown in Fig. 11a, the sulfur loading in the GF-based electrodes can be tuned from 3.3 to 10.1 mg cm^{-2}. The electrode with 10.1 mg cm^{-2} sulfur loading could deliver an extremely high areal capacity of 13.4 mA h cm^{-2}, much higher than that of the commonly reported Li–S electrodes and the commercially used lithium cobalt oxide cathode with a value of 3–4 mA h cm^{-2}. Meanwhile, the electrode with high sulfur loading retained high rate performance with reversible capacities higher than 450 mA h g^{-1} under a large current density of 6 A g^{-1}, plus stable cycling performance with only 0.07% capacity decay per cycle over 1000 cycles. These impressive results indicate that such electrodes could enable high-performance and flexible Li–S batteries with fast charge and stable performance over extended charge/discharge cycling.

2.3 Perspectives

We have highlighted the recent progress in 2D material based wearable batteries, but there is still much to do to realize the wearable battery system. The batteries for wearable applications should possess good electrochemical property, mechanical property, and operational safety. Correspondingly, studies on wearable batteries should focus on properties such as (1) high energy density and long-term cycle life without decay during operation while being bent and even folded; (2) maintaining an

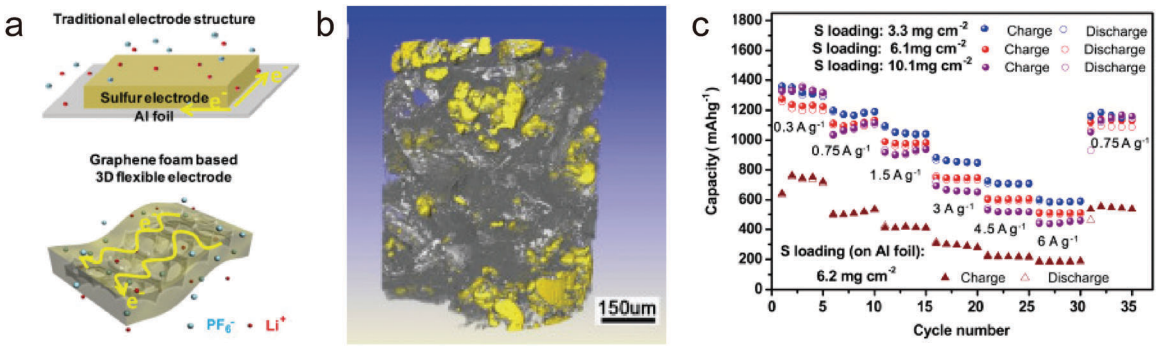

Fig. 11 Wearable Li–S batteries based on graphene. (a) Comparison between electrode design in which sulfur is coated on an Al foil and a graphene foam (GF)-based flexible electrode. (b) 3D image of the reconstructed S-PDMS/GF electrodes with 10.1 mg cm^{-2} sulfur loading (graphene and carbon black marked in gray, sulfur particles marked in yellow and PDMS marked in white). (c) Rate performance of the S-PDMS/GF electrodes with different sulfur loadings and the electrode with sulfur coated on an Al foil. Reproduced with permission from ref. 123. Copyright 2014, Elsevier Ltd.

intact and stable structure without cracking while being bent and folded; (3) good packing to prevent leakage and adaptable separator to avoid internal short-circuits. While many works have reported the flexibility of electrodes, there is a lack of data about their performance under repeated bending or folding. For practical wearable applications, merely the flexibility of the electrodes is not enough, and the whole battery needs to be robust and flexible. The development of shape-conformable solid-state package/electrolytes/separators still needs to be undertaken. Last but not least, the safety of wearable batteries is obviously crucial for realizing the wearable system and therefore should get more attention. Since the conventional liquid electrolytes used in batteries tend to be flammable, replacing them with solid-state electrolytes can provide better safety. For the same reason, safety of the overall package could be improved.

3. Wearable supercapacitors

The fast development of flexible and wearable electronic devices calls for wearable power sources. Thus, wearable energy-storage devices with high-performance are urgently needed. Batteries and supercapacitors are two typical energy storage devices.[125,126] While batteries tend to be limited by their lower power densities, supercapacitors have many advantages such as higher power densities, ultrafast charge/discharge rates, and superior cycle lifetime. As a consequence, developing wearable supercapacitors is considered to be one avenue to meet the great demand for wearable power sources. Moreover, their long-term cyclic stability makes supercapacitors more suitable than batteries as the energy storage component in sustainable power systems, which integrate energy harvesters with energy storage devices to directly power electronics. According to the working mechanisms, supercapacitors can be divided into three types (Fig. 12): (1) electric double-layer capacitors (EDLCs); (2) pseudocapacitors; and (3) hybrid supercapacitors.[127] EDLCs are based on ion adsorption/desorption that lead to fast charge/discharge rates and excellent cyclic stability.[128] Pseudocapacitors utilize fast reversible redox reactions that result in increased energy density and power density compared with EDLCs. Hybrid supercapacitors combine EDLCs with pseudocapacitors in a single device, and they have energy and power densities comparable to those of EDLCs and cyclic stability better than that of pseudocapacitors. Recently, great efforts have been made for developing high-performance supercapacitors. The requirements for wearable supercapacitors include flexibility, light weight, high power density, high energy density, durability, safety and so on.

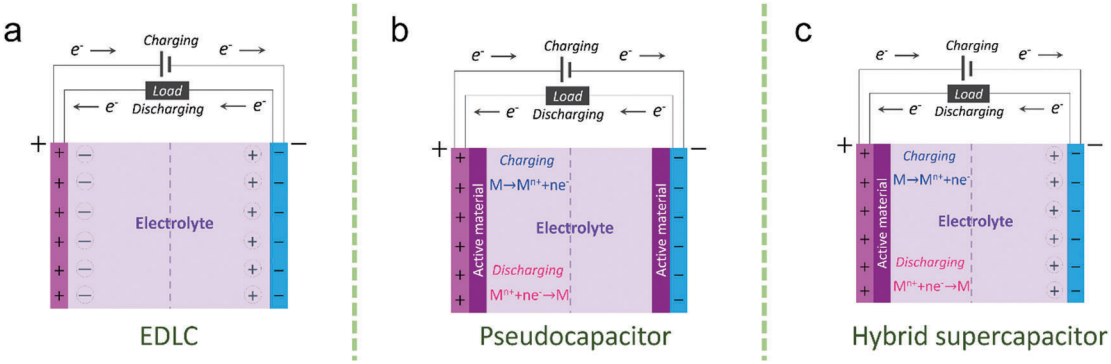

Fig. 12 Working mechanisms of supercapacitors. Schematic illustration of the mechanisms for the (a) electric double-layer capacitor (EDLC), (b) pseudocapacitor and (c) hybrid supercapacitor.

2D materials, such as graphene and its derivatives, MXenes, TMDs, and TMOs, have many advantages to meet such requirements: firstly, their high specific surface area and more active sites for electrochemical reactions can increase the capacity and power density; secondly, they have negligible thickness and high flexibility; thirdly, some 2D materials such as 2D carbon materials endow supercapacitors with lightweight property and high durability since carbon electrodes are much lighter than metal or conducting polymer electrodes and do not react with the electrolyte. In this part, 2D material based supercapacitors that have the potential for wearable power sources will be discussed.

3.1 Wearable supercapacitors based on graphene and its derivatives

As one of the most representative 2D materials, graphene and its derivatives have been widely used for supercapacitors.

3.1.1 EDLCs. Graphene and rGO have been applied as electrodes of EDLCs, which improve the high-frequency operation. Conventional porous electrode based EDLCs behave like a resistor rather than a capacitor when driven by high frequency alternating current (AC), which limits their applications for filter circuits. Thus, materials with high surface area but less inherent porosity are required. Graphene nanosheets offer a promising route to tackle this challenge due to their advantages such as a high amount of exposed and accessible edge planes, minimal porosity effects and extremely high conductivity. Holloway *et al.* demonstrated EDLCs with an efficient filtering of 120 Hz current, using electrodes made from vertically oriented graphene nanosheets grown directly on metal current collectors.[129] At 120 Hz, the derived capacitance value was 175 mF, and the measured resistance was 1.1 Ω, yielding an RC time constant of less than 200 ms. Such good high-frequency operation may be attributed to the following reasons. Firstly, these graphene nanosheets have a preponderance of edge planes that result in higher specific capacitance. Secondly, the exposed and directly accessible charge-storage edge planes of these graphene nanosheets minimize the distributed nature of the charge storage. Thirdly, the open structure of graphene nanosheets reduces the ionic resistance and therefore minimize porosity effects. Finally, these graphene nanosheets have extremely high conductivity and are directly grown on current collectors, which minimizes the electronic resistance.

For a majority of graphene based supercapacitors, the restacking of graphene sheets is always a problem that lowers the energy and power densities. Therefore, alleviating the strong sheet-to-sheet van der Waals interaction to a reasonable degree is important for graphene based supercapacitors. El-Kady *et al.* applied direct laser reduction on GO to produce graphene using a standard LightScribe DVD optical drive (Fig. 13a and b).[130] The initially stacked GO sheets were converted into graphene films with high electrical conductivity (1738 S m^{-1}) and high specific surface area (1520 m^2 g^{-1}). The LightScribe laser causes simultaneous reduction and exfoliation of GO sheets and produces an open graphene network, which prevents the agglomeration of graphene sheets and contributes to the high performance. Supercapacitors made with these electrodes presented ultrahigh energy density, high power density and excellent cyclic stability (96.5% after 10 000 cycles). Besides, these supercapacitors also exhibited excellent flexibility with only 5% loss after 1000 bending cycles. Other methods were also used for providing more interactive sites to bind graphene nanosheets. For example, Weng *et al.* developed a graphene-cellulose paper (GCP) in which graphene nanosheets cover the cellulose fibers and are distributed through the macroporous filter paper, forming a conductive interwoven network.[131] Therefore, this membrane is believed to overcome the low porosity as well as low strength of graphene or GO papers. Moreover, the GCP membrane can endure over 1000 repeated bending tests with only 6% increase in electrical resistivity, and it can be tailored to various shapes for applications of several prototypes of flexible supercapacitors. Flexible large-area hierarchical porous graphene films have also been fabricated by using GO hydrogels as the initial feedstock. Xiong *et al.* used viscous GO hydrogels to form films with desired sizes and shapes, followed by reduction of the stable GO hydrogel with HI/HAc to form graphene electrodes with macroporous/mesoporous structures.[132] The flexible supercapacitor based on these electrodes can be bent to arbitrary angles (up to 180°) with almost no capacity loss. Flexible graphene fibers integrate individual graphene nanosheets into useful and macroscopic ensembles, which can also effectively alleviate the restacking problem. Meng *et al.* reported an EDLC based on flexible graphene fibers (Fig. 13c–f).[133] The core of the graphene fiber is covered with a sheath of 3D porous network-like graphene framework. The graphene core-sheath fiber was prepared by electrochemically electrolyzing 3 mg mL^{-1} GO aqueous suspension containing 0.1 M lithium perchlorate on graphene fibers at an applied potential of −1.2 V for 5 min. The as-produced graphene fibers possess high conductivity and excellent flexibility, and have a density of 0.23 g cm^{-3}, which is 7 times and 85 times lower than that of conventional carbon fibers (>1.7 g cm^{-3}) and Au wire (~20 g cm^{-3}) respectively. The supercapacitor based on this graphene fiber has a specific capacitance of 25–40 F g^{-1}, which is lower than that of 3D graphene electrodes (>100 F g^{-1}), but is still close to that of activated carbon textiles (20–70 F g^{-1}). The energy density and power density of this supercapacitor are 0.4–1.7 × 10^{-7} W h cm^{-2} and 6–100 × 10^{-6} W cm^{-2}, respectively. The supercapacitor can be weaved into fabrics and has a capacitance of ~19 F cm^{-1} in the knotted state.

As for further improving the performance of supercapacitors, optimization of their ion transportation remains a challenge. Choi *et al.* reported a graphene based supercapacitor by assembling the thin films of functionalized rGO (f-rGO) and solvent-cast Nafion electrolyte membranes (Fig. 13g–i).[134] The produced f-rGO supercapacitors exhibited higher performance compared with the normal rGO supercapacitors, and the cyclic voltammetry (CV) curves were of almost the same shape during the bending test demonstrating their excellent flexibility. The specific capacitance was 118.5 F g^{-1} at 1 A g^{-1} and the rate was ~90% at 30 A g^{-1}. Two main factors may be responsible for such high performance: (1) the interconnected networks of

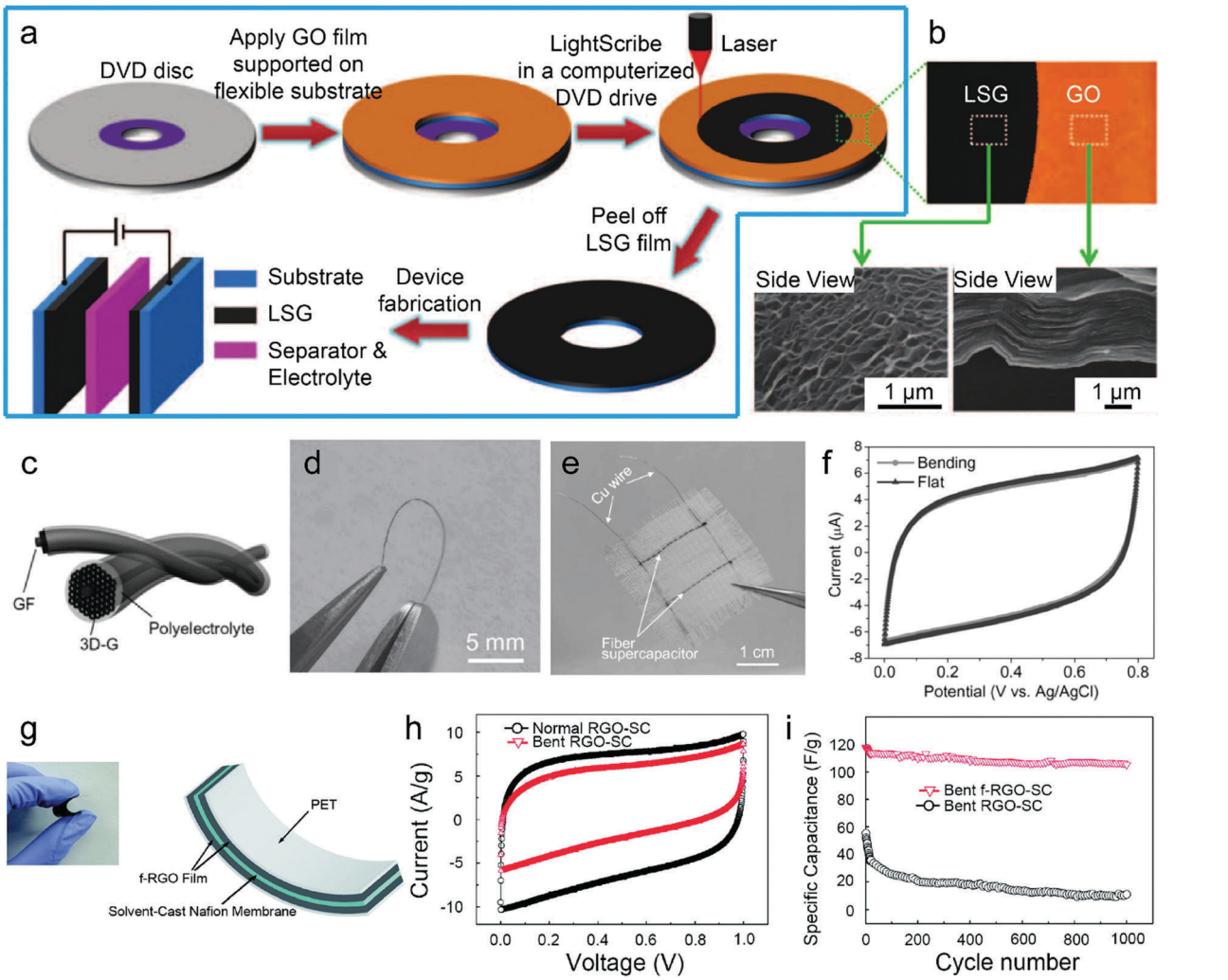

Fig. 13 Graphene and rGO for EDLCs. (a) Schematic illustration of the fabrication of supercapacitors based on laser-scribed graphene (LSG). (b) The GO film reduced to LSG with the color changed from golden brown to black. The cross-sectional SEM images show that the laser changed the stacked GO sheets into a well-exfoliated few-layered LSG film. Reproduced with permission from ref. 130. Copyright 2012, AAAS. (c) Schematic illustration of the graphene fiber based supercapacitor. (d) Photograph showing the supercapacitor in the bending state. (e) Photograph showing the textile embedded with two graphene fiber based supercapacitors. (f) The CV curves at a scan rate of 50 mV s^{-1} of two graphene fiber based supercapacitors weaved in the textile in the flat and bending state. Reproduced with permission from ref. 133. Copyright 2013, John Wiley & Sons, Inc. (g) Photograph and schematic diagram of the all-solid-state flexible functionalized rGO (f-rGO) based supercapacitor. (h) CV curves at 100 mV s^{-1} of the rGO and f-rGO based supercapacitors. (i) Durability test of the rGO and f-rGO based supercapacitors. Reproduced with permission from ref. 134. Copyright 2011, American Chemical Society.

f-rGO lead to fast charge transport and continuous transport pathways; (2) the close contact between the electrode and the electrolyte results in decreased resistance and enhanced performance.[135] Moreover, the flexible f-rGO supercapacitors demonstrated no significant changes after 1000 cycles of charge/discharge processes and the shape of the CV curve was almost unchanged after bending to a radius of 2.2 mm.

The doping of heteroatoms such as nitrogen (N) and boron (B) in graphene basal planes can further enhance the capacitance because the doped graphene can not only improve the electrode conductivity but can also result in additional pseudocapacitance contributions.[136,137] Lin *et al.* reported a supercapacitor based on N-doped ordered mesoporous graphene-like layered carbon.[136] The typical preparation of the graphene-like layered carbon used a sacrificial mesoporous silica as the template. After the synthesis of the graphene-like carbon, the silica was etched away and self-supporting ordered mesoporous graphene-like few-layered carbon was obtained. The N-doped graphene-like layered carbon had high conductivity (360 S cm^{-1}) and high specific surface area (1900 m^2 g^{-1}). The electrodes of the supercapacitor were fabricated by combining the N-doped graphene-like layered carbon powders with 3D graphene foam by using a binder (at lower mass loading, the binder is not used). In 0.5 M H_2SO_4 electrolyte, the electrode had a specific capacitance of 790 F g^{-1} at 1 A g^{-1}, and its packaged device had a specific energy density of 23.0 W h kg^{-1} and a specific power density of 18.5 kW kg^{-1}; in 2 M Li_2SO_4 (pH 1.8) electrolyte, the corresponding values were 720 F g^{-1}, 38.5 W h kg^{-1},

and 22.5 kW kg^{-1}, respectively. This high performance mostly originates from the robust redox reactions at N-associated detects that transform graphene-like layered carbon into an electrochemically active substance without compromising its electrical conductivity.

3.1.2 Pseudocapacitors and hybrid supercapacitors. Compared with EDLCs, pseudocapacitors work based on fast reversible redox reactions and have higher energy density. Conducting polymers, metal oxides, and other kinds of materials that can provide fast redox reactions act as active materials for pseudocapacitors. Graphene and rGO used in pseudocapacitors are mainly aimed to increase the specific surface area for redox reactions and improve the conductivity of active materials. Hybrid supercapacitors combine EDLCs with pseudocapacitors in a single device and have energy density and cyclic stability in between those of EDLCs and pseudocapacitors. Graphene and rGO can serve as the EDLC electrode, or combine with active materials to act as the pseudo electrode, or be used for both the electrodes of hybrid supercapacitors, playing the same roles as those in EDLCs or pseudocapacitors.

Graphene and rGO can be applied in conducting polymer based pseudocapacitors or hybrid supercapacitors to enhance the performance by providing high specific surface area. Zang *et al.* used a hybrid film as the pseudo electrode material, which was composed of graphene woven fabric (GWF) and polyaniline (PANI).[138] PANI also acts as the active material that offers the fast redox reaction of the supercapacitor and the GWF provides a high specific surface area for the supercapacitor. The GWF was grown directly on copper meshes by a CVD method. For the synthesis of the hybrid film, they used an *in situ* electropolymerization method, coating PANI on a GWF film (Fig. 14a and b). The supercapacitor had a capacitance of 23 mF cm^{-2} (Fig. 14c) and exhibited good flexibility. The device could be deformed more than 500 times while still maintaining the areal capacitance. Besides, it showed a capacitance retention of ~100% after 2000 cycles. In the same year, Xiao *et al.* also combined PANI with

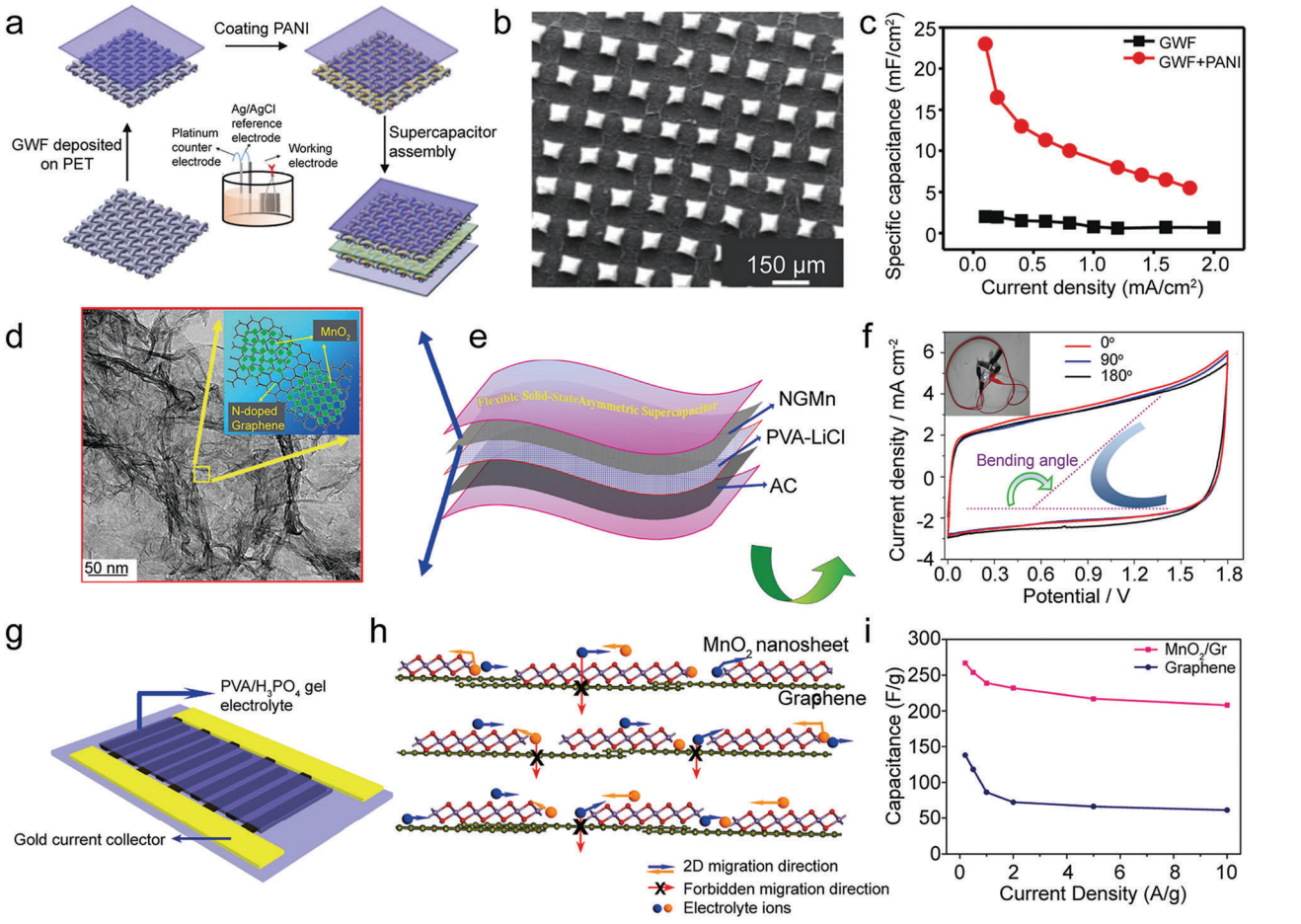

Fig. 14 Graphene and rGO for pseudocapacitors and hybrid supercapacitors. (a) Schematic illustration of the fabrication process of the pseudocapacitor based on graphene woven fabric (GWF) and PANI. (b) SEM images of GWF/PANI films. (c) Areal capacitance of GWF and GWF/PANI. Reproduced with permission from ref. 138. Copyright 2015, the Royal Society of Chemistry. (d) TEM images of the N-doped rGO/MnO_2 nanosheet (NGMn) composite. (e) The structure of the flexible supercapacitors. (f) CV curves of the flexible device under various bending conditions at 10 mV s^{-1}. Inset: Photograph of a blue LED powered by the two supercapacitors in series. Reproduced with permission from ref. 141. Copyright 2016, American Chemical Society. (g) The structure of the ultraflexible planar supercapacitors. (h) Schematic illustration of the 2D planar ion transport favored with the 2D δ-MnO_2/graphene hybrid structures. (i) Comparison of the specific capacitance of the supercapacitors based on the hybrids and based on graphene. Reproduced with permission from ref. 142. Copyright 2013, American Chemical Society.

rGO for supercapacitors.[139] They fabricated a kind of rGO/PANI/rGO nanohybrid paper that had high conductivity, good chemical stability and excellent mechanical robustness. Porous PANI nanomaterials were electropolymerized *in situ* on the rGO paper. Then the surface of the PANI coated rGO paper was wrapped by an ultrathin rGO layer, resulting in a freestanding sandwich-structured paper. This nanohybrid paper was used as the pseudo electrode for supercapacitors, and its unique structure increased the specific capacitance and improved the cyclic stability. The as-obtained supercapacitor exhibited not only high energy density but also high power density. Moreover, it also showed excellent cyclic stability and exceptional mechanical flexibility. These results demonstrated its potential for flexible energy-related devices and wearable electronics.

Graphene and rGO can also be used in metal oxide based pseudocapacitors or hybrid supercapacitors to increase the performance by improving the conductivity of the metal oxide. Metal oxide based supercapacitors have many advantages. For example, MnO_2 has high theoretical specific capacitance and low cost.[140] However, there are still some problems hindering their practical applications, such as poor electrical conductivity, low specific surface area, and dissolution in the electrolyte. Combining MnO_2 with conductive and chemically inert materials, such as graphene, may be an approach to solve such problems. Liu *et al.* reported a hybrid supercapacitor based on N-doped rGO/MnO_2 nanosheet (NGMn) composites, which showed excellent electrochemical performance.[141] N-doped rGO was used as a template to induce the growth of layered δ-MnO_2 nanosheets (Fig. 14d), which improved the electrical conductivity of the composite. The NGMn composites exhibited a large specific capacitance of about 305 F g^{-1} at a scan rate of 5 mV s^{-1}. The supercapacitor was fabricated using NGMn as the cathode, activated carbon as the anode and polyvinyl acetate (PVA)/LiCl gel as the electrolyte (Fig. 14e), and it exhibited a maximum energy density of 3.5 mW h cm^{-3} and a power density of 0.019 W cm^{-3}. Besides, the supercapacitor possessed good robustness, with CV curves almost unchanged under different bending angles (Fig. 14f). The flexibility, high energy density, and good cycle life all demonstrate that this NGMn based supercapacitor has great potential in portable and wearable electronics. Peng *et al.* reported a supercapacitor based on a 2D δ-MnO_2/graphene hybrid thin film (Fig. 14g).[142] δ-MnO_2 nanosheets were integrated onto the rGO sheets (Fig. 14h), resulting in more active surface area and extra interface at the hybridized interlayer regions. This structure not only provides benefits for absorption/desorption of ions but also facilitates charge transport during charge/discharge processes, leading to good rate capability and cyclic stability. In addition, this structure also opens up the interlayer space to allow more electrolyte ions to penetrate efficiently into the hybridized film, which helps to increase the faradaic capacitance. The specific capacitance of this supercapacitor was 267 F g^{-1} at 0.2 A g^{-1} and 208 F g^{-1} at 10 A g^{-1} (Fig. 14i) and capacitance retention was 92% after 7000 charge/discharge cycles. Moreover, after 1000 times of folding/unfolding, the capacitance retention was over 90%. Bissett *et al.* produced a MoS_2/graphene composite membrane to act as the pseudo electrode material.[143] The composite membranes were synthesized by mixing dispersions of MoS_2 and graphene, with no binders. The highest specific capacitance of supercapacitors based on the composite membranes was obtained when the weight ratio of MoS_2 to graphene was 1 : 3. The differences in flake dimensions as well as surface energies of the MoS_2 and graphene prevent restacking and improve the performance. At a scan rate of 5 mV s^{-1}, the composite membrane exhibited a specific capacitance of 1.16 mF cm^{-2}. These results demonstrate a simple and scalable approach for flexible supercapacitors.

In addition, GO has also been applied to serve as the separator of supercapacitors.[144,145] Hu *et al.* reported an all-in-one flexible fiber supercapacitor.[145] The rGO–GO–rGO fiber supercapacitor was obtained by region-specific reduction of the GO fiber under laser irradiation. The rGO parts act as the electrodes, and the GO intermediate layer acts as both the separator and the reservoir for holding the electrolyte. The capacitance of this fiber supercapacitor can reach a value of 1.2 mF cm^{-2} at a current density of 80 μA cm^{-2}. The capacitance shows no obvious degradation after 1000 cycles of charge/discharge processes. The energy and power densities of the fiber supercapacitor are 2–5.4 × 10^{-4} W h cm^{-2} and 3.6–9 × 10^{-2} W cm^{-2}, respectively. This kind of graphene fiber based supercapacitors could be woven into textile and are promising for use in wearable electronics.

Graphene nanosheets have been used as the electrodes of EDLCs, which endow EDLCs with improved high-frequency performance because they have exposed and accessible edge planes that lead to minimal porosity effects and high conductivity. The restacking of graphene is a big challenge, which can be resolved by methods such as direct laser reduction of GO or constructing graphene with interwoven network structures. By doping graphene with heteroatoms, the electronic structure and density of state can be further improved and additional pseudocapacitance contributions can be introduced, leading to higher electrochemical performance. However, the doping processes require precise control, which may elevate the fabrication cost. Graphene and rGO have also been introduced into conducting polymer based supercapacitors to increase the specific surface area and cyclic stability, and into metal oxide based supercapacitors to improve the conductivity of the metal oxide. GO has been applied to act as the separator of supercapacitors.

3.2 Wearable supercapacitors based on other 2D materials

3.2.1 Transition metal carbides (MXenes). MXenes are a class of 2D materials that have the general formula of $M_{n+1}X_nT_x$, where 'M' is a transition metal, X is C and/or N, n means an integer between 1 and 3, and T_x represents surface functional groups.[146] MXenes have been used for supercapacitors due to their excellent properties, such as the extra active pseudocapacitive centers from the inorganic frameworks and the capability of electrosorption of electrolyte ions. Their unique structure brings about many advantages for energy storage: (1) fast electron supply to electrochemically active sites is enabled because of

the conductive transition metal carbide layer; (2) a redox-active transition metal oxide-like surface is generated during the synthesis; (3) fast ion transport is permitted due to the 2D morphology and pre-intercalated water.[147]

Lukatskaya *et al.* reported high-performance EDLCs with layered Ti_3C_2 MXene serving as the electrode materials.[148] The Ti_3C_2 MXene layers can be intercalated with a variety of cations, including Na^+, K^+, NH_4^+, Mg^{2+}, and Al^{3+} (Fig. 15a and b). As a consequence, the excellent performance based on the flexible $Ti_3C_2T_x$ paper resulted from both the double-layer capacitance and intercalation, and the latter made up for the shortcoming of the low specific surface area. The capacitance of this material was in excess of 300 F cm^{-3}. This study demonstrates the potential of 2D carbides and carbonitrides for electrochemical energy storage applications.

In 2017, Lukatskaya *et al.* further applied $Ti_3C_2T_x$ MXene for pseudocapacitors that have pseudocapacitive energy storage with ultrahigh rate.[149] The macroporous $Ti_3C_2T_x$ MXene film delivered a high specific capacitance of 210 F g^{-1} at a scan rate of 10 V s^{-1}. Moreover, the volumetric capacitance (about 1500 F cm^{-3}) reached the previously unmatched performance of RuO_2. The high performance can be attributed to the unique structure of the $Ti_3C_2T_x$ MXene film, the macroporous electrode and the increased concentration of the electrolyte. Firstly, the conductive inner transition metal carbide layer enables fast electron supply to the electrochemically active sites; the transition metal oxide-like surface generated during the synthesis is redox active; and the intercalated water molecules enable high accessibility of protons to the redox-active sites. Secondly, the electrodes were characterized by 1–2 μm-diameter macropores with a submicrometer-thick MXene wall, which greatly reduce the ion transport length. Thirdly, 3 M H_2SO_4 was used as the electrolyte in this study, and the higher concentration of proton results in slightly higher capacitance values and superior rate performance than that using 1 M H_2SO_4 solution.

3.2.2 TMDs and TMOs. TMDs and TMOs have also been applied for supercapacitors. Feng *et al.* demonstrated that vanadium disulfide (VS_2) is a potential material for high-performance planar supercapacitors, because of the synergy between its metallic nature and exfoliative characteristics brought by the conducting S–V–S layers stacked up by weak van der Waals interlayer interactions.[150] The electrical resistivity increased with increasing temperature, demonstrating the typical metallic conducting behavior and confirming the metallicity of VS_2 nanosheets (Fig. 15c).[150] The highly conductive VS_2 thin films were successfully assembled as the electrodes of the planar EDLCs (Fig. 15d) with a specific capacitance of 4760 μF cm^{-2} in a 150 nm in-plane configuration. The capacitance showed no obvious degradation after 1000 charge/discharge cycles. Wu *et al.* reported a flexible ultrathin pseudocapacitor based on α_1-vanadyl phosphate ($VOPO_4$) ultrathin nanosheets with less than six atomic layers.[151] These nanosheets could undergo a reversible pseudocapacitive reaction with Li^+:

$$VOPO_4 + xLi^+ + xe^- \leftrightarrow 2Li_xVOPO_4.$$

The energy density of the as-obtained flexible supercapacitor was 1.7 mW h cm^{-2}, and the power density was 5.2 mW cm^{-2}. In addition, the specific capacitance showed negligible degradation even after 400 bending cycles.

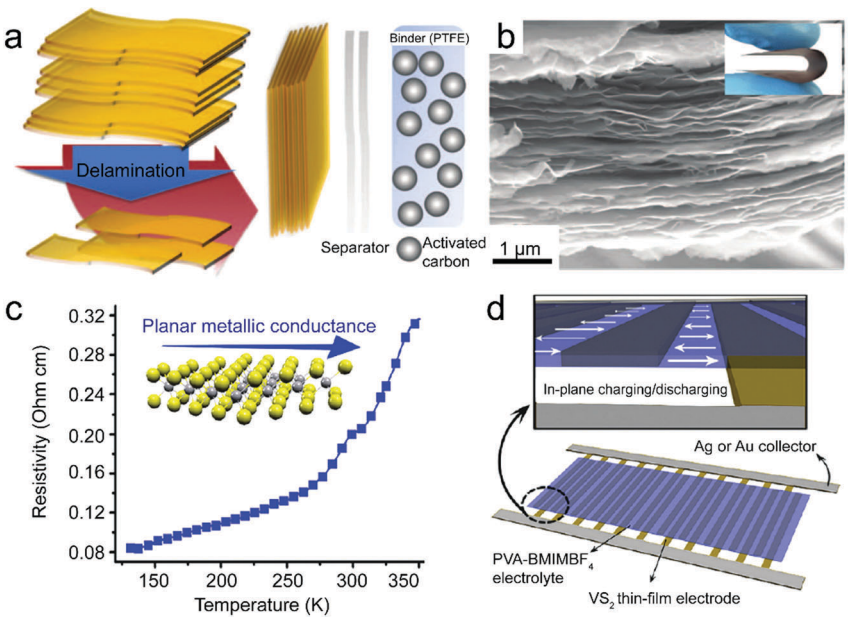

Fig. 15 Supercapacitors based on MXenes and TMDs. (a) Schematic illustration of the electrode fabrication process. First, the multilayer $Ti_3C_2T_x$ powders are delaminated to produce few-layer MXene flakes; then the resulting colloidal solution is filtered through a porous membrane, producing binder and additive-free $Ti_3C_2T_x$ paper electrodes for use in capacitance tests. (b) SEM image of the paper electrode. Inset: photograph showing its flexibility. Reproduced with permission from ref. 148. Copyright 2013, AAAS. (c) Temperature dependence of planar resistivity of the VS_2 thin film. (d) Up: the migration path of ions for the planar supercapacitor; bottom: schematic illustration of the as-fabricated supercapacitor configuration. Reproduced with permission from ref. 150. Copyright 2011, American Chemical Society.

The unique structure of MXenes enables fast electron supply, a redox-active layer surface, and high proton accessibility, which endow MXene based supercapacitors with high performance. TMOs and TMDs have also been applied for flexible supercapacitors, and their layered structure makes them promising for flexible supercapacitors with planar structure.

It should be noted that for wearable purposes, the configuration of the supercapacitor electrodes is of great importance. Big challenges emerge for conventional sandwich-structured supercapacitors when further decreasing the thickness to achieve high performance and flexibility, such as how to prevent short circuit and ensure a smooth transportation of ions during bending. Planar supercapacitors, with the electrode material, electrolyte, and current collector integrated onto the same plane, are a promising solution to address these issues. Even when the supercapacitors are rolled or even folded, planar supercapacitors can offer planar channels for ions without affecting the ion transportation.[152] Due to their layered structures, 2D materials are desirable for use in flexible planar supercapacitors. The wearable planar supercapacitors based on 2D materials usually feature two parallel or interdigital electrodes, on a flexible substrate.[131,153] The fabrication techniques of planar supercapacitors include photolithography, plasma etching, laser scribe, and inkjet printing.[154–157] Chen *et al.* reported a flexible planar supercapacitor based on graphene prepared by liquid–air interfacial assembly.[158] The GO film supported by the PET substrate was reduced into electrically conductive graphene by using hydriodic acid as the reducing agent. Then the flexible planar supercapacitor was constructed on the PET supported graphene, without the substrate-transfer procedure. The fabricated planar supercapacitors with MnO_2 and PANI as the active materials presented an areal specific capacitance of up to 963 and 2561 μF cm^{-2}, respectively. Further development of wearable planar supercapacitors based on 2D materials can involve improving the electrochemical properties of the electrode materials, optimizing the device geometry (number of finger electrodes, interspace between adjacent electrodes, *etc.*), and reducing the cost of the manufacturing processes.

3.3 Perspectives

Supercapacitors have advantages over batteries in terms of higher power density, ultrafast charge/discharge rates and superior operating lifetime. The excellent cyclic stability also makes supercapacitors more suitable than batteries to serve as the energy storage component of sustainable power systems that combine energy harvesters with energy storage devices to power electronics. Therefore, wearable/flexible supercapacitors are promising to meet the demand for wearable power sources. The flexibility of 2D materials satisfies the basic requirement for flexible supercapacitors. But what really tantalizes researchers is that the potential of 2D materials for flexible supercapacitors goes well beyond flexibility. Graphene nanosheets possess exposed and accessible edge planes that result in minimal porosity effects and high conductivity, and thereby improve the high-frequency operation of EDLCs. Doping graphene with heteroatoms can further improve the supercapacitor performance by enhancing the conductivity and introducing additional pseudocapacitive contributions. Graphene and rGO can increase the specific surface area and cyclic stability of conducting polymer based pseudocapacitors and improve the conductivity of the metal oxide for metal oxide based supercapacitors. GO has been used as the separator of supercapacitors. The unique structure of MXenes endows the supercapacitors with high performance due to the fast electron supply, redox-active layer surface and high proton accessibility. TMOs and TMDs are promising for flexible supercapacitors with planar structure due to their layered structure. The performance of the supercapacitors based on these 2D materials is summarized in Table 2.

For future studies, there are lots of challenges that require tremendous efforts. Precise control over the structural stability and doping processes of graphene and its derivatives without compromising the cost is still needed. Some other 2D carbon materials such as graphdiyne are predicted to have great potential for the electrodes of supercapacitors, and yet the experimental performance is not ideal.[159] The quality, stability, and synthesis method of these 2D carbon materials need to be improved. For non-carbon 2D materials, more controllable approaches are needed to precisely manipulate their thickness and crystallographic structures, and effective procedures are needed to tune the electrochemical properties at the atomic and molecular level.

In addition, further fundamental studies are still required to understand the operation mechanism so as to achieve optimized device performance and fulfill large-scale production standards. For practical wearable applications, devices are required to have strong robustness and high bending stability. Planar structured supercapacitors seem to be an effective route to tackle this challenge. Still, it is necessary to design new architectures and optimize both the electrochemical and mechanical properties of the 2D material based wearable supercapacitors.

4. Wearable energy harvesters

The unique properties of 2D materials also make them promising for energy harvesting. For example, due to their tunable light absorption property and band gap, some 2D materials such as MoS_2, WS_2, $MoSe_2$ and WSe_2 show great potential for the construction of solar cells with high power density and ultrathin thickness; some 2D materials such as BN, MoS_2, $MoSe_2$, $MoTe_2$, WS_2, WSe_2, and WTe_2 show stronger piezoelectric coupling than conventional bulk wurtzite structures, thereby offering new opportunities for piezoelectric nanogenerators; some 2D materials such as SnS_2 have increased electrical conductivity and decreased thermal conductivity compared with their bulk material counterparts, which provide new platforms for thermoelectric nanogenerators. In this section, applications of 2D materials for wearable energy harvesters will be reviewed and discussed.

4.1 Solar cells based on 2D materials

Solar radiation is an abundant energy source that is sustainable and renewable. Solar cells that convert sunlight into electricity

Table 2 Summary of performance of supercapacitors based on 2D materials

2D material	Electrode	Specific surface area	Specific capacitance	Cyclic stability	Flexibility	Ref.
TMD/graphene	MoS_2/graphene composite membranes	—	11 mF cm^{-2} at 5 mV s^{-1}	~250% after 10 000 cycles	—	143
rGO	Functionalized reduced graphene oxide thin films	—	118.5 F g^{-1} at 1 A g^{-1}	No significant changes after 1000 cycles	Almost the same in CV curves when bending to a radius of 2.2 mm	134
Doped graphene	Nitrogen-doped graphitic carbon sheets	50 m^2 g^{-1}	176 F g^{-1} at 0.1 A g^{-1}	120% after 2000 cycles at 0.5 A g^{-1}	—	265
Graphene/GO	GO/pristine graphene/PANI composite sheets	—	793.7 F g^{-1} at 1.0 A g^{-1}	80% after 1000 cycles at a scan rate of 100 mV s^{-1}	—	266
Doped graphene	Nitrogen-doped graphene/MnO_2 nanosheets	—	305 F g^{-1} at 5 mV s^{-1}	>90% after 1500 cycles	No significant change under various bending conditions	141
Doped graphene	Boron/nitrogen co-doped carbon nanosheets	416 m^2 g^{-1} (powder) and 393 m^2 g^{-1} (film)	358 F g^{-1} at 0.1 A g^{-1} (powder)	113% after 15 000 cycles (film)	—	267
Graphdiyne	Graphdiyne	—	71.4 F g^{-1} at 3.5 A g^{-1}	97% over 1000 cycles	—	159
Graphene	Graphene woven fabric and PANI hybrid films	—	23 mF cm^{-2}	~100% after 2000 cycles	The device could be deformed more than 500 times, while still maintaining the areal capacitance	138
Graphene	Hierarchical porous graphene films	1316 m^2 g^{-1}	71.0 mF cm^{-2} at 1 mA cm^{-2}	98.3% after 5000 cycles	The electrodes can be bent to arbitrary angles (even 180°) with an almost negligible capacity loss	132
Graphene	Graphene nanosheets cotton cloth composite fabric	—	326.8 F g^{-1} in 6 M KOH solution	93.8% after 1500 cycles	—	268
Graphene	Graphene-cellulose paper membranes	—	81 mF cm^{-2}	99.1% after 5000 cycles	1000 repeated bending tests with only 6% increase of electrical resistivity	131
Graphene	Graphene	—	394 μF cm^{-2}	no degradation in performance after 1500 cycles	—	152
Graphene	Graphene	1520 m^2 g^{-1}	2.07 mF cm^{-2} at 1000 A g^{-1} (inorganic electrolyte)	96.5% after 10 000 cycles	5% loss after 1000 bending cycles	130
Graphene	Quasi-2D ultrathin MnO_2/graphene nanosheets	—	267 F g^{-1} at 0.2 A g^{-1}	92% after 7000 cycles	Slight difference after thousands of times	142
Graphene	Co–Al hydroxide nanosheets/graphene multilayer films	—	880 F g^{-1} and 70 F m^{-2} at 5 mV s^{-1}	Over 99% after 2000 cycles	—	269
Graphene	Sandwich-structured graphene/PANI/graphene nanocomposite paper	—	581 F g^{-1} at 1 A g^{-1}	85% after 10 000 cycles	—	139
TMD	VS_2 nanosheets	—	4760 μF cm^{-2}	Higher than 90% after 1000 cycles	Very small degradation even after 200 bending cycles	150
TMO	α_1-Vanadyl phosphate nanosheets ($VOPO_4$)	—	8360.5 μF cm^{-2}	96% after 2000 cycles	Negligible degradation even after 400 bending cycles	151
MXene	Macroporous $Ti_3C_2T_x$ films	—	210 F g^{-1} at 10 V s^{-1}	90% after 10 000 cycles	—	149

can be mounted or integrated into the human body or clothes/accessories to serve as a power source for wearable electronics. 2D materials such as graphene and its derivatives, 2D TMDs, and phosphorene (monolayer BP) show great potential for application as solar cells due to their unique optoelectronic properties.

Graphene possesses a lot of merits for wearable solar cells, such as high optical transparency, high electron mobility, and excellent mechanical flexibility, which make it promising to replace the traditional indium tin oxide (ITO) or fluorine-doped tin oxide (FTO) electrodes. Compared with the brittle ITO, graphene is much more flexible and therefore is more desirable for flexible solar cells. Also, ITO is opaque to ultraviolet light (wavelength <320 nm) due to its band gap of ~ 4 eV and to infrared light because of free carrier absorption; on the other hand, the monolayer graphene has an optical transparency of $\sim 97.7\%$ over the entire solar spectrum, with the addition of each layer corresponding to a $\sim 2.3\%$ decrease in transparency. For graphene, the increase in layers leads to a decrease in optical transparency but an increase in conductivity; thus there should be a balance when it comes to graphene layers. The main limitation faced by graphene is its lack of an intrinsic band gap. This limitation can be alleviated through functionalization. Due to the excellent transparency, high carrier mobility and chemical stability, graphene and rGO have been applied to act as the anode of dye sensitized solar cells (DSSCs), heterojunction silicon solar cells and organic solar cells (OSCs) (Fig. 16a–c),[160–165] the cathode of heterojunction photovoltaic solar cells and OSCs,[166–169] the charge transport layer of DSSCs and OSCs,[170–173] and the intermediate layer of tandem OSCs.[174,175] Graphene has also been used to serve as the active layer of OSCs for light harvesting/accepting since its 2D structure and high aspect ratio can facilitate the desired donor/acceptor interface formation for charge separation and charge transfer.[176,177] Functionalized graphene has been applied as the counter electrode of DSSCs due to the large density of lattice defects and oxygen-containing functional groups.[178,179] Chemically doped graphene has been applied for Schottky-junction solar cells, and the presented high performance is because the doping-induced shift in the graphene's chemical potential increases the graphene's carrier density and enhances the cell's built-in potential.[180–182] The reported solar cells based on graphene

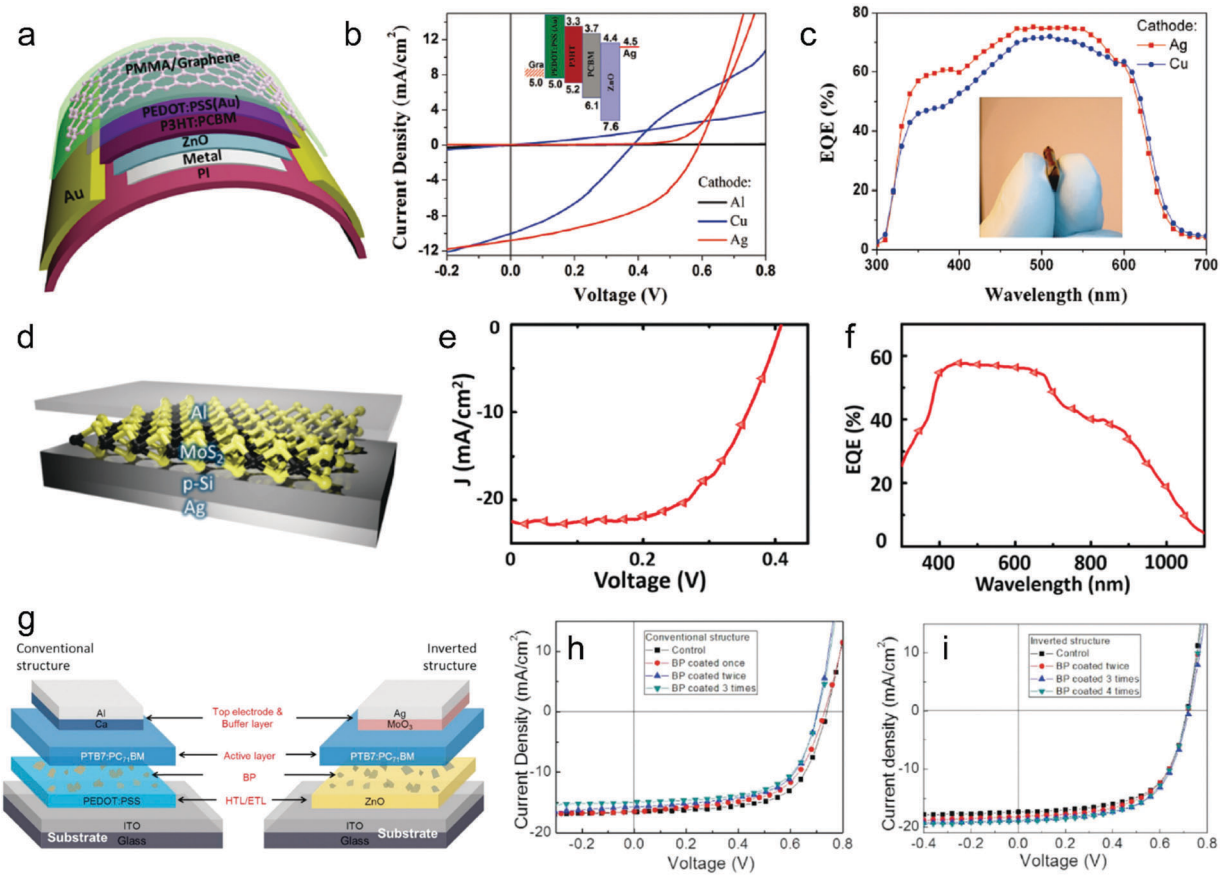

Fig. 16 2D materials for solar cells. (a) Schematic diagram showing the detailed structure of the organic solar cell. (b and c) The (b) J–V characteristics and (c) EQEs of solar cells with different metals as cathode and monolayer graphene as anode. Reproduced with permission from ref. 160. Copyright 2013, John Wiley & Sons, Inc. (d) Schematic illustration showing the structure of the MoS_2/p-Si heterojunction solar cell. (e and f) The (e) J–V characteristics and (f) EQE spectrum of the solar cell. Reproduced with permission from ref. 185. Copyright 2014, American Chemical Society. (g) Schematic illustrations showing the structures of organic solar cells with and without BP incorporation. (h–i) The J–V characteristics of the organic solar cells (h) without and (i) with BP. Reproduced with permission from ref. 195. Copyright 2016, John Wiley & Sons, Inc.

and its derivatives have a power conversion efficiency of up to ~10.34%.

Like graphene, the band gaps of some 2D TMDs are also layer-dependent (*e.g.*, monolayer MoS_2 has a direct band gap of ~1.8 eV while bulk MoS_2 has an indirect band gap of ~1.3 eV) and this kind of tunable energy levels enable them to be coupled with various donor/acceptor systems in OSCs. Compared with graphene, semiconducting 2D TMDs such as MoS_2, WS_2, $MoSe_2$, and WSe_2 have more suitable band gaps that are predicted to absorb up to 5–10% of incident sunlight, which is about one order of magnitude higher than that of Si or GaAs with the same thickness (below 1 nm). In this regard, 2D TMDs have been applied as the photoactive semiconductor layer in Schottky or p–n junctions (Fig. 16d–f).[183–189] Besides, 2D TMDs have also been used for the catalytic counter electrode in DSSCs and the hole-extraction layer in OSCs due to their good catalytic activity and hole-extraction capability.[190–193] Although solar cells based on 2D TMDs are predicted to have high solar energy conversion efficiencies, the reported experimental power conversion efficiencies (0.1–8.11%) are still low compared with those of conventional solar cells based on silicon (15–30%).

Phosphorene and its derivatives have balanced properties between graphene and 2D TMDs, with high optical transparency, good charge carrier mobility and excellent electronic properties. Phosphorene has been demonstrated to serve as the light absorber and charge transfer layer in solar cells, with enhanced light absorption and electron recombination (Fig. 16g–i).[194,195] The reported solar cells based on phosphorene exhibited a power conversion efficiency of up to ~8.25%. Theoretical works have shown that phosphorene is a promising material for solar cells with good stability and high power conversion efficiency (as high as ~20%).[196,197] However, there is still a lack of experimental demonstrations revealing the use of phosphorene in solar cells with corresponding extraordinary properties.

Graphene is a candidate to replace ITO electrodes in flexible solar cells, due to its excellent flexibility, transparency over the entire solar spectrum, high electron mobility and chemical stability. 2D TMDs have tunable band gaps and are predicted to absorb more incident sunlight than conventional Si or GaAs with the same thickness. Phosphorene has balanced properties between graphene and 2D TMDs, and can bridge the gap between these two kinds of materials. All these 2D materials are promising for wearable solar cells, but right now the power conversion efficiencies of the corresponding solar cells are still not comparable to those of conventional solar cells based on silicon. Therefore, efforts are required to further improve the performance of 2D material based solar cells; for example, optimizing the incorporation of 2D materials may lead to enhancement of light absorption, charge collection, and efficient exciton dissociation.

4.2 Mechanical energy harvesters based on 2D materials

Human motion produces kinetic energy that can be converted into electricity. Harvesting biomechanical energy is an important approach to provide electricity for wearable electronics. The piezoelectric nanogenerator and triboelectric nanogenerator are two common energy harvesters for scavenging biomechanical energy because of their advantages such as light weight and high energy conversion efficiency. 2D materials have been used for these two types of nanogenerators.

4.2.1 Piezoelectric nanogenerators. Graphene and its derivatives have been applied in piezoelectric nanogenerators for two main roles. One role is acting as the electrode of piezoelectric nanogenerators due to their excellent flexibility, carrier mobility and transparency.[198–203] Kwon *et al.* reported a flexible and semi-transparent piezoelectric nanogenerator based on $PbZr_{0.52}Ti_{0.48}O_3$ with graphene as the electrode, which showed an output voltage of ~2 V, a current density of ~2.2 μA cm^{-2}, and a power density of ~88 mW cm^{-3} at an applied force of 0.9 kgf (Fig. 17a–c).[201] The other role is serving as an additive to the conventional piezoelectric materials to enhance the performance.[204–210] Graphene has zigzag-structured carbon atoms that match the zigzag-structured β phase of the PVDF. The hydrophilic interaction between the CF_2 in PVDF and the –C═O and COOH groups in GO leads to the attachment of PVDF chains to the GO. Hence, the addition of graphene or GO to the PVDF matrix can enhance the nucleation of β phase crystals and thereby improve the performance of piezoelectric nanogenerators. Yaqoob *et al.* reported a tri-layer piezoelectric nanogenerator based on PVDF, barium titanate, and surface-modified n-type graphene, which shows a current of 1.5 μA at a force of 2 N and an instantaneous power of 5.8 mW (Fig. 17d–f).[210] The n-type graphene enhances the outputs of the piezoelectric nanogenerator by aligning the dipoles in one direction. In addition, although graphene is non-piezoelectric, it has been discovered theoretically that piezoelectricity can be generated in doped graphene with atoms on one side, where the doping atoms break the inversion symmetry of graphene.[211]

2D TMDs (monolayer or few layers) such as MoS_2, $MoSe_2$, $MoTe_2$, WS_2, WSe_2, and WTe_2 are found to have piezoelectricity, which is different from their bulky counterparts that are not expected to be piezoelectric because of the presence of an interlayer inversion center.[212–214] The observed piezoelectricity can be attributed to the strain induced lattice distortion and the associated ion charge polarization of the mono- or few-layer TMDs. The magnitude of the piezoelectricity strongly depends on the number of layers, usually decreasing when more than two layers are present (Fig. 17g).[215,216] The most experimentally studied 2D TMD material for piezoelectricity is MoS_2.[214–218] The reported piezoelectric nanogenerators based on MoS_2 showed an open-circuit voltage on the order of ~15 mV, a short-circuit current on the order of ~20 to 65 pA, a power density of up to ~2 mW m^{-2} and an energy conversion efficiency of up to ~5.08%.[214,216] The reported piezoelectric nanogenerators based on other 2D TMDs showed electrical outputs at levels similar to those of MoS_2. Lee *et al.* reported that WSe_2 bilayers fabricated through turbostratic stacking have reliable piezoelectric properties (Fig. 17h and i).[219] The fabricated piezoelectric nanogenerator exhibited an output voltage of 45 mV, a short-circuit current of 100 pA and a maximum instantaneous power of 2.54 pW. Compared with traditional piezoelectric nanogenerators based on $Pb(Zr_xTi_{1-x})O_3$, the energy conversion

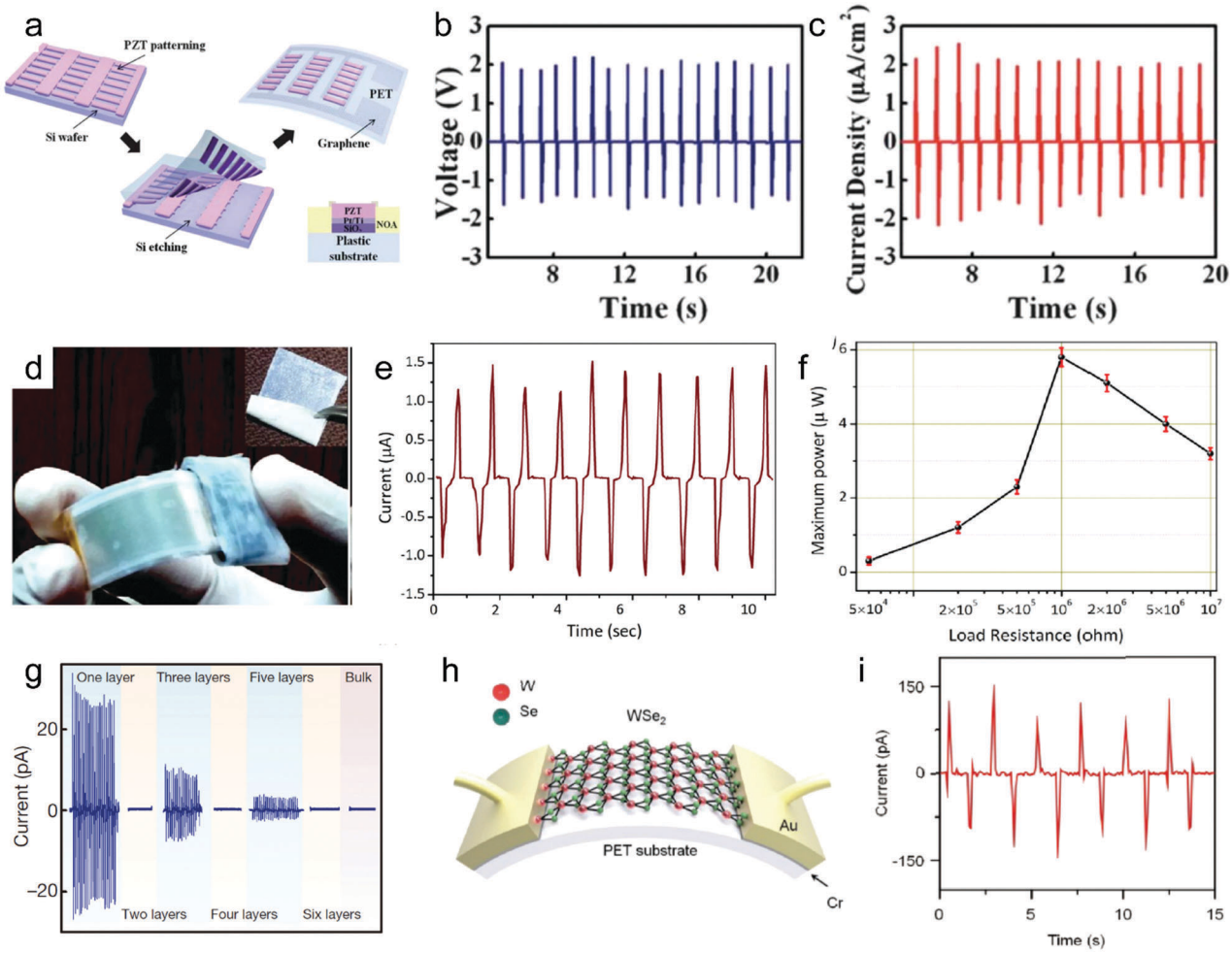

Fig. 17 Piezoelectric nanogenerators based on 2D materials. (a) Schematic overview of the fabrication process for the piezoelectric nanogenerator. (b and c) The output (b) voltage and (c) current density of the piezoelectric nanogenerator. Reproduced with permission from ref. 201. Copyright 2012, the Royal Society of Chemistry. (d) Photograph of the piezoelectric nanogenerator under bending. (e and f) The output (e) current and (f) instantaneous power of the piezoelectric nanogenerator. Reproduced with permission from ref. 210. Copyright 2017, Elsevier Ltd. (g) Evolution of the piezoelectric outputs with increasing number of MoS_2 atomic layers. Reproduced with permission from ref. 216. Copyright 2014, Nature Publishing Group. (h) Schematic illustration of the piezoelectric nanogenerator based on monolayer WSe_2. (i) The short-circuit current response of the monolayer WSe_2 under periodic tensile strain. Reproduced with permission from ref. 219. Copyright 2017, John Wiley & Sons, Inc.

efficiency of piezoelectric nanogenerators based on 2D TMDs (*e.g.*, MoS_2: 5.08%) is about one order of magnitude lower. Therefore efforts are required to further improve the energy conversion efficiencies of these piezoelectric nanogenerators, which may be achieved by improving the interface properties and optimizing the device structure.

Other 2D materials such as hexagonal BN and phosphorene have also been discovered theoretically to possess piezoelectricity.[220–223] However, there have been few experimental studies on them.

4.2.2 Triboelectric nanogenerators. Graphene and its derivatives have been applied in triboelectric nanogenerators and they mainly serve as the electrode or the triboelectric layer, which endow the triboelectric nanogenerators with features such as thin thickness, transparency, flexibility or even stretchability (*e.g.*, crumpled graphene).[224–231] Nanjegowda *et al.* reported a triboelectric nanogenerator based on graphene that is transferred from copper to a polymer substrate by a roll-to-roll method (Fig. 18a–c).[230] The triboelectric nanogenerator showed a current density of $\sim$0.075 μA cm^{-2} at a frequency of 4.3 Hz. When graphene is used as the electrode, its lower conductivity compared with bulk metal films has little negative impact on the performance because of the large internal impedance of triboelectric nanogenerators (usually on the order of tens or hundreds of MΩ).[232,233] Graphene is not a desirable material for the triboelectric layer since it is less triboelectrically active compared with the commonly used triboelectric layers such as polytetrafluoroethylene (PTFE), Kapton, rubber, Al, and nylon. But it has been reported that aligned graphene sheets embedded in PDMS can improve the surface triboelectric charge density and thereby enhance the performance of the triboelectric nanogenerator.[234] Moreover, an rGO/polyimide composite has been introduced into the triboelectric layer (beneath the negatively charged dielectric surface) to help trap electrons and increase the triboelectric

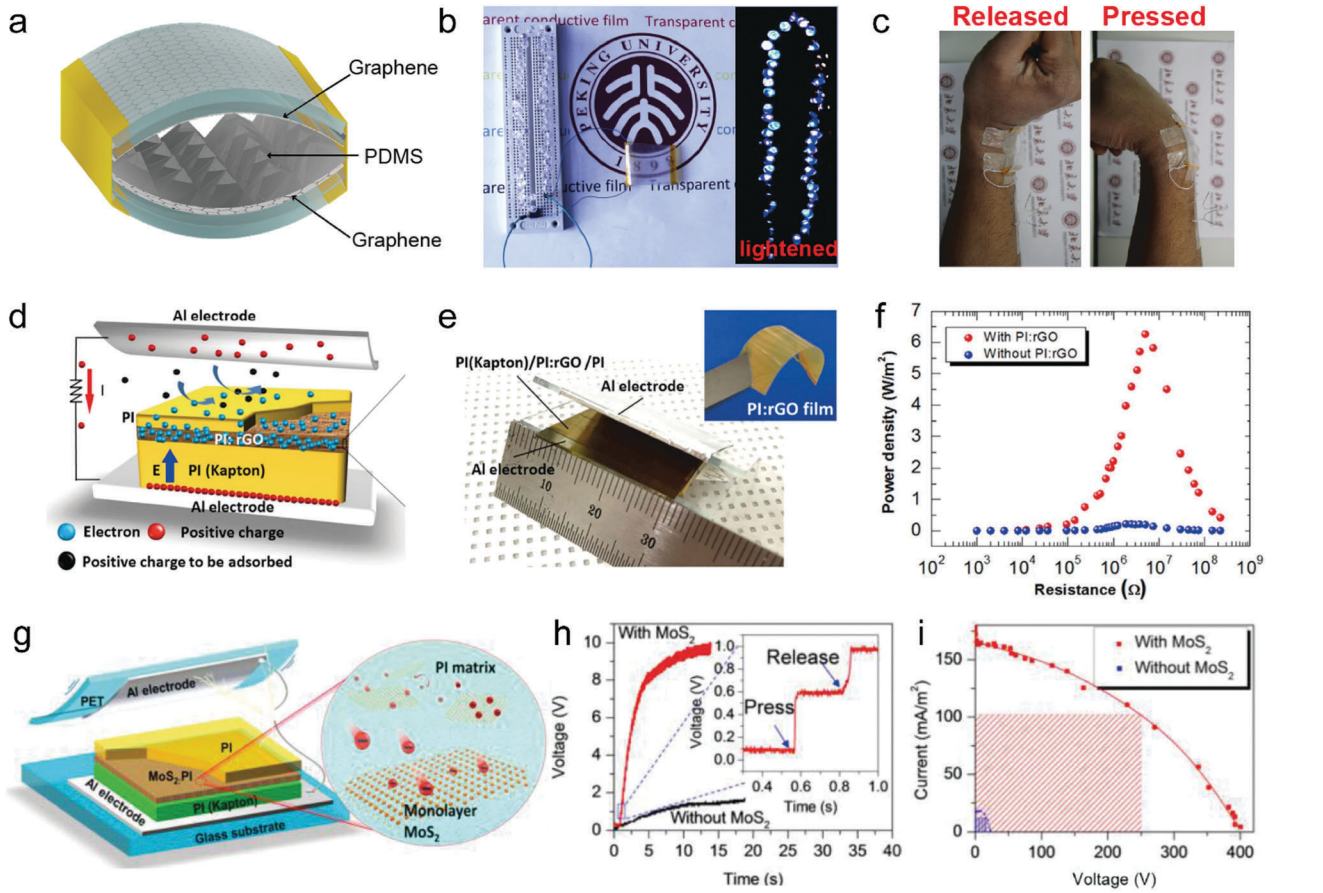

Fig. 18 Triboelectric nanogenerators based on 2D materials. (a) Schematic diagram of the graphene/EVA/PET based triboelectric nanogenerator. (b) Photographs showing 56 LED bulbs lighted up by the triboelectric nanogenerator. (c) Photographs showing the nanogenerator mounted on the wrist to harvest biomechanical energy. Reproduced with permission from ref. 230. Copyright 2015, John Wiley & Sons, Inc. (d) Schematic illustration of the triboelectric nanogenerator with a polyimide (PI):rGO film. (e) Photographs showing the fabricated flexible triboelectric nanogenerator. (f) Dependence of the output power density on the external load resistance. Reproduced with permission from ref. 235. Copyright 2017, Elsevier Ltd. (g) Schematic illustration of the triboelectric nanogenerator with monolayer MoS_2. (h and i) The (h) charging processes and (i) peak current as a function of the peak voltage for the triboelectric nanogenerators with and without monolayer MoS_2. Reproduced with permission from ref. 236. Copyright 2017, American Chemical Society.

charge density (Fig. 18d–f). The power density of the triboelectric nanogenerator with rGO is $\sim$6.3 W m^{-2}, which is about 30 times higher than that without it.[235]

Recently, MoS_2 has also been applied in the negatively charged dielectric layer to serve as the triboelectric electron-acceptor layer and enhance the output performance (Fig. 18g–i).[236] The triboelectric nanogenerator modified with MoS_2 showed an open-circuit voltage of $\sim$120 V, a power density of 25.7 W m^{-2}, and improved cyclic stability. It is predicted that other 2D materials may also be promising for providing electron-trapping sites for triboelectric nanogenerators and enhancing their performance.

Graphene and its derivatives have been applied as the electrodes of flexible piezoelectric and triboelectric nanogenerators, and also as additives to enhance the performance of these two types of nanogenerators. Some 2D TMDs show layer-dependent higher piezoelectricity than their bulky counterparts, and more experimental studies are still needed to demonstrate the theoretically predicted piezoelectric properties of other 2D TMDs. MoS_2 has been used as an additive layer to enhance the performance of triboelectric nanogenerators and it is predicted that other 2D materials may also be able to improve the performance of triboelectric nanogenerators.

4.3 Thermoelectric nanogenerators based on 2D materials

The idea of converting human body heat into electricity has been tantalizing researchers for years. A resting human male gives off approximately 100–128 Watts of energy as heat. Harvesting body heat energy is an important route toward green and sustainable wearable power sources. Currently, the favored technology to harvest body heat energy is the thermoelectric nanogenerator, which generates electricity from the temperature difference between the human body and the ambient environment. The performance of the thermoelectric nanogenerator relies on the thermoelectric figure of merit of the material, which is given by

$$ZT = \frac{\sigma S^2 T}{\kappa} \quad (1)$$

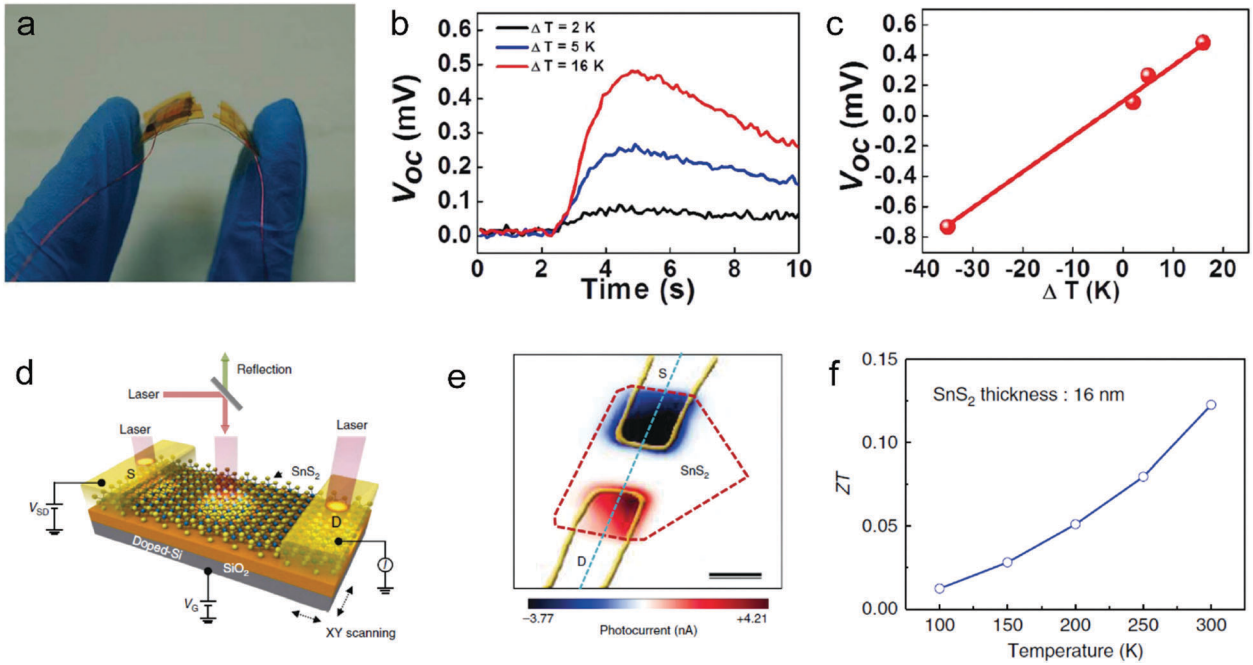

Fig. 19 2D materials for harvesting thermal energy. (a) Photograph of the flexible thermoelectric nanogenerator based on the MoS_2/graphene nanocomposite. (b) The output voltage of the thermoelectric nanogenerator under various temperature differences. (c) Dependence of the output voltage on the temperature difference. Reproduced with permission from ref. 248. Copyright 2017, IOP Publishing Ltd. (d) Schematic illustration of the thermoelectric nanogenerator under the photo-thermoelectric measurement setup. (e) Scanning photo-thermoelectric current imaging demonstrating the thermocurrent-dominated profile. (f) Calculated *ZT* values for temperatures from 100 to 300 K. Reproduced with permission from ref. 251. Copyright 2016, Nature Publishing Group.

where σ, S and κ are the electrical conductivity, the Seebeck coefficient and the thermal conductivity of the material respectively. It can be seen that a higher Seebeck coefficient, larger electron conductivity and smaller thermal conductivity all contribute to a higher *ZT*.

Graphene has a reported Seebeck coefficient of ~40 to 180 μV K^{-1} at ~250 to 300 K and thermal conductivity of ~2000 to 5000 W m^{-1} K^{-1} at 300 K.[237–244] Although the relatively low Seebeck coefficient and high thermal conductivity limit the use of graphene as a thermoelectric material, it has been reported that graphene or rGO added to other thermoelectric materials can enhance the power factor (PF = σS^2).[245–248] Xie *et al.* reported a flexible thermoelectric nanogenerator based on the MoS_2/graphene nanocomposite (Fig. 19a–c).[248] This thermoelectric nanogenerator exhibited higher performance than that without graphene, with an output voltage of −0.73 mV under a temperature difference of −35 K and a power density of 8.8 nW cm^{-2}.

Some other 2D materials have been found to possess higher *ZT* than their bulky counterparts.[249–251] For example, it has been discovered by Lee *et al.* that 2D SnS_2 has higher electrical conductivity and lower thermal conductivity than its bulky counterpart, and the Seebeck coefficient of the 16 nm-thick 2D SnS_2 materials is 34.7 mV K^{-1} at 300 K (Fig. 19d–f).[251] The negative correlation between the electrical conductivity and thermal conductivity of such 2D materials makes them promising for thermoelectric nanogenerators, but there's still a lot of work, both theoretical and experimental, to be done to turn that promise into reality.

Graphene's relatively low Seebeck coefficient and high thermal conductivity limit its use as a thermoelectric material, but it can be used as an additive to other thermoelectric materials to improve the power factor; some 2D layered IV–VI metal chalcogenides are found to have higher thermoelectricity than their bulky counterparts, but lots of efforts are still required to demonstrate their wearable applications.

4.4 Other types of energy harvesters based on 2D materials

Graphene and its derivatives have also been applied to generate electricity from other types of ambient energy sources, such as moisture and water drops.[252–256]

GO with oxygen-containing groups has been used in energy harvesters that produce electricity from ambient moisture. Zhao *et al.* reported an energy harvester to generate electricity from moisture diffusion based on GO film. The concentration gradient of the oxygen-containing groups in the GO provides an ionic gradient under adsorbed moisture, which leads to a periodic electric output when humidity varies (Fig. 20a).[252] This energy harvester showed an output voltage of ~35 mV, a power density of ~4.2 mW m^{-2}, and an energy conversion efficiency of up to ~62%. It was demonstrated to generate electricity from human respiration (Fig. 20b–e). To act as wearable power sources, the electrical outputs of this energy harvester still need to be improved, and it should be combined with energy storage devices to directly power wearable electronics. For use as a self-powered respiration sensor, long-term cycle stability is required. Some concentration cells based on GO have also been

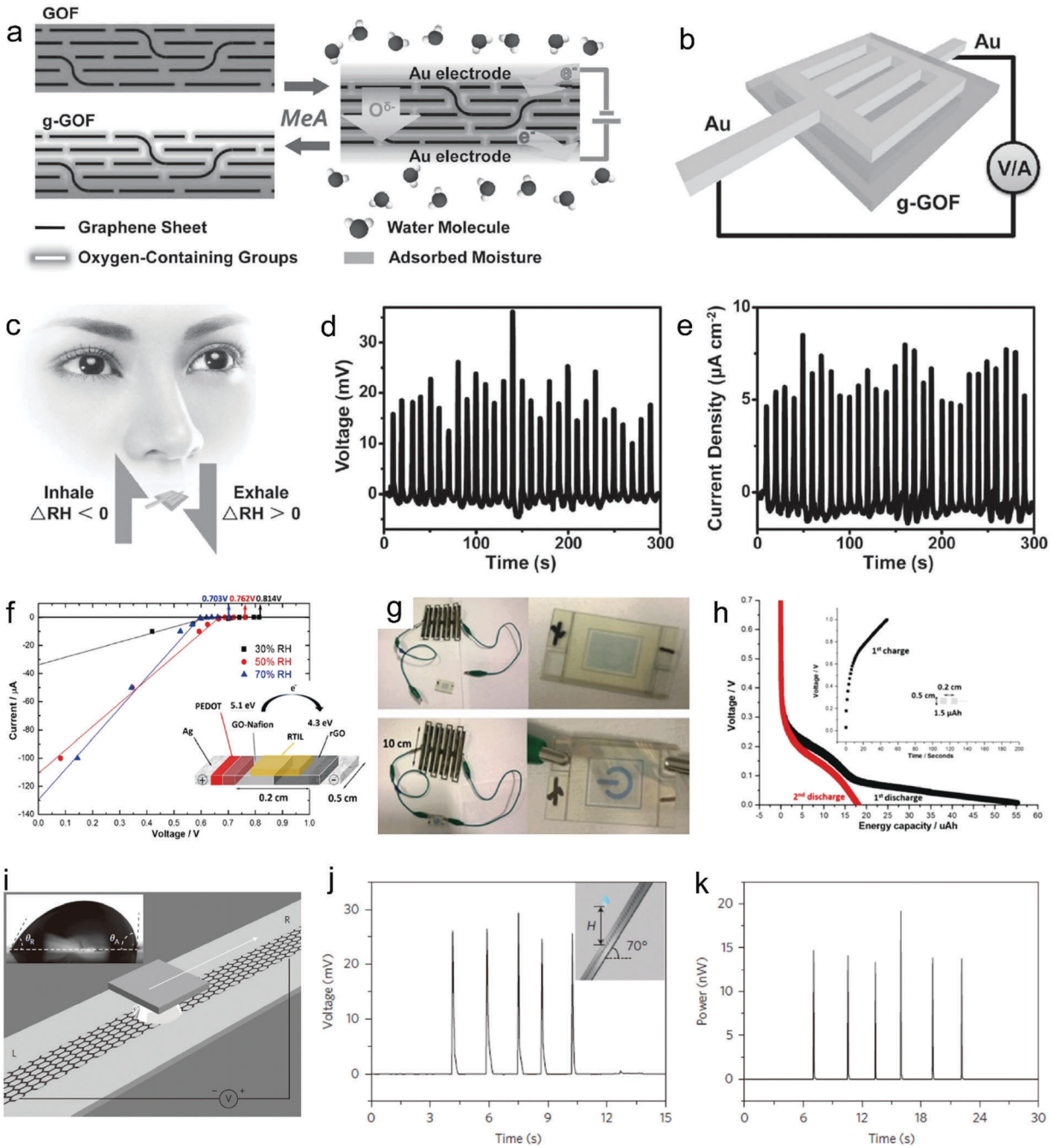

Fig. 20 2D materials for harvesting other types of energy. (a) Schematic illustration showing the moisture-electric annealing process of GO film with applied voltage under a humid environment. The $O^{\delta-}$ represents the oxygen-containing ions. (b) Schematic diagram showing the structure of the energy harvester. (c) Schematic illustration showing the energy harvester driven by human breathing. (d and e) The output (d) voltage and (e) current density generated by respiratory moisture-tide with a ΔRH of ~21%. Reproduced with permission from ref. 252. Copyright 2015, John Wiley & Sons, Inc. (f) *I*–*V* characteristics of the PEDOT/GO-Nafion/rGO concentration cell that was coated on the polymer substrate with a room temperature ionic liquid (RTIL) under different relative humidity (RH) of 30%, 50% and 70%. Insets: Structure of the GO concentration cell. (g) Discharge of the GO concentration cell printed in series on a polyethylene naphthalate (PEN) substrate under an ambient environment. (h) The first and second discharge at 1 μA and the inset picture shows the first charge at 100 μA with a size of 2 × 10 cm at an RH of 70%. Reproduced with permission from ref. 258. Copyright 2015, Nature Publishing Group. (i) Schematic illustration showing electricity generated by moving an ionic water drop on graphene. (j and k) The (j) voltage and (k) power produced by dropping droplets of 0.6 M $CuCl_2$ solution onto graphene at an angle of 70°. Reproduced with permission from ref. 255. Copyright 2014, Nature Publishing Group.

used to generate electricity from moisture.[257,258] Wei *et al.* reported a GO based concentration cell that was demonstrated on an arbitrary insulating substrate (*e.g.*, polymer sheet/paper) by coating poly(3,4-ethylenedioxythiophene) (PEDOT), GO ink and rGO on Ag charge collectors (Fig. 20d–f).[258] The generated electricity from humidity depends on the device size.

When integrated with a room temperature ionic liquid (RTIL), one unit cell with a length of 0.5 cm can generate an energy capacity of 30 A h L^{-1} and a voltage of up to 0.7 V. With a power density of up to 0.4 W cm^{-3} and an energy density of 4 W h L^{-1}, the GO based concentration cell was demonstrated to drive an electrochromic device. A disposable energy source made of GO was also written on a plastic glove to demonstrate its wearability. This work provides new platforms for futuristic wearable electronics.

It has been discovered that the relative motion between graphene and ionic or non-ionic water can produce electricity, explained by various mechanisms. Dhiman *et al.* reported that an output power of ~85 nW was generated when a ~0.6 M HCl solution flows over graphene at a speed of ~0.01 m s^{-1}, and they proposed that the power generation may be attributed to the surface ion hopping mechanism.[254] Yin *et al.* reported that electricity can be generated by moving ionic water over monolayer graphene. They proposed that the adsorption of Na^+ ions at the front boundary and the desorption of Na^+ ions at the rear boundary of the ionic droplet drive free electrons to move across graphene under the droplet from the rear end to the front end. Dropping ionic water onto a 70° tilted graphene surface produces a voltage of ~30 mV, a current of ~1.7 μA and a power of ~19.2 nW (Fig. 20f–h).[259] Kwak *et al.* introduced a PTFE layer beneath the ionic water droplet and graphene, which led to an improved performance with an output voltage, current and power of ~1.1 V, ~8 μA, and ~1.9 μW respectively.[260] Lee *et al.* reported that a voltage of ~48.2 μV was generated when nonionic water flows over graphene with a velocity of 0.1 m s^{-1}. They suggested that distilled water is a polar liquid that can form "ordered" structures near hydrophobic interfaces, and these "ordered" structures can interact with charge carriers in graphene, leading to charge redistribution. This charge redistribution in graphene results in a potential difference, and a consistent voltage is generated with the distilled water flowing over graphene.[259] The nanogenerators based on non-ionic water/graphene have an output voltage of up to ~0.1 V.[259,261] Although the mechanism seems unclear, this kind of energy harvesters may have the potential for wearable applications because of the excellent flexibility of graphene. For example, graphene based raincoats may be developed to harvest energy from the raindrops. However, the delivered power needs to be further enhanced, and suitable device designs are also needed.

In conclusion, GO has been used to produce electricity from ambient moisture diffusion, which can be applied to harvest energy from human respiration or serve as self-powered respiration sensors. Relative motion between water and graphene can generate electricity, which shows the potential for wearable power sources.

5. Conclusions and future prospects

With the rapid development of power-hungry wearable smart devices and flexible electronics, wearable energy sources with high energy density and power density, operational safety, long-term stability, in addition to mechanical flexibility, light weight, thin thickness, and low cost are in urgent need.

Emerging 2D materials open a new window for developing wearable energy sources. On the one hand, the atomic-scale thickness of the mono- or few-layered 2D materials renders them flexibility, which enables them to meet the criteria including flexibility and thin thickness. On the other hand, 2D materials show extraordinary properties differing from their bulky counterparts. These unique properties give them an edge in certain energy devices, which are summarized as follows. (1) The high carrier mobility, chemical inertness and lightweight property make graphene desirable to serve as the conducting additives and current collectors for energy storage devices, and with its transparency in the whole solar spectrum, it is also desirable to act as the electrode of energy harvesters such as solar cells. Graphene including rGO with hierarchical or porous interconnected structures can help improve the performance of batteries by facilitating the storage and transport of ions, buffering the volume expansion of electrode materials and enhancing the surface/interface ion storage properties. Graphene nanosheets vertically grown on current collectors can enhance the high-frequency operation of EDLCs due to their exposed and accessible edge planes that lead to minimal porosity effects and high conductivity. Doped graphene can further improve the supercapacitor performance by improving the conductivity and introducing additional pseudocapacitive contributions. Due to the unimpeded permeation of humidity through GO,[262] GO with oxygen containing groups can be applied to generate electricity from ambient moisture. (2) 2D TMDs such as MoS_2 show improved performance for LIBs compared with their bulky counterparts due to the shorter diffusion path length for Li^+ ions, enlarged surface active sites and prevention of pulverization of active materials during cycling. 2D TMDs are also promising for solar cells because they have tunable band gaps and can theoretically absorb more incident sunlight than conventional Si or GaAs with the same thickness. Some 2D TMDs such as MoS_2 present layer-dependent higher piezoelectricity than their bulky counterparts. Some 2D IV–VI metal chalcogenides such as SnS_2 show higher thermoelectricity than their bulky counterparts. (3) MXenes have a unique structure that endows them with advantages for energy storage: their conductive transition metal carbide layer can allow fast electron supply to electrochemically active sites; they have transition metal oxide-like surface that is redox-active; and their 2D morphology and pre-intercalated water can permit fast ion transport. (4) BP has a high theoretical specific capacity of 2596 mA h g^{-1} for LIBs, which is approximately 7 times that of the widely used graphite (372 mA h g^{-1}). Phosphorene also has a theoretical solar power conversion efficiency of as high as ~20% and good stability for solar cells. Fig. 21 presents the evaluated performance of 2D material based wearable energy sources involved in this review in comparison to their peers based on conventional materials. The quantified scoring is presented in the form of spider charts, which can be used as a reference for researchers to visually see which energy devices each class of 2D materials are suitable for.

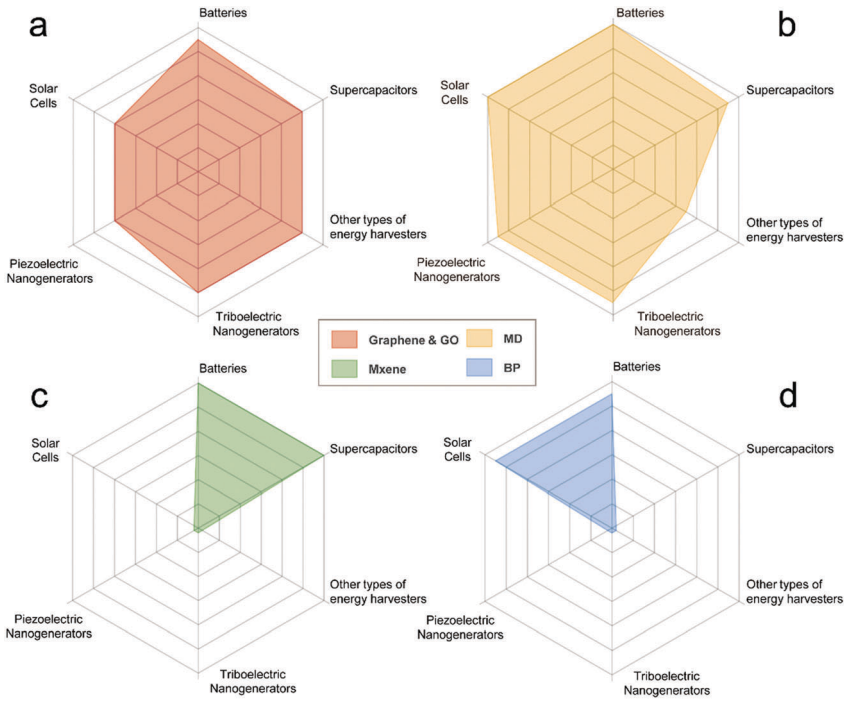

Fig. 21 Schematic illustration of the evaluated performance of wearable energy sources based on 2D materials. Each kind of material, (a) graphene and GO, (b) metal dichalcogenides (MDs, including TMDs: MoS_2, WS_2, VS_2, $MoSe_2$, and IV–VI MDs: SnS_2), (c) MXenes, (d) black phosphorus (BP), has been evaluated in terms of device performance (batteries; supercapacitors; solar cells; triboelectric nanogenerators; piezoelectric nanogenerators; and other types of energy harvesters including thermoelectric nanogenerators and energy harvesters scavenging energy from moisture). Note that the device performance of wearable energy sources based on 2D materials mentioned in this review was evaluated in comparison with that of the same kind of devices based on conventional materials. Excellent, good, general and poor device performance are scored 5.5–6, 4–5.4, 1–3.9 and <1, respectively. Scale: each ring counts 1 and the full mark is 6.

The research of 2D materials started in around 2004, the year that scientists successfully gained monolayer graphene. Over the past few decades, the number of published journal articles about 2D materials each year has been consistently increasing (Fig. 22a). With researchers delving deeper into 2D materials' synthesis and property, the proportion of publications devoted to the field of energy keeps expanding. Compared with journal articles, patents are more critical for entrepreneurs to gain strategic advantages. The number of issued worldwide patents about wearable energy sources based on 2D materials has also been increasing rapidly (Fig. 22b), suggesting ongoing product development and vast prospects for future industrialization.

As for future research, many challenges need to be addressed and a lot of work needs to be done for wearable energy sources based on 2D materials.

From the perspective of material, efforts are required to further improve the synthesis methods, and fundamental studies are still required to better understand the physics behind the unique properties. (1) The restacking of 2D materials is a big challenge for their use in energy storage devices. This challenge could be addressed by growing vertically oriented 2D materials on current collectors and synthesizing 2D materials with hierarchical or porous interconnected structures. (2) The yields of 2D materials with the current synthesis methods

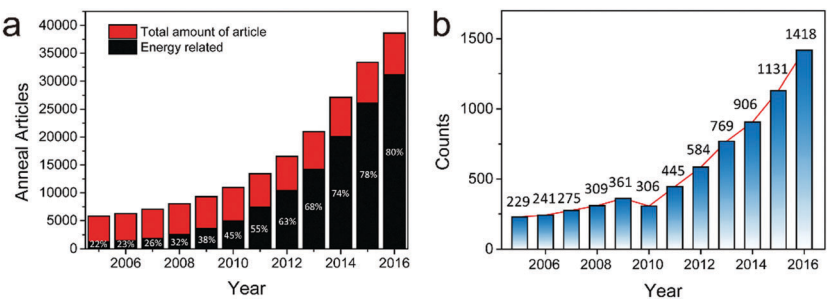

Fig. 22 (a) Journal publication trends in 2D materials and their energy source related research (2005–2016), data queried from Web of Science™. (b) The issued worldwide patents related to wearable energy sources based on 2D materials per year (2005–2016), data queried from Derwent Innovations Index™.

(*e.g.* CVD, solution exfoliation, mechanical exfoliation, *etc.*) are still low. Therefore, exploring new preparation approaches and improving the existing synthesis processes are needed, with precise manipulation over the crystallographic structures along with the thickness. For industrialization, low-cost and large-scale production methods that yield 2D materials with desired qualities need to be developed. (3) A full understanding of the physics behind the unique properties of 2D materials can not only help manipulate their structures and properties during the synthesis process but can also help design energy devices with high performance. Thus, with the new born members and novel properties of 2D materials, it is essential to promote the relevant fundamental studies.

From the perspective of device, lots of efforts are still required to improve the device design, fabrication and performance. (1) It is preferable to avoid the etching of substrates and transfer processes of 2D materials during device fabrication while maintaining the device performance, and to achieve this, suitable device designs and material synthesis methods are required. (2) The performance and safety (especially the energy storage devices) of the wearable energy devices should be maintained during the possible deformation such as bending and folding. Some efforts are still needed to improve the fabrication processes of the energy storage devices such as developing high-performance solid electrolytes and improving the packaging techniques. (3) The incorporation of different 2D materials may achieve synergetic properties that lead to better performance of energy devices. For example, an optimized incorporation of 2D materials for solar cells may result in improvements in light absorption, charge collection and efficient exciton dissociation. (4) Some wearable energy sources (*e.g.*, piezoelectric and thermoelectric nanogenerators) based on 2D materials (*e.g.*, MoS_2 and SnS_2) are still at the stage of fundamental research, and efforts are needed to demonstrate their wearable applications. Moreover, the energy conversion efficiencies of the energy harvesters based on 2D materials still need to be improved. (5) It is a beautiful vision that wearable devices can be powered sorely by the energy harvested from the ambient environment, without frequent charging or replacement of power supply components. This vision could be achieved by a sustainable power system that combines the energy storage device with the energy harvester, where the energy scavenged from the environment is higher than that consumed by the wearable devices. For a high-performance sustainable power system, wearable energy storage devices with excellent cycle lifetime and high energy and power densities as well as wearable energy harvesters with high energy conversion efficiencies need to be developed. Moreover, power management would be required to improve the storage efficiency of the harvested energy and optimize the generated electrical outputs when several types of energy harvesters are combined together.

With their extraordinary properties, 2D materials offer new routes toward wearable energy sources. 2D material based wearable energy sources have certain unparalleled advantages over energy sources based on conventional materials. Although challenges still remain, it is predicted that wearable energy sources based on 2D materials would herald the coming of a new generation of wearable electronic systems.

Abbreviations

2D	Two-dimensional
Al	Aluminum
B	Boron
Li	Lithium
N	Nitrogen
Na	Sodium
Li–S	Lithium–sulfur
VS_2	Vanadium disulfide
FTO	Fluorine-doped tin oxide
ITO	Tranditional indium tin oxide
BP	Black phosphorus
TMD	Transition metal dichalcogenide
TMO	Transition metal oxide
MXene	Transition metal carbides and carbonitride
FTO	Fluorine-doped tin oxide
G	Graphene
rGO	Reduced graphene oxide
f-rGO	Functionalized rGO
GAs	Graphene aerogels
GCP	Graphene-cellulose paper
GF	Graphene foam
GNHPG	Graphene nanoribbons on highly porous 3D graphene
GO	Graphene oxide
GWF	Graphene woven fabric
HPGA	Hierachical porous graphene aerogel
HsGDY	Hydrogen-substituted graphdiyne
LCGO	Liquid crystalline graphene oxide
NGMn	N-Doped rGO/MnO_2 nanosheet
n-Gr	n-Type graphene
CNP	Carbon nanotube paper
Si NWs	Silicon nanowires
PANI	Polyaniline
PDMS	Poly(dimethylsiloxane)
PTFE	Polytetrafluoroethylene
PVA	Polyvinyl acetate
PVDF	Poly(vinylidenefluoride)
EDLC	Electric double-layer capacitor
LIB	Lithium ion battery
SIB	Sodium-ion battery
CVD	Chemical vapor deposition
RTIL	Room temperature ionic liquid
DSSC	Dye sensitized solar cell
OSC	Organic solar cell

Conflicts of interest

There are no conflicts to declare.

Acknowledgements

This work was financially supported by the National Basic Research Program of China (No. 2016YFA0200101 and 2014CB932500), the National Natural Science Foundation of China (No. 51432002, 51520105003 and 51362029), and the National Postdoctoral Program for Innovative Talents (BX201600001).

Notes and references

1 C. Narayanaswami, N. Kamijoh, K. Yamazaki, M. Raghunath, T. Inoue, T. Cipolla, J. Sanford, E. Schlig, S. Venkiteswaran and D. Guniguntala, *Computer*, 2002, **35**, 33–41.
2 P. Bonato, *Engineering in Medicine & Biology Magazine IEEE*, 2010, vol. 29, pp. 25–36.
3 R. Want, B. N. Schilit and S. Jenson, *Computer*, 2015, **48**, 28–35.
4 D.-H. Kim, N. Lu, R. Ma, Y.-S. Kim, R.-H. Kim, S. Wang, J. Wu, S. M. Won, H. Tao, A. Islam, K. J. Yu, T.-i. Kim, R. Chowdhury, M. Ying, L. Xu, M. Li, H.-J. Chung, H. Keum, M. McCormick, P. Liu, Y.-W. Zhang, F. G. Omenetto, Y. Huang, T. Coleman and J. A. Rogers, *Science*, 2011, **333**, 838–843.
5 Y. Fu, X. Cai, H. Wu, Z. Lv, S. Hou, M. Peng, X. Yu and D. Zou, *Adv. Mater.*, 2012, **24**, 5713–5718.
6 J. H. Lee, K. Y. Lee, M. K. Gupta, T. Y. Kim, D. Y. Lee, J. Oh, C. Ryu, W. J. Yoo, C. Y. Kang, S. J. Yoon, J. B. Yoo and S. W. Kim, *Adv. Mater.*, 2014, **26**, 765–769.
7 Z. Liu, J. Li and F. Yan, *Adv. Mater.*, 2013, **25**, 4296.
8 W. Jie, S. Li, Y. Fang, Y. Zi, J. Lin, X. Wang, Y. Xu and L. W. Zhong, *Nat. Commun.*, 2016, **7**, 12744.
9 R. Trestian, A. N. Moldovan, O. Ormond and G. M. Muntean, *Network Operations and Management Symposium*, 2012.
10 M. Chan, D. Estève, J. Y. Fourniols, C. Escriba and E. Campo, *Artif. Intell. Med.*, 2012, **56**, 137.
11 J. A. Rogers, *Nat. Nanotechnol.*, 2017, **12**, 839–840.
12 Y. Liu, J. J. Norton, R. Qazi, Z. Zou, K. R. Ammann, H. Liu, L. Yan, P. L. Tran, K. I. Jang and J. W. Lee, *Sci. Adv.*, 2016, **2**, e1601185.
13 B. C. Tee, A. Chortos, A. Berndt, A. K. Nguyen, A. Tom, A. Mcguire, Z. C. Lin, K. Tien, W. G. Bae and H. Wang, *Science*, 2015, **350**, 313.
14 T. Someya, Z. Bao and G. G. Malliaras, *Nature*, 2016, **540**, 379.
15 D. Son, J. Lee, S. Qiao, R. Ghaffari, J. Kim, J. E. Lee, C. Song, S. J. Kim, D. J. Lee and S. W. Jun, *Nat. Nanotechnol.*, 2014, **9**, 397.
16 D. Wei, D. Cotton and T. Ryhänen, *Nanomaterials*, 2012, **2**, 268–274.
17 R. Raccichini, A. Varzi, D. Wei and S. Passerini, *Adv. Mater.*, 2016, **29**, 1603421.
18 D. Wei, P. Andrew, H. Yang, Y. Jiang, F. Li, C. Shan, W. Ruan, D. Han, N. Li and C. Bower, *J. Mater. Chem.*, 2011, **21**, 9762–9767.
19 D. Wei, M. R. Astley, N. Harris, R. White, T. Ryhänen and J. Kivioja, *Nanoscale*, 2014, **6**, 9536.
20 D. Wei, S. Haque, P. Andrew, J. Kivioja, T. Ryhanen, A. Pesquera, A. Centeno, B. Alonso, A. Chuvilin and A. Zurutuza, *J. Mater. Chem. A*, 2013, **1**, 3177–3181.
21 C. K. Chan, H. Peng, G. Liu, K. Mcilwrath, X. F. Zhang, R. A. Huggins and Y. Cui, *Nat. Nanotechnol.*, 2007, **3**, 187–191.
22 L. X. Yuan, Z. H. Wang, W. X. Zhang, X. L. Hu, J. T. Chen, Y. H. Huang and J. B. Goodenough, *Energy Environ. Sci.*, 2011, **4**, 269–284.
23 Y. Zhu, X. Han, Y. Xu, Y. Liu, S. Zheng, K. Xu, L. Hu and C. Wang, *ACS Nano*, 2013, **7**, 6378.
24 M.-C. Lin, M. Gong, B. Lu, Y. Wu, D.-Y. Wang, M. Guan, M. Angell, C. Chen, J. Yang and B.-J. Hwang, *Nature*, 2015, **520**, 324–328.
25 D. Wei, M. R. Scherer, C. Bower, P. Andrew, T. Ryhänen and U. Steiner, *Nano Lett.*, 2012, **12**, 1857.
26 D. Wei and T. W. Ng, *Electrochem. Commun.*, 2009, **11**, 1996–1999.
27 D. Wei, S. J. Wakeham, T. W. Ng, M. J. Thwaites, H. Brown and P. Beecher, *Electrochem. Commun.*, 2009, **11**, 2285–2287.
28 D. Wei, H. Wang, P. Hiralal, P. Andrew, T. Ryhänen, Y. Hayashi and G. A. Amaratunga, *Nanotechnology*, 2010, **21**, 435702.
29 S. Pan, Z. Yang, P. Chen, J. Deng, H. Li and H. Peng, *Angew. Chem.*, 2014, **53**, 6110.
30 B. J. Kim, H. K. Dong, Y. Y. Lee, H. W. Shin, G. S. Han, J. S. Hong, K. Mahmood, T. K. Ahn, Y. C. Joo, K. S. Hong, N. G. Park, S. Lee and H. S. Jung, *Energy Environ. Sci.*, 2015, **8**, 916–921.
31 Z. L. Wang and J. Song, *Science*, 2006, **312**, 242.
32 M. Zhang, T. Gao, J. Wang, J. Liao, Y. Qiu, Q. Yang, H. Xue, Z. Shi, Y. Zhao and Z. Xiong, *Nano Energy*, 2015, **13**, 298–305.
33 F. Yi, L. Lin, S. Niu, P. K. Yang, Z. Wang, J. Chen, Y. Zhou, Y. Zi, J. Wang and Q. Liao, *Adv. Funct. Mater.*, 2015, **25**, 3688–3696.
34 F. Yi, L. Lin, S. Niu, J. Yang, W. Wu, S. Wang, Q. Liao, Y. Zhang and Z. L. Wang, *Adv. Funct. Mater.*, 2015, **24**, 7488–7494.
35 X. Wang, Y. Yin, F. Yi, K. Dai, S. Niu, Y. Han, Y. Zhang and Z. You, *Nano Energy*, 2017, **39**, 429–436.
36 Y. Du, K. Cai, S. Chen, H. Wang, S. Z. Shen, R. Donelson and T. Lin, *Sci. Rep.*, 2015, **5**, 6411.
37 Y. Yang, K. C. Pradel, Q. Jing, J. M. Wu, F. Zhang, Y. Zhou, Y. Zhang and Z. L. Wang, *ACS Nano*, 2012, **6**, 6984–6989.
38 J. Wang, S. Li, F. Yi, Y. Zi, J. Lin, X. Wang, Y. Xu and Z. L. Wang, *Nat. Commun.*, 2016, **7**, 12744.
39 X. Wang, S. Niu, Y. Fang, Y. Yin, C. Hao, K. Dai, Z. Yue, Y. Zheng and L. W. Zhong, *ACS Nano*, 2017, **11**, 1728.
40 S. Wang, Z. H. Lin, S. Niu, L. Lin, Y. Xie, K. C. Pradel and Z. L. Wang, *ACS Nano*, 2013, **7**, 11263.
41 H. Ren, H. Wang, L. Lin, M. Tang, S. Zhao, B. Deng, M. K. Priydarshi, J. Zhang, H. Peng and Z. Liu, *Nano Res.*, 2017, **10**, 1189–1199.
42 H. Ren, M. Tang, B. Guan, K. Wang, J. Yang, F. Wang, M. Wang, J. Shan, Z. Chen and D. Wei, *Adv. Mater.*, 2017, **29**, 1702590.

43 X. Sun, L. Lin, L. Sun, J. Zhang, D. Rui, J. Li, M. Wang, C. Tan, N. Kang and D. Wei, *Small*, 2017, **14**, 1702916.
44 W. Gao, *Graphene oxide: reduction recipes, spectroscopy, and applications*, Springer International Publishing, Cham, 2015, pp. 61–95.
45 L. Xie, X. Ling, Y. Fang, J. Zhang and Z. Liu, *J. Am. Chem. Soc.*, 2009, **131**, 9890.
46 K. S. Novoselov, A. K. Geim, S. V. Morozov, D. Jiang, Y. Zhang, S. V. Dubonos, I. V. Grigorieva and A. A. Firsov, *Science*, 2004, **306**, 666–669.
47 A. K. Geim and K. S. Novoselov, *Nat. Mater.*, 2007, **6**, 183.
48 S. W. Cranford and M. J. Buehler, *Carbon*, 2011, **49**, 4111–4121.
49 S. Zhang, J. Wang, Z. Li, R. Zhao, L. Tong, Z. Liu, J. Zhang and Z. Liu, *J. Phys. Chem. C*, 2016, **120**, 10605–10613.
50 X. Gao, J. Zhou, R. Du, Z. Xie, S. Deng, R. Liu, Z. Liu and J. Zhang, *Adv. Mater.*, 2016, **28**, 168–173.
51 J. Zhou, X. Gao, R. Liu, Z. Xie, J. Yang, S. Zhang, G. Zhang, H. Liu, Y. Li and J. Zhang, *J. Am. Chem. Soc.*, 2015, **137**, 7596–7599.
52 Q. H. Wang, K. Kalantarzadeh, A. Kis, J. N. Coleman and M. S. Strano, *Nat. Nanotechnol.*, 2012, **7**, 699–712.
53 X. Xu, W. Yao, D. Xiao and T. F. Heinz, *Nat. Phys.*, 2014, **10**, 1–2.
54 J. Shi, D. Ma, G. F. Han, Y. Zhang, Q. Ji, T. Gao, J. Sun, X. Song, C. Li and Y. Zhang, *ACS Nano*, 2014, **8**, 10196.
55 Z. Sun, T. Liao, Y. Dou, S. M. Hwang, M.-S. Park, L. Jiang, J. H. Kim and S. X. Dou, *Nat. Commun.*, 2014, **5**, 3813.
56 M. Naguib, O. Mashtalir, J. Carle, V. Presser, J. Lu, L. Hultman, Y. Gogotsi and M. W. Barsoum, *ACS Nano*, 2012, **6**, 1322–1331.
57 O. Mashtalir, M. Naguib, V. N. Mochalin, Y. Dall'Agnese, M. Heon, M. W. Barsoum and Y. Gogotsi, *Nat. Commun.*, 2013, **4**, 1716.
58 J. Qiao, X. Kong, Z.-X. Hu, F. Yang and W. Ji, *Nat. Commun.*, 2014, **5**, 4475.
59 L. Li, Y. Yu, G. J. Ye, Q. Ge, X. Ou, H. Wu, D. Feng, X. H. Chen and Y. Zhang, *Nat. Nanotechnol.*, 2014, **9**, 372.
60 H. Zhang, *ACS Nano*, 2015, **9**, 9451–9469.
61 S. Z. Butler, S. M. Hollen, L. Cao, Y. Cui, J. A. Gupta, H. R. Gutiérrez, T. F. Heinz, S. S. Hong, J. Huang and A. F. Ismach, *ACS Nano*, 2013, **7**, 2898–2926.
62 M. Armand and J.-M. Tarascon, *Nature*, 2008, **451**, 652–657.
63 W. Liu, M. S. Song, B. Kong and Y. Cui, *Adv. Mater.*, 2017, **29**, 1603436.
64 G. Zhou, F. Li and H.-M. Cheng, *Energy Environ. Sci.*, 2014, **7**, 1307–1338.
65 F. Bonaccorso, L. Colombo, G. Yu, M. Stoller, V. Tozzini, A. C. Ferrari, R. S. Ruoff and V. Pellegrini, *Science*, 2015, **347**, 1246501.
66 L. Peng, Y. Zhu, D. Chen, R. S. Ruoff and G. Yu, *Adv. Energy Mater.*, 2016, **6**, 1600025.
67 L. Peng, Y. Zhu, H. Li and G. Yu, *Small*, 2016, **12**, 6183–6199.
68 T. Stephenson, Z. Li, B. Olsen and D. Mitlin, *Energy Environ. Sci.*, 2014, **7**, 209–231.
69 L. Cong, H. Xie and J. Li, *Adv. Energy Mater.*, 2017, **7**, 1601906.
70 C. Tan, X. Cao, X.-J. Wu, Q. He, J. Yang, X. Zhang, J. Chen, W. Zhao, S. Han and G.-H. Nam, *Chem. Rev.*, 2017, **117**, 6225–6331.
71 M. D. Stoller, S. Park, Y. Zhu, J. An and R. S. Ruoff, *Nano Lett.*, 2008, **8**, 3498–3502.
72 C. Lee, X. Wei, J. W. Kysar and J. Hone, *Science*, 2008, **321**, 385–388.
73 E. Yoo, J. Kim, E. Hosono, H. S. Zhou, T. Kudo and I. Honma, *Nano Lett.*, 2008, **8**, 2277–2282.
74 G. Kucinskis, G. Bajars and J. Kleperis, *J. Power Sources*, 2013, **240**, 66–79.
75 R. Raccichini, A. Varzi, S. Passerini and B. Scrosati, *Nat. Mater.*, 2015, **14**, 271–279.
76 S. Hu, M. LozadaHidalgo, F. C. Wang, A. Mishchenko, F. Schedin, R. R. Nair, E. W. Hill, D. W. Boukhvalov, M. I. Katsnelson and R. A. W. Dryfe, *Nature*, 2014, **516**, 227–230.
77 X. Huang, X. Qi, F. Boey and H. Zhang, *Chem. Soc. Rev.*, 2012, **41**, 666–686.
78 M. Reddy, G. Subba Rao and B. Chowdari, *Chem. Rev.*, 2013, **113**, 5364–5457.
79 J. R. Dahn, T. Zheng, Y. Liu and J. S. Xue, *Science*, 1995, **270**, 590–593.
80 Y. Liu, J. S. Xue, T. Zheng and J. R. Dahn, *Carbon*, 1996, **34**, 193–200.
81 J. I. Martínez, I. Cabria, M. J. López and J. A. Alonso, *J. Phys. Chem. C*, 2009, **113**, 939.
82 Y. Liu, V. I. Artyukhov, M. Liu, A. R. Harutyunyan and B. I. Yakobson, *J. Phys. Chem. Lett.*, 2013, **4**, 1737–1742.
83 C. Wang, D. Li, C. O. Too and G. G. Wallace, *Chem. Mater.*, 2009, **21**, 2604–2606.
84 X. Zhao, C. M. Hayner, M. C. Kung and H. H. Kung, *ACS Nano*, 2011, **5**, 8739.
85 T. Hu, X. Sun, H. Sun, M. Yu, F. Lu, C. Liu and J. Lian, *Carbon*, 2013, **51**, 322–326.
86 A. V. Talyzin, G. Mercier, A. Klechikov, M. Hedenström, J. Dan, W. Di, D. Cotton, A. Opitz and E. Moons, *Carbon*, 2017, **115**, 430–440.
87 R. Mukherjee, A. V. Thomas, A. Krishnamurthy and N. Koratkar, *ACS Nano*, 2012, **6**, 7867–7878.
88 L. Ren, K. N. Hui, K. S. Hui, Y. Liu, X. Qi, J. Zhong, Y. Du and J. Yang, *Sci. Rep.*, 2015, **5**, 14229.
89 K. Chen, C. Li, L. Shi, T. Gao, X. Song, A. Bachmatiuk, Z. Zou, B. Deng, Q. Ji and D. Ma, *Nat. Commun.*, 2016, **7**, 13440.
90 B. Liu, J. G. Zhang and G. Shen, *Nano Today*, 2016, **11**, 82–97.
91 B. Wang, X. Li, X. Zhang, B. Luo, M. Jin, M. Liang, S. A. Dayeh, S. T. Picraux and L. Zhi, *ACS Nano*, 2013, **7**, 1437–1445.
92 L. Shi, C. Pang, S. Chen, M. Wang, K. Wang, Z. Tan, G. Peng, J. Ren, Y. Huang and H. Peng, *Nano Lett.*, 2017, **17**, 3681.
93 H. Gwon, H. S. Kim, K. U. Lee, D. H. Seo, C. P. Yun, Y. S. Lee, B. T. Ahn and K. Kang, *Energy Environ. Sci.*, 2011, **4**, 1277–1283.

94 N. Li, Z. Chen, W. Ren, F. Li and H. M. Cheng, *Proc. Natl. Acad. Sci. U. S. A.*, 2012, **109**, 17360–17365.
95 G. Li, Y. Li, H. Liu, Y. Guo, Y. Li and D. Zhu, *Chem. Commun.*, 2010, **46**, 3256–3258.
96 Y. Li, L. Xu, H. Liu and Y. Li, *Chem. Soc. Rev.*, 2014, **43**, 2572–2586.
97 S. Zhang, H. Liu, C. Huang, G. Cui and Y. Li, *Chem. Commun.*, 2015, **51**, 1834.
98 J. He, N. Wang, Z. Cui, H. Du, L. Fu, C. Huang, Z. Yang, X. Shen, Y. Yi and Z. Tu, *Nat. Commun.*, 2017, **8**, 1172.
99 G. Du, Z. Guo, S. Wang, R. Zeng, Z. Chen and H. Liu, *Chem. Commun.*, 2010, **46**, 1106–1108.
100 M. Chhowalla, Z. Liu and H. Zhang, *Chem. Soc. Rev.*, 2015, **44**, 2584–2586.
101 H. Li, X. Wang, B. Ding, G. Pang, P. Nie, L. Shen and X. Zhang, *ChemElectroChem*, 2014, **1**, 1118–1125.
102 Y. Chao, R. Jalili, Y. Ge, C. Wang, T. Zheng, K. Shu and G. G. Wallace, *Adv. Funct. Mater.*, 2017, **27**, 1700234.
103 H. Wang, H. Feng and J. Li, *Small*, 2014, **10**, 2165–2181.
104 J. Sun, G. Zheng, H.-W. Lee, N. Liu, H. Wang, H. Yao, W. Yang and Y. Cui, *Nano Lett.*, 2014, **14**, 4573–4580.
105 L. Chen, G. Zhou, Z. Liu, X. Ma, J. Chen, Z. Zhang, X. Ma, F. Li, H. M. Cheng and W. Ren, *Adv. Mater.*, 2016, **28**, 510.
106 N. Li, G. Zhou, R. Fang, F. Li and H. M. Cheng, *Nanoscale*, 2013, **5**, 7780–7784.
107 L. Yu, W. Wei, G. Lin, Y. Wang, Y. Ying, Y. Mao, L. Sun and X. Peng, *ACS Appl. Mater. Interfaces*, 2013, **5**, 9850.
108 L. Peng, P. Xiong, L. Ma, Y. Yuan, Y. Zhu, D. Chen, X. Luo, J. Lu, K. Amine and G. Yu, *Nat. Commun.*, 2017, **8**, 15139.
109 L. Peng, Y. Zhu, X. Peng, Z. Fang, W. Chu, Y. Wang, Y. Xie, Y. Li, J. J. Cha and G. Yu, *Nano Lett.*, 2017, **17**, 6273–6279.
110 L. Peng, Z. Fang, Y. Zhu, C. Yan and G. Yu, *Adv. Energy Mater.*, 2017, 1702179.
111 C. Yan, C. Lv, Y. Zhu, G. Chen, J. Sun and G. Yu, *Adv. Mater.*, 2017, **29**, 1703909.
112 B. Dunn, H. Kamath and J. M. Tarascon, *Science*, 2011, **334**, 928–935.
113 H. Pan, Y. S. Hu and L. Chen, *Energy Environ. Sci.*, 2013, **6**, 2338–2360.
114 M. D. Slater, D. Kim, E. Lee and C. S. Johnson, *Adv. Funct. Mater.*, 2013, **23**, 947–958.
115 D. Aurbach, Z. Lu, A. Schechter, Y. Gofer, H. Gizbar, R. Turgeman, Y. Cohen, M. Moshkovich and E. Levi, *Nature*, 2000, **407**, 724–727.
116 Y. Xue, Q. Zhang, W. Wang, H. Cao, Q. Yang and L. Fu, *Adv. Energy Mater.*, 2017, 1602684.
117 D. Kundu, E. Talaie, V. Duffort and L. F. Nazar, *Angew. Chem.*, 2015, **54**, 3431.
118 H. Li, Y. Ding, H. Ha, Y. Shi, L. Peng, X. Zhang, C. J. Ellison and G. Yu, *Adv. Mater.*, 2017, **29**, 1700898.
119 M. Angell, C.-J. Pan, Y. Rong, C. Yuan, M.-C. Lin, B.-J. Hwang and H. Dai, *Proc. Natl. Acad. Sci. U. S. A.*, 2017, **114**, 834–839.
120 X. Yu, B. Wang, D. Gong, Z. Xu and B. Lu, *Adv. Mater.*, 2017, **29**, 1604118.
121 Z. Yang, J. Deng, X. Chen, J. Ren and H. Peng, *Angew. Chem.*, 2013, **52**, 13453.
122 Z. W. Seh, Y. Sun, Q. Zhang and Y. Cui, *Chem. Soc. Rev.*, 2016, **45**, 5605.
123 G. Zhou, *Nano Energy*, 2015, **11**, 356–365.
124 L. Xiao, Y. Cao, J. Xiao, B. Schwenzer, M. H. Engelhard, L. V. Saraf, Z. Nie, G. J. Exarhos and J. Liu, *Adv. Mater.*, 2012, **24**, 1176.
125 J. R. Miller and P. Simon, *Science*, 2008, **321**, 651–652.
126 J.-M. Tarascon and M. Armand, *Nature*, 2001, **414**, 359–367.
127 M. Winter and R. J. Brodd, *Chem. Rev.*, 2004, **104**, 4245–4270.
128 P. Simon and Y. Gogotsi, *Nat. Mater.*, 2008, **7**, 845–854.
129 J. R. Miller, R. Outlaw and B. Holloway, *Science*, 2010, **329**, 1637–1639.
130 M. F. El-Kady, V. Strong, S. Dubin and R. B. Kaner, *Science*, 2012, **335**, 1326–1330.
131 Z. Weng, Y. Su, D. W. Wang, F. Li, J. Du and H. M. Cheng, *Adv. Energy Mater.*, 2011, **1**, 917–922.
132 Z. Y. Xiong, C. L. Liao, W. H. Han and X. G. Wang, *Adv. Mater.*, 2015, **27**, 4469–4475.
133 Y. Meng, Y. Zhao, C. Hu, H. Cheng, Y. Hu, Z. Zhang, G. Shi and L. Qu, *Adv. Mater.*, 2013, **25**, 2326–2331.
134 B. G. Choi, J. Hong, W. H. Hong, P. T. Hammond and H. Park, *ACS Nano*, 2011, **5**, 7205–7213.
135 X. Peng, L. Peng, C. Wu and Y. Xie, *Chem. Soc. Rev.*, 2014, **43**, 3303–3323.
136 T. Lin, I. W. Chen, F. Liu, C. Yang, H. Bi, F. Xu and F. Huang, *Science*, 2015, **350**, 1508.
137 Z.-S. Wu, K. Parvez, A. Winter, H. Vieker, X. Liu, S. Han, A. Turchanin, X. Feng and K. Müllen, *Adv. Mater.*, 2014, **26**, 4552–4558.
138 X. B. Zang, X. Li, M. Zhu, X. M. Li, Z. Zhen, Y. J. He, K. L. Wang, J. Q. Wei, F. Y. Kang and H. W. Zhu, *Nanoscale*, 2015, **7**, 7318–7322.
139 F. Xiao, S. Yang, Z. Zhang, H. Liu, J. Xiao, L. Wan, J. Luo, S. Wang and Y. Liu, *Sci. Rep.*, 2015, **5**, 9359.
140 R. S. Kalubarme, H. S. Jadhav and C.-J. Park, *Electrochim. Acta*, 2013, **87**, 457–465.
141 Y. C. Liu, X. F. Miao, J. H. Fang, X. X. Zhang, S. J. Chen, W. Li, W. D. Feng, Y. Q. Chen, W. Wang and Y. N. Zhang, *ACS Appl. Mater. Interfaces*, 2016, **8**, 5251–5260.
142 L. Peng, X. Peng, B. Liu, C. Wu, Y. Xie and G. Yu, *Nano Lett.*, 2013, **13**, 2151–2157.
143 M. A. Bissett, I. A. Kinloch and R. A. W. Dryfe, *ACS Appl. Mater. Interfaces*, 2015, **7**, 17388–17398.
144 Y. M. Shulga, S. A. Baskakov, V. A. Smirnov, N. Y. Shulga, K. G. Belay and G. L. Gutsev, *J. Power Sources*, 2014, **245**, 33–36.
145 Y. Hu, H. Cheng, F. Zhao, N. Chen, L. Jiang, Z. Feng and L. Qu, *Nanoscale*, 2014, **6**, 6448–6451.
146 M. Naguib, V. N. Mochalin, M. W. Barsoum and Y. Gogotsi, *Adv. Mater.*, 2014, **26**, 992–1005.
147 M. Ghidiu, M. R. Lukatskaya, M.-Q. Zhao, Y. Gogotsi and M. W. Barsoum, *Nature*, 2014, **516**, 78–U171.
148 M. R. Lukatskaya, O. Mashtalir, C. E. Ren, Y. Dall'Agnese, P. Rozier, P. L. Taberna, M. Naguib, P. Simon, M. W. Barsoum and Y. Gogotsi, *Science*, 2013, **341**, 1502–1505.

149 M. R. Lukatskaya, S. Kota, Z. Lin, M.-Q. Zhao, N. Shpigel, M. D. Levi, J. Halim, P.-L. Taberna, M. W. Barsoum, P. Simon and Y. Gogotsi, *Nat. Energy*, 2017, **6**, 17105.
150 J. Feng, X. Sun, C. Wu, L. Peng, C. Lin, S. Hu, J. Yang and Y. Xie, *J. Am. Chem. Soc.*, 2011, **133**, 17832–17838.
151 C. Wu, X. Lu, L. Peng, K. Xu, X. Peng, J. Huang, G. Yu and Y. Xie, *Nat. Commun.*, 2013, **4**, 2431.
152 J. J. Yoo, K. Balakrishnan, J. Huang, V. Meunier, B. G. Sumpter, A. Srivastava, M. Conway, A. L. Mohana Reddy, J. Yu and R. Vajtai, *Nano Lett.*, 2011, **11**, 1423–1427.
153 J. Yun, D. Kim, G. Lee and J. S. Ha, *Carbon*, 2014, **79**, 156–164.
154 Z. Niu, L. Zhang, L. Liu, B. Zhu, H. Dong and X. Chen, *Adv. Mater.*, 2013, **25**, 4035–4042.
155 W. Liu, C. Lu, X. Wang, R. Y. Tay and B. K. Tay, *ACS Nano*, 2015, **9**, 1528–1542.
156 W. Gao, N. Singh, L. Song, Z. Liu, A. L. M. Reddy, L. Ci, R. Vajtai, Q. Zhang, B. Wei and P. M. Ajayan, *Nat. Nanotechnol.*, 2011, **6**, 496–500.
157 L. T. Le, M. H. Ervin, H. Qiu, B. E. Fuchs and W. Y. Lee, *Electrochem. Commun.*, 2011, **13**, 355–358.
158 X. Chen, T. Xiang, Z. Li, Y. Wu, H. Wu, Z. Cheng, J. J. Shao and Q. H. Yang, *Adv. Mater. Interfaces*, 2017, **4**, 1601127.
159 K. Krishnamoorthy, S. Thangavel, J. C. Veetil, N. Raju, G. Venugopal and S. J. Kim, *Int. J. Hydrogen Energy*, 2016, **41**, 1672–1678.
160 Z. Liu, J. Li and F. Yan, *Adv. Mater.*, 2013, **25**, 4296–4301.
161 X. Wang, L. Zhi and K. Müllen, *Nano Lett.*, 2008, **8**, 323–327.
162 Z. Yin, S. Sun, T. Salim, S. Wu, X. Huang, Q. He, Y. M. Lam and H. Zhang, *ACS Nano*, 2010, **4**, 5263–5268.
163 Y. Wang, S. W. Tong, X. F. Xu, B. Özyilmaz and K. P. Loh, *Adv. Mater.*, 2011, **23**, 1514–1518.
164 Y. Wu, X. Zhang, J. Jie, C. Xie, X. Zhang, B. Sun, Y. Wang and P. Gao, *J. Phys. Chem. C*, 2013, **117**, 11968–11976.
165 C.-L. Hsu, C.-T. Lin, J.-H. Huang, C.-W. Chu, K.-H. Wei and L.-J. Li, *ACS Nano*, 2012, **6**, 5031–5039.
166 Z. Yin, S. Wu, X. Zhou, X. Huang, Q. Zhang, F. Boey and H. Zhang, *Small*, 2010, **6**, 307–312.
167 D. Zhang, F. Xie, P. Lin and W. C. H. Choy, *ACS Nano*, 2013, **7**, 1740–1747.
168 H. Bi, F. Huang, J. Liang, X. Xie and M. Jiang, *Adv. Mater.*, 2011, **23**, 3202–3206.
169 H. Park, S. Chang, J. Jean, J. J. Cheng, P. T. Araujo, M. Wang, M. G. Bawendi, M. S. Dresselhaus, V. Bulović, J. Kong and S. Gradečak, *Nano Lett.*, 2013, **13**, 233–239.
170 N. Yang, J. Zhai, D. Wang, Y. Chen and L. Jiang, *ACS Nano*, 2010, **4**, 887–894.
171 Y.-B. Tang, C.-S. Lee, J. Xu, Z.-T. Liu, Z.-H. Chen, Z. He, Y.-L. Cao, G. Yuan, H. Song, L. Chen, L. Luo, H.-M. Cheng, W.-J. Zhang, I. Bello and S.-T. Lee, *ACS Nano*, 2010, **4**, 3482–3488.
172 J.-M. Yun, J.-S. Yeo, J. Kim, H.-G. Jeong, D.-Y. Kim, Y.-J. Noh, S.-S. Kim, B.-C. Ku and S.-I. Na, *Adv. Mater.*, 2011, **23**, 4923–4928.
173 J. Liu, Y. Xue, Y. Gao, D. Yu, M. Durstock and L. Dai, *Adv. Mater.*, 2012, **24**, 2228–2233.
174 V. C. Tung, J. Kim and J. Huang, *Adv. Energy Mater.*, 2012, **2**, 299–303.
175 S. W. Tong, Y. Wang, Y. Zheng, M.-F. Ng and K. P. Loh, *Adv. Funct. Mater.*, 2011, **21**, 4430–4435.
176 X. Yan, X. Cui, B. Li and L.-s. Li, *Nano Lett.*, 2010, **10**, 1869–1873.
177 Z. Liu, Q. Liu, Y. Huang, Y. Ma, S. Yin, X. Zhang, W. Sun and Y. Chen, *Adv. Mater.*, 2008, **20**, 3924–3930.
178 J. D. Roy-Mayhew, D. J. Bozym, C. Punckt and I. A. Aksay, *ACS Nano*, 2010, **4**, 6203–6211.
179 S. Li, Y. Luo, W. Lv, W. Yu, S. Wu, P. Hou, Q. Yang, Q. Meng, C. Liu and H.-M. Cheng, *Adv. Energy Mater.*, 2011, **1**, 486–490.
180 Y. Lin, X. Li, D. Xie, T. Feng, Y. Chen, R. Song, H. Tian, T. Ren, M. Zhong, K. Wang and H. Zhu, *Energy Environ. Sci.*, 2013, **6**, 108–115.
181 X. Li, H. Zhu, K. Wang, A. Cao, J. Wei, C. Li, Y. Jia, Z. Li, X. Li and D. Wu, *Adv. Mater.*, 2010, **22**, 2743–2748.
182 X. Miao, S. Tongay, M. K. Petterson, K. Berke, A. G. Rinzler, B. R. Appleton and A. F. Hebard, *Nano Lett.*, 2012, **12**, 2745–2750.
183 M. Bernardi, M. Palummo and J. C. Grossman, *Nano Lett.*, 2013, **13**, 3664–3670.
184 M. Shanmugam, C. A. Durcan and B. Yu, *Nanoscale*, 2012, **4**, 7399–7405.
185 M.-L. Tsai, S.-H. Su, J.-K. Chang, D.-S. Tsai, C.-H. Chen, C.-I. Wu, L.-J. Li, L.-J. Chen and J.-H. He, *ACS Nano*, 2014, **8**, 8317–8322.
186 M. Shanmugam, R. Jacobs-Gedrim, E. S. Song and B. Yu, *Nanoscale*, 2014, **6**, 12682–12689.
187 A. Pospischil, M. M. Furchi and T. Mueller, *Nat. Nanotechnol.*, 2014, **9**, 257–261.
188 M. M. Furchi, A. Pospischil, F. Libisch, J. Burgdörfer and T. Mueller, *Nano Lett.*, 2014, **14**, 4785–4791.
189 O. Lopez-Sanchez, E. Alarcon Llado, V. Koman, A. Fontcuberta i Morral, A. Radenovic and A. Kis, *ACS Nano*, 2014, **8**, 3042–3048.
190 W. Liu, S. He, Y. Wang, Y. Dou, D. Pan, Y. Feng, G. Qian, J. Xu and S. Miao, *Electrochim. Acta*, 2014, **144**, 119–126.
191 D. Song, M. Li, Y. Jiang, Z. Chen, F. Bai, Y. Li and B. Jiang, *J. Photochem. Photobiol., A*, 2014, **279**, 47–51.
192 W. Liu, S. He, T. Yang, Y. Feng, G. Qian, J. Xu and S. Miao, *Appl. Surf. Sci.*, 2014, **313**, 498–503.
193 X. Gu, W. Cui, H. Li, Z. Wu, Z. Zeng, S.-T. Lee, H. Zhang and B. Sun, *Adv. Energy Mater.*, 2013, **3**, 1262–1268.
194 Y. Yang, J. Gao, Z. Zhang, S. Xiao, H.-H. Xie, Z.-B. Sun, J.-H. Wang, C.-H. Zhou, Y.-W. Wang, X.-Y. Guo, P. K. Chu and X.-F. Yu, *Adv. Mater.*, 2016, **28**, 8937–8944.
195 S. Lin, S. Liu, Z. Yang, Y. Li, T. W. Ng, Z. Xu, Q. Bao, J. Hao, C.-S. Lee, C. Surya, F. Yan and S. P. Lau, *Adv. Funct. Mater.*, 2016, **26**, 864–871.
196 J. Dai and X. C. Zeng, *J. Phys. Chem. Lett.*, 2014, **5**, 1289–1293.
197 W. Hu, L. Lin, C. Yang, J. Dai and J. Yang, *Nano Lett.*, 2016, **16**, 1675–1682.
198 O. J. Cheong, J. S. Lee, J. H. Kim and J. Jang, *Small*, 2016, **12**, 2567–2574.

199 Y. K. Fuh, C. C. Kuo, Z. M. Huang, S. C. Li and E. R. Liu, *Small*, 2016, **12**, 1875–1881.
200 D. Choi, M.-Y. Choi, W. M. Choi, H.-J. Shin, H.-K. Park, J.-S. Seo, J. Park, S.-M. Yoon, S. J. Chae, Y. H. Lee, S.-W. Kim, J.-Y. Choi, S. Y. Lee and J. M. Kim, *Adv. Mater.*, 2010, **22**, 2187–2192.
201 J. Kwon, W. Seung, B. K. Sharma, S.-W. Kim and J.-H. Ahn, *Energy Environ. Sci.*, 2012, **5**, 8970–8975.
202 M. Lanza, M. Reguant, G. Zou, P. Lv, H. Li, R. Chin, H. Liang, D. Yu, Y. Zhang, Z. Liu and H. Duan, *Adv. Mater. Interfaces*, 2014, **1**, 1300101.
203 X. Li, Y. Chen, A. Kumar, A. Mahmoud, J. A. Nychka and H.-J. Chung, *ACS Appl. Mater. Interfaces*, 2015, **7**, 20753–20760.
204 M. M. Abolhasani, K. Shirvanimoghaddam and M. Naebe, *Compos. Sci. Technol.*, 2017, **138**, 49–56.
205 C. Lu, L. Zhang, C. Xu, Z. Yin, S. Zhou, J. Wang, R. Huang, X. Zhou, C. Zhang, W. Yang and J. Lu, *RSC Adv.*, 2016, **6**, 67400–67408.
206 V. Bhavanasi, V. Kumar, K. Parida, J. Wang and P. S. Lee, *ACS Appl. Mater. Interfaces*, 2016, **8**, 521–529.
207 L. Wu, Alamusi, J. Xue, T. Itoi, N. Hu, Y. Li, C. Yan, J. Qiu, H. Ning, W. Yuan and B. Gu, *J. Intell. Mater. Syst. Struct.*, 2014, **25**, 1813–1824.
208 M. A. Rahman, B. C. Lee, D. T. Phan and G. S. Chung, *Smart Mater. Struct.*, 2013, **22**, 085017.
209 M. Kandpal, V. Palaparthy, N. Tiwary and V. R. Rao, *IEEE Trans. Nanotechnol.*, 2017, **16**, 259–264.
210 U. Yaqoob, A. S. M. I. Uddin and G.-S. Chung, *Appl. Surf. Sci.*, 2017, **405**, 420–426.
211 M. T. Ong and E. J. Reed, *ACS Nano*, 2012, **6**, 1387–1394.
212 L. Dong, J. Lou and V. B. Shenoy, *ACS Nano*, 2017, **11**, 8242–8248.
213 K.-A. N. Duerloo, M. T. Ong and E. J. Reed, *J. Phys. Lett.*, 2012, **3**, 2871–2876.
214 X. Song, F. Hui, T. Knobloch, B. Wang, Z. Fan, T. Grasser, X. Jing, Y. Shi and M. Lanza, *Appl. Phys. Lett.*, 2017, **111**, 083107.
215 H. Zhu, Y. Wang, J. Xiao, M. Liu, S. Xiong, Z. J. Wong, Z. Ye, Y. Ye, X. Yin and X. Zhang, *Nat. Nanotechnol.*, 2015, **10**, 151–155.
216 W. Wu, L. Wang, Y. Li, F. Zhang, L. Lin, S. Niu, D. Chenet, X. Zhang, Y. Hao, T. F. Heinz, J. Hone and Z. L. Wang, *Nature*, 2014, **514**, 470–474.
217 Y. Zhou, W. Liu, X. Huang, A. Zhang, Y. Zhang and Z. L. Wang, *Nano Res.*, 2016, **9**, 800–807.
218 Y. Huang, L. Liu, J. Sha and Y. Chen, *Appl. Phys. Lett.*, 2017, **111**, 063902.
219 J.-H. Lee, J. Y. Park, E. B. Cho, T. Y. Kim, S. A. Han, T.-H. Kim, Y. Liu, S. K. Kim, C. J. Roh, H.-J. Yoon, H. Ryu, W. Seung, J. S. Lee, J. Lee and S.-W. Kim, *Adv. Mater.*, 2017, **29**, 1606667.
220 K. H. Michel and B. Verberck, *Phys. Rev. B: Condens. Matter Mater. Phys.*, 2009, **80**, 224301.
221 K.-A. N. Duerloo and E. J. Reed, *Nano Lett.*, 2013, **13**, 1681–1686.
222 L. B. Drissi, S. Sadki and K. Sadki, *J. Phys. Chem. Solids*, 2018, **112**, 137–142.
223 M. N. Blonsky, H. L. Zhuang, A. K. Singh and R. G. Hennig, *ACS Nano*, 2015, **9**, 9885–9891.
224 S. Kim, M. K. Gupta, K. Y. Lee, A. Sohn, T. Y. Kim, K.-S. Shin, D. Kim, S. K. Kim, K. H. Lee, H.-J. Shin, D.-W. Kim and S.-W. Kim, *Adv. Mater.*, 2014, **26**, 3918–3925.
225 H. Chu, H. Jang, Y. Lee, Y. Chae and J.-H. Ahn, *Nano Energy*, 2016, **27**, 298–305.
226 S. A. Shankaregowda, C. B. Nanjegowda, X. L. Cheng, M. Y. Shi, Z. F. Liu and H. X. Zhang, *2015 IEEE 15th International Conference on Nanotechnology (IEEE-Nano)*, 2015, pp. 1477–1480.
227 C. Wu, T. W. Kim, F. Li and T. Guo, *ACS Nano*, 2016, **10**, 6449–6457.
228 H. Chen, Y. Xu, L. Bai, Y. Jiang, J. Zhang, C. Zhao, T. Li, H. Yu, G. Song, N. Zhang and Q. Gan, *Adv. Mater. Technol.*, 2017, **2**, 1700044.
229 J. Zhou, Y. Chen, X. Song, B. Zheng, P. Li, J. Liu, F. Qi, X. Hao and W. Zhang, *Energy Technol.*, 2017, **5**, 599–603.
230 B. N. Chandrashekar, B. Deng, A. S. Smitha, Y. Chen, C. Tan, H. Zhang, H. Peng and Z. Liu, *Adv. Mater.*, 2015, **27**, 5210–5216.
231 H. Guo, T. Li, X. Cao, J. Xiong, Y. Jie, M. Willander, X. Cao, N. Wang and Z. L. Wang, *ACS Nano*, 2017, **11**, 856–864.
232 F. Yi, X. Wang, S. Niu, S. Li, Y. Yin, K. Dai, G. Zhang, L. Lin, Z. Wen, H. Guo, J. Wang, M.-H. Yeh, Y. Zi, Q. Liao, Z. You, Y. Zhang and Z. L. Wang, *Sci. Adv.*, 2016, **2**, e1501624.
233 F. Yi, J. Wang, X. Wang, S. Niu, S. Li, Q. Liao, Y. Xu, Z. You, Y. Zhang and Z. L. Wang, *ACS Nano*, 2016, **10**, 6519–6525.
234 X. Xia, J. Chen, G. Liu, M. S. Javed, X. Wang and C. Hu, *Carbon*, 2017, **111**, 569–576.
235 C. Wu, T. W. Kim and H. Y. Choi, *Nano Energy*, 2017, **32**, 542–550.
236 C. Wu, T. W. Kim, J. H. Park, H. An, J. Shao, X. Chen and Z. L. Wang, *ACS Nano*, 2017, **11**, 8356–8363.
237 T. A. Amollo, G. T. Mola, M. S. K. Kirui and V. O. Nyamori, *Crit. Rev. Solid State Mater. Sci.*, 2017, 1–25, DOI: 10.1080/10408436.2017.1300871.
238 J. G. Checkelsky and N. P. Ong, *Phys. Rev. B: Condens. Matter Mater. Phys.*, 2009, **80**, 081413.
239 D. Wang and J. Shi, *Phys. Rev. B: Condens. Matter Mater. Phys.*, 2011, **83**, 113403.
240 X. Wu, Y. Hu, M. Ruan, N. K. Madiomanana, C. Berger and W. A. d. Heer, *Appl. Phys. Lett.*, 2011, **99**, 133102.
241 X. Liu, D. Wang, P. Wei, L. Zhu and J. Shi, *Phys. Rev. B: Condens. Matter Mater. Phys.*, 2012, **86**, 155414.
242 A. V. Babichev, V. E. Gasumyants and V. Y. Butko, *J. Appl. Phys.*, 2013, **113**, 076101.
243 S.-G. Nam, D.-K. Ki and H.-J. Lee, *Phys. Rev. B: Condens. Matter Mater. Phys.*, 2010, **82**, 245416.
244 D. Sim, D. Liu, X. Dong, N. Xiao, S. Li, Y. Zhao, L.-J. Li, Q. Yan and H. H. Hng, *J. Phys. Chem. C*, 2011, **115**, 1780–1785.
245 J. Gao, C. Liu, L. Miao, X. Wang, Y. Peng and Y. Chen, *RSC Adv.*, 2016, **6**, 31580–31587.
246 J. Dong, W. Liu, H. Li, X. Su, X. Tang and C. Uher, *J. Mater. Chem. A*, 2013, **1**, 12503–12511.

247 B. Liang, Z. Song, M. Wang, L. Wang and W. Jiang, *J. Nanomater.*, 2013, 6.
248 X. Yannan, C. Ting-Mao, Y. Weifeng, H. Minghui, Z. Yingru, L. Ning and L. Zong-Hong, *Semicond. Sci. Technol.*, 2017, **32**, 044003.
249 R. Venkatasubramanian, E. Siivola, T. Colpitts and B. O'Quinn, *Nature*, 2001, **413**, 597–602.
250 L.-D. Zhao, S.-H. Lo, Y. Zhang, H. Sun, G. Tan, C. Uher, C. Wolverton, V. P. Dravid and M. G. Kanatzidis, *Nature*, 2014, **508**, 373–377.
251 M.-J. Lee, J.-H. Ahn, J. H. Sung, H. Heo, S. G. Jeon, W. Lee, J. Y. Song, K.-H. Hong, B. Choi, S.-H. Lee and M.-H. Jo, *Nature*, 2016, **7**, 12011.
252 F. Zhao, H. Cheng, Z. Zhang, L. Jiang and L. Qu, *Adv. Mater.*, 2015, **27**, 4351–4357.
253 F. Zhao, Y. Liang, H. Cheng, L. Jiang and L. Qu, *Energy Environ. Sci.*, 2016, **9**, 912–916.
254 P. Dhiman, F. Yavari, X. Mi, H. Gullapalli, Y. Shi, P. M. Ajayan and N. Koratkar, *Nano Lett.*, 2011, **11**, 3123–3127.
255 J. Yin, X. Li, J. Yu, Z. Zhang, J. Zhou and W. Guo, *Nat. Nanotechnol.*, 2014, **9**, 378–383.
256 J. Yin, Z. Zhang, X. Li, J. Yu, J. Zhou, Y. Chen and W. Guo, *Nat. Commun.*, 2014, **5**, 3582.
257 D. Wei, *Adv. Mater. Technol.*, 2016, **1**, 1600145.
258 D. Wei, *Sci. Rep.*, 2015, **5**, 15173.
259 S. H. Lee, Y. Jung, S. Kim and C.-S. Han, *Appl. Phys. Lett.*, 2013, **102**, 063116.
260 S. S. Kwak, S. Lin, J. H. Lee, H. Ryu, T. Y. Kim, H. Zhong, H. Chen and S.-W. Kim, *ACS Nano*, 2016, **10**, 7297–7302.
261 H. Zhong, J. Xia, F. Wang, H. Chen, H. Wu and S. Lin, *Adv. Funct. Mater.*, 2017, **27**, 1604226.
262 R. R. Nair and A. K. Geim, *Science*, 2011, **335**, 442.
263 Z. W. Seh, J. H. Yu, W. Li, P.-C. Hsu, H. Wang, Y. Sun, H. Yao, Q. Zhang and Y. Cui, *Nat. Commun.*, 2014, **5**, 5017–5024.
264 O. Mashtalir, M. R. Lukatskaya, M. Q. Zhao, M. W. Barsoum and Y. Gogotsi, *Adv. Mater.*, 2015, **27**, 3501.
265 R. Atchudan, T. Edison, S. Perumal and Y. R. Lee, *Appl. Surf. Sci.*, 2017, **393**, 276–286.
266 Y. L. Zhang, L. Si, B. Zhou, B. Zhao, Y. Y. Zhu, L. H. Zhu and X. Q. Jiang, *Chem. Eng. J.*, 2016, **288**, 689–700.
267 Z. Ling, Z. Wang, M. Zhang, C. Yu, G. Wang, Y. Dong, S. Liu, Y. Wang and J. Qiu, *Adv. Funct. Mater.*, 2016, **26**, 111–119.
268 W.-w. Liu, X.-b. Yan, J.-w. Lang, C. Peng and Q.-j. Xue, *J. Mater. Chem.*, 2012, **22**, 17245–17253.
269 X. Dong, L. Wang, D. Wang, C. Li and J. Jin, *Langmuir*, 2011, **28**, 293–298.

